For Reference

NOT TO BE TAKEN FROM THIS ROOM

For Reference

NOT TO BE TAKEN FROM THIS ROOM

Ex libris
universitatis
albertaensis

QUAECUMQUE VERA

The University of Alberta
Printing Department
Edmonton, Alberta

THE UNIVERSITY OF ALBERTA

A DOUBLY TUNED TUNNEL DIODE OSCILLATOR

by

© ROBERT KENT TIEDEMANN

A THESIS
SUBMITTED TO THE FACULTY OF GRADUATE STUDIES
IN PARTIAL FULFILLMENT OF THE REQUIREMENTS FOR THE
DEGREE OF MASTER OF SCIENCE

DEPARTMENT OF ELECTRICAL ENGINEERING

EDMONTON, ALBERTA
JULY, 1967

UNIVERSITY OF ALBERTA

FACULTY OF GRADUATE STUDIES

The undersigned certify that they have read and recommend to the Faculty of Graduate Studies for acceptance, a thesis entitled "A Doubly Tuned Tunnel Diode Oscillator" submitted by Robert Kent Tiedemann in partial fulfillment of the requirements for the degree of Master of Science.

ABSTRACT

This thesis deals primarily with the development of an approximate method of analysis of a tunnel diode oscillator. Because of the non-linear voltage-current characteristic of the tunnel diode, relatively simple systems may exhibit certain phenomena which cannot be explained in terms of linear circuit theory.

If two mutually coupled parallel resonant circuits comprise the linear portion of a tunnel diode oscillator, under certain conditions, two distinct modes of oscillation will be exhibited. Furthermore, as the degree of coupling is varied, two critical points can be found for which the oscillator will switch from one mode to the other. A form of hysteresis is also exhibited in that the point at which the oscillator will switch to its second mode occurs for a larger degree of coupling than does the point at which it will switch back to its original mode.

The objective of this thesis is thus to present a method of analysis sufficiently accurate as to account for the above phenomenon. This is done by first analysing an oscillator using a single tank circuit, and then considering the effect of the second tank circuit.

ACKNOWLEDGEMENTS

The author wishes to express his appreciation to Professor Y.J. Kingma, under whose supervision this project has been completed.

The assistance and co-operation received from the staff and graduate students of the Department of Electrical Engineering is also gratefully acknowledged.

The author is indebted to the National Research Council and the University of Alberta for the financial assistance provided.

TABLE OF CONTENTS

1. INTRODUCTION

1.1 The Tunnel Diode 1
1.2 Tunnel Diode Characteristics 2
1.3 Parasitic Elements 3
1.4 Basic Oscillator Circuit 5
1.5 Methods of Analysis 7

2. FEEDBACK OSCILLATOR MODEL

2.1 Equivalent Biasing Network 8
2.2 Small-Signal Equivalent Circuit 10

3. PROPERTIES OF THE PARALLEL RESONANT CIRCUIT

3.1 Resonance 13
3.2 Frequency-Normalized Impedance 14
3.3 Frequency Response Above Resonance 15
3.4 Bode Plot 16

4. DESCRIBING FUNCTION METHOD

4.1 Quantitative Description of the D.C. Characteristic 19
4.2 Expansion of f(V) About the Operating Point 21
4.3 Basic Circuit Equations 23
4.4 Describing Function and Biasing Equations 27

5. SOLUTION TO DESCRIBING FUNCTION AND BIASING EQUATIONS

5.1 Discussion of $G_{eq}(A,V_Q)$ 35
5.2 Radius of Curvature 39
5.3 Constant-G_{eq} Chart 41
5.4 Properties of the Constant-G_{eq} Chart 43
5.5 Discussion of the Biasing Function 48
5.6 Unique Determination of A and V_Q 50
5.7 Stability of Solutions 53
5.8 Relative Stability 59
5.9 Further Comments on Distortion 60
5.10 Effect of Self-Oscillation 62

6. EFFECT OF SECOND TUNED CIRCUIT

6.1 Resonant Frequencies 69
6.2 Discussion of $F(u^2, K^2)$ 78
6.3 Resistance at Resonance 90
6.4 Discussion of the Function R_o'/R_o 92
6.5 Explanation of the Switching Phenomenon 103
6.6 Limitations of the Method of Analysis 109
6.7 Summary 110

7. EXPERIMENTAL VERIFICATION

7.1 Basic Computer Set-Up 113
7.2 Oscillator without Mutual Coupling 115
7.3 Distortion with an Infinite-Q Circuit 120
7.4 Distortion with Finite-Q Circuits 123
7.5 Oscillator with Mutual Coupling 125
7.6 Possible Sources of Error 136

CONCLUSIONS 138

APPENDIX I MATHEMATICAL JUSTIFICATIONS 139

APPENDIX II ANALOGUE COMPUTER SIMULATION 155

REFERENCES 173

LIST OF FIGURES

Figure No.	Title	Page
1.1	Tunnel Diode Characteristic	2
1.2	Symbol for a Tunnel Diode	3
1.3	Equivalent Circuit for a Real Tunnel Diode	4
1.4	Basic Oscillator Circuit	5
1.5	Switching Phenomenon	6
2.1	Equivalent Biasing Network	8
2.2	Steady-State Equivalent Circuits	9
2.3	Small-Signal Equivalent Circuits	10
3.1	Approximate Bode Plot	17
4.1	Tunnel Diode Characteristics	21
4.2	Expansion About the Operating Point	22
4.3	Basic Oscillator Circuit	24
5.1	Describing Function Curves	36
5.2	Graphical Interpretation of Theorem 5.1	40
5.3	Constant-G_{eq} Chart	42
5.4	Graphical Interpretation of Theorem 5.3	46
5.5	Basic Properties of the Constant-G_{eq} Chart	47
5.6	Biasing Curves	49
5.7	Biasing Curves and Load-Lines	51
5.8	Constant-G_{eq} Chart and Loci	52
5.9	Comparative Linear System	54
5.10	Differential Displacement from a Solution	56

Figure No.	Title	Page
5.11	Determination of Stability	57
5.12	Equivalent Circuit for a Real Tunnel Diode	63
5.13	Derivation of the Modified D.C. Characteritic	64
5.14	Modified D.C. Characteristic	66
5.15	An Oscillator Using a Real Tunnel Diode	67
6.1	Mutually Coupled Tank Circuits	69
6.2	Equivalent Circuits	72
6.3	Equivalent Circuit for Mutually Coupled Tank Circuits	75
6.4	Approximate Form of $F(u^2,K^2)$	84
6.5	Graph of $F(u^2,K^2)$	85
6.6	Approximate Form of $F(u^2,K^2)$ for Very Small K^2	86
6.7	Resonant Frequency Loci	88
6.8	Approximate Form of R_o'/R_o and its Relationship to $F(u^2,K^2)$	95
6.9	Graph of R_o'/R_o	98
6.10	Approximate Resonant Resistance Loci	99
6.11	Resonant Frequency Loci	101
6.12	Resonant Resistance Loci	102
6.13	Constant-G_{eq} Chart and Locus	104
6.14	Resonant Frequency and Resonant Resistance Loci	104
7.1	Block Diagram of Computer Simulation	114
7.2	Portions of Diode Characteristic Covered During Steady-State Oscillation	117

Figure No.	Title	Page
7.3	Typical Solutions	119
7.4	Waveforms Using an Infinite-Q Tank Circuit	122
7.5	Waveforms Using a Tank Circuit with a Q of 10	125
7.6	Waveforms Using a Tank Circuit with a Q of 20	126
7.7	Transient Response of Mutually Coupled Circuits to a Current Step	130
7.8	Voltage Waveforms with Mutually Coupled Tank Circuits	131
7.9	Continuous Solution with Increasing Coupling	132
7.10	Continuous Solution with Decreasing Coupling	133
7.11	Servo-Multiplier Used to Vary Coupling	135
A1.1	Radius of Curvature	139
A1.2	Graphical Representation of $g_1(V_Q)$, $d\rho/dS$, and $g_3(V_Q)$	142
A1.3	Approximation of $f(V)$ by a Cubic Equation	143
A1.4	Graphical Interpretation of the Gradient Vector	147
A1.5	Illustration of Theorem 5.2	151
A1.6	Describing Function Curve Near the Vertical Axis	152
A1.7	Contour Near the Vertical Axis	152
A2.1	Derivation of the Function Generator	155
A2.2	The Function Generator	157
A2.3	Simulation of the Biasing Network	158

Figure No.	Title	Page
A2.4	Signal Flow Graph for Equation A2.6	160
A2.5	Signal Flow Graph for Equation A2.5	160
A2.6	Signal Flow Graph for a Single Tank Circuit	161
A2.7	Computer Schematic for a Single Tank Circuit	161
A2.8	Computer Schematic for an Oscillator Using a Single Tank Circuit	162
A2.9	Circuits with Mutual Coupling	163
A2.10	Block Schematic for Simulation of Mutually Coupled Tank Circuits	165
A2.11	Signal Flow Graph for Equation A2.14	167
A2.12	Signal Flow Graph for Equation A2.13	167
A2.13	Signal Flow Graph for Feedback Portion of Fig. A2.10	168
A2.14	Computer Schematic for Feedback Portion of Fig. A2.10	168
A2.15	Block Schematic for Oscillator with Mutually Coupled Tank Circuits	169
A2.16	Computer Schematic for Oscillator with Mutually Coupled Tank Circuits	170
A2.17	Accurate Adjustment of K^2	171

I. INTRODUCTION

1.1 The Tunnel Diode

In the analysis of any non-linear system, the factors of primary importance are the characteristics of the non-linear device. Thus, only a brief qualitative discussion of the operation of the tunnel diode itself will be presented. A more sophisticated treatment can be found in a variety of literature.

The tunnel diode is a semiconductor device containing a single p-n junction. It differs primarily from the conventional semiconductor diode in that the levels of doping in both the p-type and n-type materials are many times higher. This high concentration of impurities results in an extremely thin depletion region at the junction. For very low values of bias, this depletion region represents an energy barrier which electrons are unable to surmount. However, because of the tunnel effect, whereby a particle may disappear from one side of such a barrier, and appear on the other side without loss of energy, an appreciable current will flow across the junction. As bias is subsequently increased, the tunnelling current increases up to a point, and then decreases to approximately zero. This gives rise to the "negative resistance" region of the tunnel diode. Upon further increase in bias,the electrons are given sufficient energy to surmount the barrier,

and conduction takes place by means of the same mechanism as in an ordinary diode.

1.2 Tunnel Diode Characteristic

The d.c. voltage-current characteristic for a typical tunnel diode is illustrated in Fig. 1.1. The meanings of a number of important parameters are also indicated.

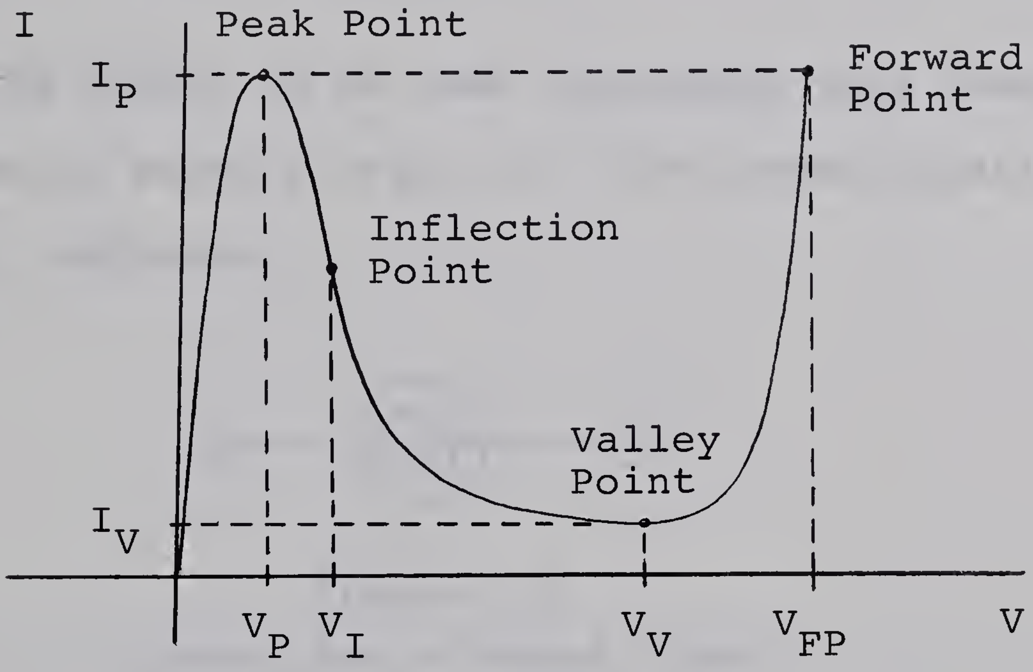

Figure 1.1
Tunnel Diode Characteristic

The functional notation I = f(V) shall be used for a mathematical description of the d.c. characteristic. Within the region between V_p and V_v, where f'(V) is negative, the tunnel diode can be thought of as a small-signal negative resistance. Hence it can be used as a source of a.c. power, and

readily lends itself to amplifier and oscillator applications.

The quantity r_d shall be defined, in the interval $V_p < V < V_v$, by the equation

$$-\frac{1}{r_d} = f'(V) \quad . \tag{1.1}$$

Also, the quantity $-G_d$ shall be defined as the minimum value of $f'(V)$, or

$$-G_d = f'(V_I) \quad . \tag{1.2}$$

The symbol to be used throughout this thesis for a tunnel diode is shown in Fig. 1.2. The normal biasing polarity is also indicated.

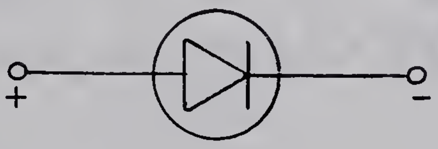

Figure 1.2
Symbol for a Tunnel Diode

1.3 Parasitic Elements

Any tunnel diode, when used in conjunction with external circuitry, will have associated with it parasitic circuit elements, R_s, L_s, and C_s, where:

R_s represents a series resistance due to the bulk material of the diode and associated wiring;

L_s represents a series inductance mainly due to the wiring; and

C_s represents a shunt capacitance depending on the junction, the package, and the wiring.

If an "ideal" tunnel diode is now defined as a device which produces only the d.c. characteristic, $I = f(V)$, the parasitic elements can be lumped and connected externally to this ideal diode. The resulting network can be used as the equivalent circuit for a "real" tunnel diode. This is shown in Fig. 1.3.

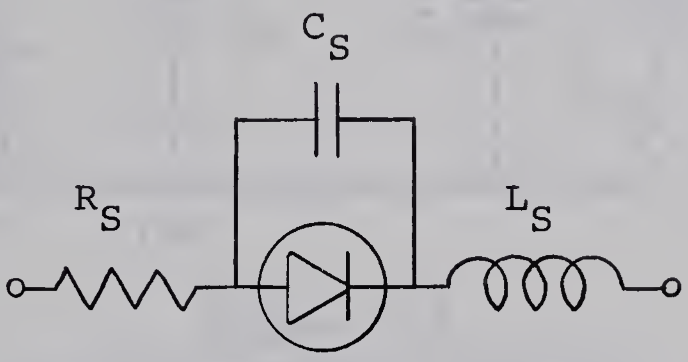

Figure 1.3
Equivalent Circuit for a Real Tunnel Diode

Note that since the series resistance associated with the tunnel diode itself will be included in determining the d.c. characteristic, R_S, as indicated in Fig. 1.3, represents only the series resistance external to the actual diode.

In the analysis of the tunnel diode oscillator, the parasitic elements have first been neglected, and their possible consequence are later considered in Sec. 5.10.

1.4 Basic Oscillator Circuit

Figure 1.4 shows the basic form of oscillator to be analysed in this thesis. The biasing network (V_{BB}, R_{B_1}, R_{B_2}, and C_B) is used to bias the tunnel diode in the "negative resistance" region. It will be assumed that C_B is sufficiently large that its impedance can be neglected at the frequency of oscillation.

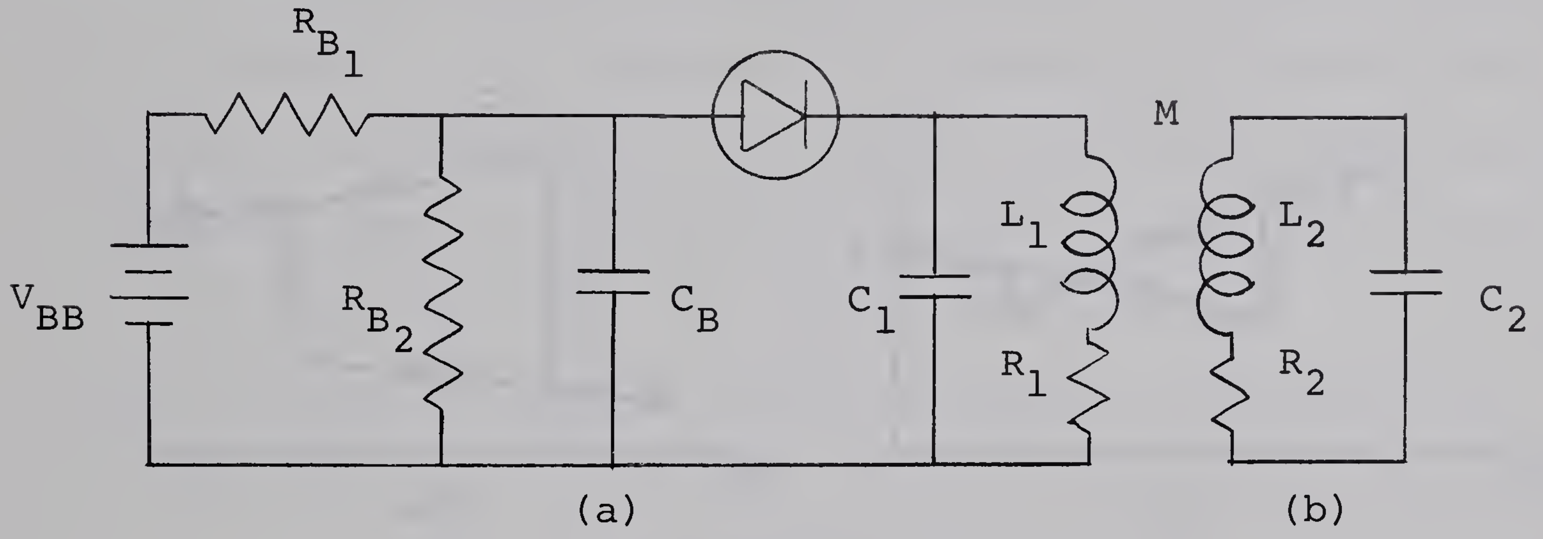

Figure 1.4
Basic Oscillator Circuit

If the secondary tank circuit (Fig. 1.4(a)) is first neglected, the operation of the oscillator can be qualitatively understood by considering the tunnel diode as a source of a.c. energy, which compensates for the energy losses in the primary tank circuit.

When the secondary tank circuit is mutually coupled to the primary, the coefficient of coupling can be defined as

$$K^2 = \frac{M^2}{L_1 L_2} \; ; \tag{1.3}$$

where M is the mutual inductance between L_1 and L_2. Thus, varying the distance between L_1 and L_2 will result in an opposite variation in K^2.

The nature of the switching phenomenon, as discussed in this thesis, is qualitatively illustrated in Fig. 1.5. In Fig. 1.5(a), f refers to the fundamental frequency of oscillation, and in Fig. 1.5(b), A refers to the fundamental amplitude of time-varying voltage across the tunnel diode.

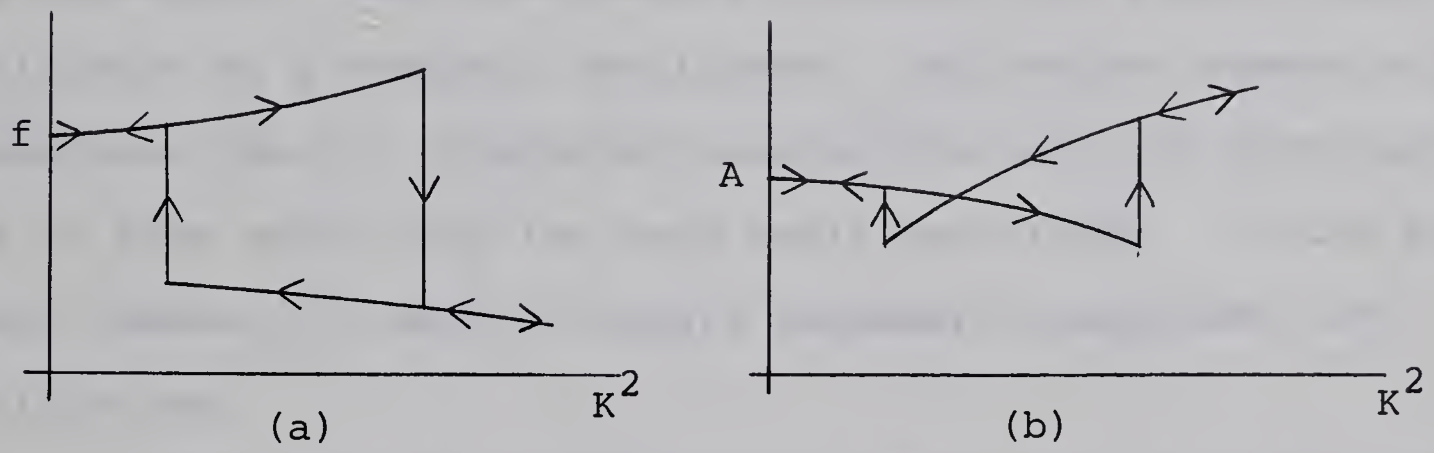

(a) (b)

Figure 1.5
Switching Phenomenon

As can be seen from Fig. 1.5, two distinct modes of oscillation are exhibited, and there are two critical values of K^2 for which the oscillator will switch modes. If K^2 is between these two values, both modes are available, and the mode assumed by the oscillator depends on whether K^2 has recently been increased from a small value or decreased from a large value.

A further experimental observation is that the patterns shown in Fig. 1.5 seem to be exhibited only when the secondary tank circuit has a considerably higher Q and a slightly lower resonant frequency than the primary.

1.5 Methods of Analysis

Two methods of analysis of the oscillator circuit are presented. The first method considers the tunnel diode oscillator as a feedback oscillator. This method essentially linearizes the d.c. characteristic at the point of operation, and is thus valid only for very small amplitudes. It can be used, however, to derive certain necessary conditions for oscillation.

The second method, which is much more fruitful than the first, is essentially the describing-function method. The basic assumption of this method is that time-varying voltage across the tunnel diode is purely sinusoidal. The essential differences between this method and the conventional describing-function method, are that (1) the describing-function equation is a function of both amplitude and operating point, and (2) the shift in operating point due to a change in amplitude is considered.

II. FEEDBACK OSCILLATOR MODEL

2.1 Equivalent Biasing Network

If the d.c. bias voltage, V_{BB}, in Fig. 1.4(a), is applied suddenly at some instant, it can be considered as a voltage step, which has the Laplace Transform V_{BB}/S. The biasing network can thus be represented as shown in Fig.2.1(a).

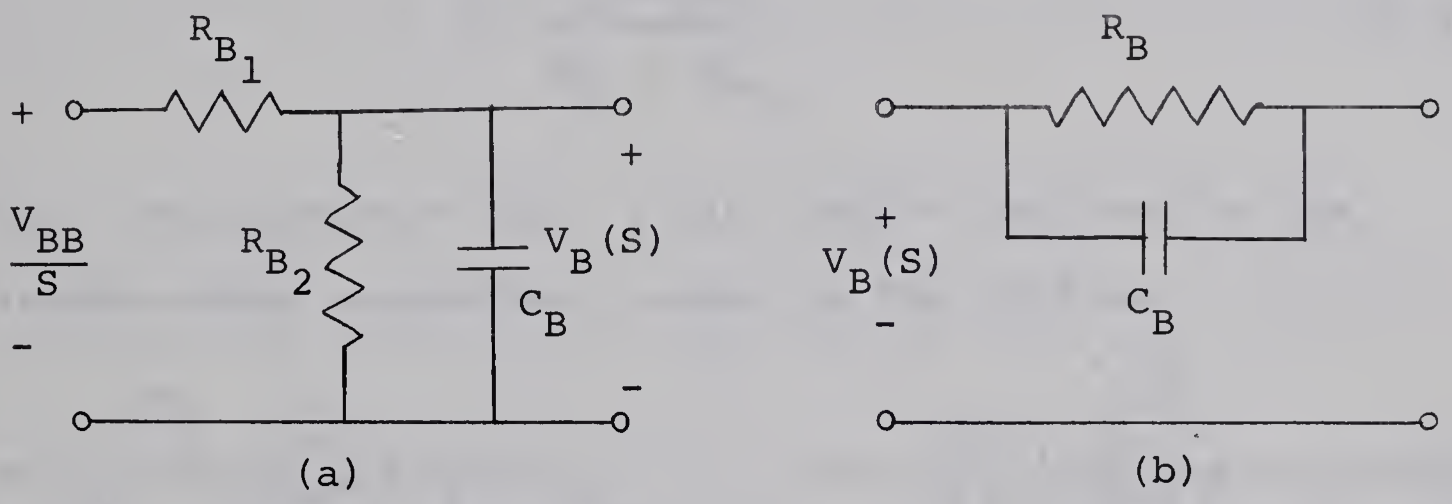

Figure 2.1
Equivalent Biasing Network

Application of Thevenin's Theorem now results in the equivalent circuit shown in Fig. 2.1(b), if

$$R_B = \frac{R_{B_1} R_{B_2}}{R_{B_1} + R_{B_2}} \tag{2.1}$$

Simple analysis shows that

$$V_B(S) = \frac{V_{BB}\ R_{B_2}}{S(R_{B_1} + R_{B_2} + SC_B R_{B_1} R_{B_2})} \tag{2.2}$$

If the analysis is now confined to steady-state conditions, $V_B(S)$ in Fig. 2.1(b), can be replaced by its steady-state value. Using the Final Value Theorem of Laplace Transforms,

$$V_B = \lim_{t\to\infty} V_B(t) = \lim_{S\to 0} SV_B(S)$$
$$= \frac{V_{BB}R_{B_2}}{R_{B_1} + R_{B_2}} \tag{2.3}$$

Thus, the circuit of Fig. 1.4(a) can be replaced by its "steady-state" equivalent, shown in Fig. 2.2(a).

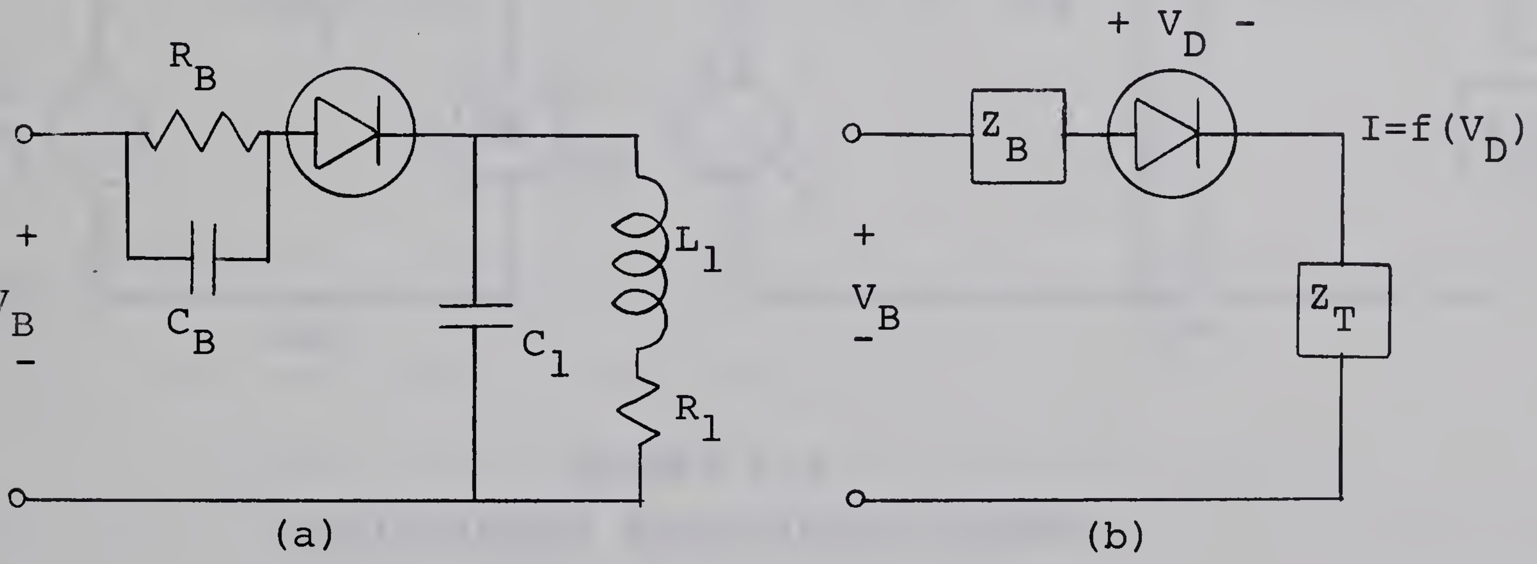

(a) (b)

Figure 2.2
Steady-State Equivalent Circuits

The circuit of Fig. 2.2(a) can in turn be represented by Fig. 2.2(b), if Z_T represents the tank circuit impedance, and Z_B the biasing network impedance.

2.2 Small Signal Equivalent Circuit

For very small signals about some operating point, the tunnel diode can be approximated by a linear negative resistance, $-r_d$. Furthermore, it has already been assumed that at all frequencies of interest, $Z_B = 0$. Thus, assuming that all d.c. currents and voltages remain constant, the circuit of Fig. 2.2(b) can be replaced by its small signal equivalent, shown in Fig. 2.3(a).

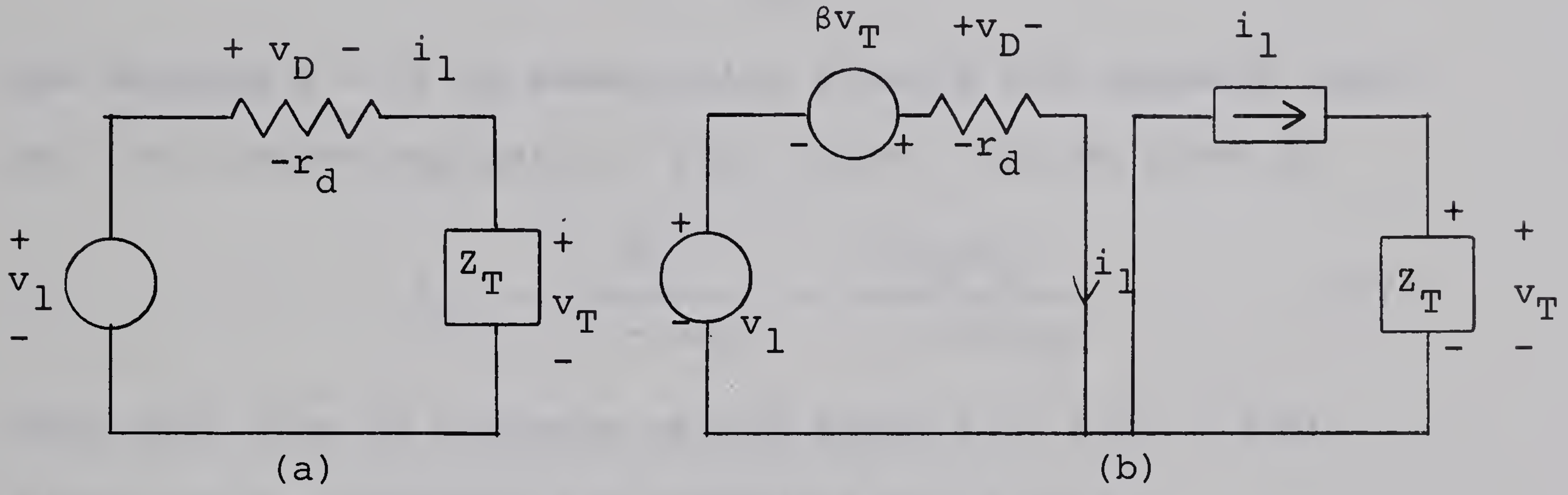

Figure 2.3
Small-Signal Equivalent Circuits

Note that for generality, an external signal, v_1, has been added.

Two equations can be written for the circuit of Fig. 2.3(a):

$$v_1 = i_1 Z_T + v_D \ ; \quad \text{and} \tag{2.4}$$

$$i_1 = \frac{v_D}{-r_d} \tag{2.5}$$

Referring now to Fig. 2.3(b), if $\beta = -1$, the same two equations apply, so that this circuit will be identical to that of Fig. 2.3(a).

The circuit of Fig. 2.3(b) is easily recognized as a feedback amplifier, with a feedback factor β, and an open-loop gain $A_v = \left.\frac{v_T}{v_1}\right|_{\beta=0}$. For $\beta = 0$, $i_1 = \frac{v_1}{-r_d}$ and $v_T = i_1 Z_T$. Hence,

$$A_v = -\frac{Z_T}{r_d} \tag{2.6}$$

Now setting $\beta = -1$ is essentially closing the feedback loop, and the closed-loop gain of Fig. 2.3(b) will be given by

$$A_f = \frac{A_v}{1 - \beta A_v} = \frac{-Z_T/r_d}{1 - Z_T/r_d} \tag{2.7}$$

This must also be the gain of the circuit in Fig. 2.3(a), since the two circuits are identical for $\beta = -1$.

Since for oscillation of a feedback amplifier, $\beta A_v = 1$, it follows that the circuit shown in Fig. 2.3(a) will oscillate if $Z_T/r_d = 1$, or

$$Z_T = r_d \tag{2.8}$$

If ω_o is now defined such that $\text{Im}\left[Z_T(j\omega_o)\right] = 0$, and R_o is defined as $R_o = Z_T(j\omega_o)$, Eq. 2.8 implies that oscillation of frequency ω_o will occur if

$$R_o = r_d \tag{2.9}$$

Note that if R_o is greater than r_d, the open-loop gain will be greater than one, and upon closing the loop, oscillations will build up until some form of limiting occurs. This is what normally occurs in a tunnel diode oscillator.

III. PROPERTIES OF THE PARALLEL RESONANT CIRCUIT

3.1 Resonance

Since the oscillator can be expected to oscillate with frequency ω_o, such that $Z_T(j\omega_o) = R_o$, this frequency shall be referred to as the resonant frequency of the tank circuit. Similarly, R_o shall be referred to as the resonant resistance. Note that for this circuit, ω_o does not correspond to an extremum of $|Z_T(j\omega)|$.

The impedance of the primary tank circuit can be expressed in terms of S as

$$Z_T(S) = \frac{R_1 + SL_1}{S^2L_1C_1 + SC_1R_1 + 1} ; \qquad (3.1)$$

or in terms of $j\omega$ as

$$Z_T(j\omega) = \frac{R_1 + j\omega L_1}{(1 - \omega^2L_1C_1) + j\omega C_1R_1} . \qquad (3.2)$$

Setting $\mathrm{Im}\left[Z_T(j\omega_o)\right] = 0$, it can easily be shown that

$$\omega_o = \sqrt{\frac{1}{L_1C_1} - \frac{R_1^2}{L_1^2}} . \qquad (3.3)$$

Substituting (3.3) into (3.2);

$$R_o = \frac{L_1}{R_1C_1} . \qquad (3.4)$$

3.2 Frequency-Normalized Impedance

Normalized frequency, u, shall be defined such that

$$u^2 = \omega^2 L_1 C_1 \tag{3.5}$$

The tank circuit impedance can now be expressed in terms of ju as

$$Z_T(ju) = \frac{R_1(1 + j\frac{u}{R_1}\sqrt{L_1/C_1})}{(1 - u^2) + ju\,R_1\sqrt{C_1/L_1}} \; . \tag{3.6}$$

If Q_1 is defined as

$$Q_1 = \frac{1}{R_1}\sqrt{\frac{L_1}{C_1}} \quad , \tag{3.7}$$

Eq. (3.6) can be rewritten as

$$Z_T(ju) = \frac{R_1(1 + jQ_1u)}{(1 - u^2) + j\frac{u}{Q_1}} \; . \tag{3.8}$$

With the above definition of Q_1 in mind, (3.3) can be rewritten as

$$\omega_o = \frac{1}{\sqrt{L_1C_1}}\sqrt{1 - \frac{1}{Q_1{}^2}} \tag{3.9}$$

from which the normalized resonant frequency will be

$$u_o = \sqrt{1 - \frac{1}{Q_1{}^2}} \tag{3.10}$$

Thus, if $Q_1^2 >> 1$, $\omega_o \simeq \frac{1}{\sqrt{L_1 C_1}}$, and $u_o \simeq 1$.

3.3 Frequency Response Above Resonance

Equation 3.8 can be used to determine approximately the impedance to any harmonic of the resonant frequency. The square of the magnitude of (3.8) will be given by:

$$|Z_T(ju)|^2 = \frac{R_1^2(1 + Q_1^2 u^2)}{(1 - u^2)^2 + \frac{u^2}{Q_1^2}} \tag{3.11}$$

If it is assumed that $Q_1^2 >> 1$, $u_o \simeq 1$. Thus, for the n^{th} harmonic above resonance, $u \simeq n$. Since $n \geq 2$, $u \gtrsim 2$, and thus $Q_1^2 u^2 >> 1$. Also, $(1 - u^2)^2 >> \frac{u^2}{Q_1^2}$. Hence,

$$|Z_T(jnu_o)|^2 \simeq |Z_T(jn)|^2 \simeq \frac{R_1^2 Q_1^2 n^2}{(n^2-1)^2} = \frac{L_1}{C_1} \frac{n^2}{(n^2 - 1)^2} \text{; or}$$

$$|Z_T(jn)| \simeq \sqrt{\frac{L_1}{C_1}} \frac{n}{(n^2 - 1)} \text{ .} \tag{3.12}$$

Thus, the magnitude of impedance to the n^{th} harmonic above resonance is nearly independent of R_1 (if Q_1 is high), and depends almost directly on $\sqrt{L_1/C_1}$. The significance of this will be seen later.

Also the ratio of the magnitude of the impedance to the n^{th} harmonic to the impedance at resonance can be found;

or

$$\frac{|Z(jnu_o)|}{|Z(ju_o)|} \simeq \frac{|Z(jn)|}{R_o} \simeq \sqrt{\frac{L_1}{C_1}}\ \frac{n}{(n^2 - 1)R_o} .$$

But $\frac{1}{R_o}\sqrt{\frac{L_1}{C_1}} = \frac{1}{Q_1}$; so that

$$\frac{|Z(jnu_o)|}{|Z(ju_o)|} \simeq \frac{n}{(n^2-1)Q_1} \tag{3.13}$$

3.4 Bode Plot

An approximate Bode Plot of $|Z_T(ju)|$ will now be derived. This is shown in Fig. 3.1. Note that absolute magnitudes of impedance (in db) are used, so that $|Z_T(ju)| = 1$ corresponds to 0 - db. Equation 3.11 can be used to determine the as~~s~~ymptotes, critical frequencies, and magnitudes. The following steps are required to derive the Bode Plot:

(1) If $u^2 << 1$, $|Z_T(ju)|^2 \simeq R_1{}^2(1 + Q_1{}^2u^2)$. This has a corner frequency at $u = 1/Q_1$.

For $u < 1/Q_1$, the as~~s~~ymptote is a horizontal line of ordinate value $20 \log_{10} R_1$.

For $u^2 > 1/Q_1$, the as~~s~~ymptote will be determined by the equation $|Z_T(ju)| \simeq R_1Q_1u = u\sqrt{L_1/C_1}$. This as~~s~~ymptote will have a slope of +20db/decade, and will intersect the 0 - db line when $u\sqrt{L_1/C_1} = 1$, or $u = \sqrt{C_1/L_1}$.

(2) If $u^2 >> 1$, $|Z_T(ju)| \simeq \frac{R_1Q_1}{u} = \frac{1}{u}\sqrt{L_1/C_1}$. The corresponding as~~s~~ymptote will have a slope of -20db/decade, and will intersect the 0 - db line at $u = \sqrt{L_1/C_1}$.

(3) The as~~s~~ymptotes having positive and negative slopes will intersect where $u\sqrt{L_1/C_1} = \frac{1}{u}\sqrt{L_1/C_1}$, or $u = 1$. At this point the ordinate value (on either as~~s~~ymptote) will be $20 \log_{10} \sqrt{L_1/C_1} = 10 \log_{10} L_1/C_1$.

(4) At $u = 1$, $|Z_T(ju)| \simeq R_1Q_1^{\,2} = R_o$. Thus the ordinate value of the actual curve, at $u = 1$, will be approximately $20 \log_{10} R_o = 20 \log_{10} L_1/R_1C_1$. The approximate Bode Plot can now be sketched.

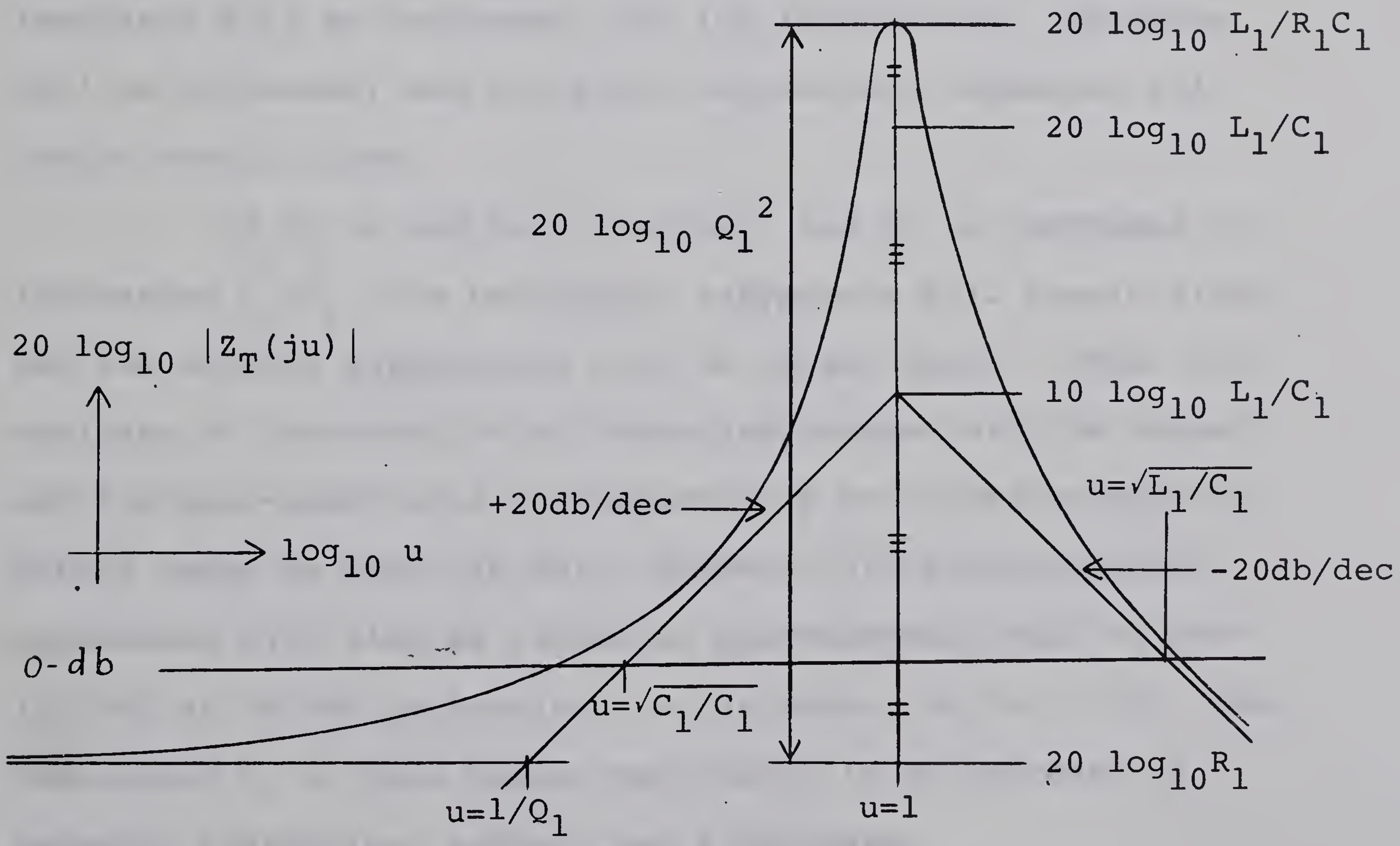

Figure 3.1
Approximate Bode Plot

Figure 3.1 can be used to study the effect of varying the circuit components. It is first noticed that the only two separate factors appearing in the derivation of the Bode Plot are R_1 and (L_1/C_1). (i.e. $Q_1 = \frac{1}{R_1}\sqrt{L_1/C_1}$, and $R_o = \frac{1}{R_1}(L_1/C_1)$.)

If it is desired to increase Q_1, this can be done by either decreasing R_1 or increasing (L_1/C_1). If R_1 is first decreased, it is apparent from Fig. 3.1 that the horizontal as~~s~~ymptote will be shifted downward, but the two sloping as~~s~~ymptotes will remain fixed. Furthermore, the peak-point will be shifted upward. Thus, near the resonant frequency, impedance will be increased; for low frequencies, impedance will be decreased; and for high frequencies, impedance will remain nearly fixed.

If R_1 is now held constant, and Q_1 is increased by increasing L_1/C_1, the horizontal as~~s~~ymptote will remain fixed, and the sloping as~~s~~ymptotes will be spread apart. Thus, the ordinate of intersection of these as~~s~~ymptotes will be raised, and the peak-point will correspondingly be raised by approximately twice as much (in db). However, all high-frequency impedances will also be raised by approximately half as much (in db) as is the peak-point. It is shown, in Sec. 5.11, that increasing Q_1 in this manner may result in an increase in harmonic distortion, rather than a decrease.

IV. DESCRIBING-FUNCTION METHOD

4.1 Quantitative Description of the D.C. Characteristic

The analysis to follow is numerically based on a 1N2940 Germanian tunnel diode. Table 4.1 lists the typical parameters for this diode. These values have been taken from the first edition of the "General Electric Tunnel Diode Manual". (Ref.3)

Table 4.1

Typical Parameters

I_p	1.00	ma
I_v	0.13	ma
V_p	60.0	mv
V_v	350.0	mv
V_{fp}	500.0	mv
G_d	6.60	mmho

Before beginning any sort of numerical analysis, a mathematical description of the curve I = f(V) must be found. Such a curve can be approximated by a K^{th} order polynomial in V, where the value of K as chosen depends on the degree of accuracy required.

i.e.

$$I = f(V) = \sum_{n=1}^{K} h_n V^n \qquad (4.1)$$

In this case, K has been chosen to be ten. The d.c. characteristic for a 1N2940 tunnel diode has been obtained graphically, using an analogue computer*, and is shown in Fig. 4.1 (a).

If ten points (V_n, I_n), excluding the origin, are chosen on the d.c. characteristic, ten simultaneous equations in h_n can be written.
i.e.

$$\begin{aligned} I_1 &= h_1V_1 + h_2V_1^2 + \ldots + h_{10}V_1^{10} \\ &\vdots \\ I_{10} &= h_1V_{10} + h_2V_{10}^2 + \ldots + h_{10}V_{10}^{10} \end{aligned} \tag{4.2}$$

This was done for the ten points indicated in Fig. 4.1(a), and Eq. 4.2 were then solved by means of a digital computer. The resulting ten coefficients are listed in Table 4.2

Table 4.2

Characteristic Coefficients

$h_1 = +0.34887421 \times 10^{-1}$ A/V
$h_2 = -0.42478878$ A/V^2
$h_3 = +0.30580876 \times 10$ A/V^3
$h_4 = -0.30233254 \times 10^2$ A/V^4
$h_5 = +0.26704247 \times 10^3$ A/V^5
$h_6 = -0.14331515 \times 10^4$ A/V^6
$h_7 = +0.45227742 \times 10^4$ A/V^7
$h_8 = -0.83121280 \times 10^4$ A/V^8
$h_9 = +0.82619199 \times 10^4$ A/V^9
$h_{10} = -0.34370567 \times 10^4$ A/V^{10}

---

* Analogue computer simulation is discussed in AII.

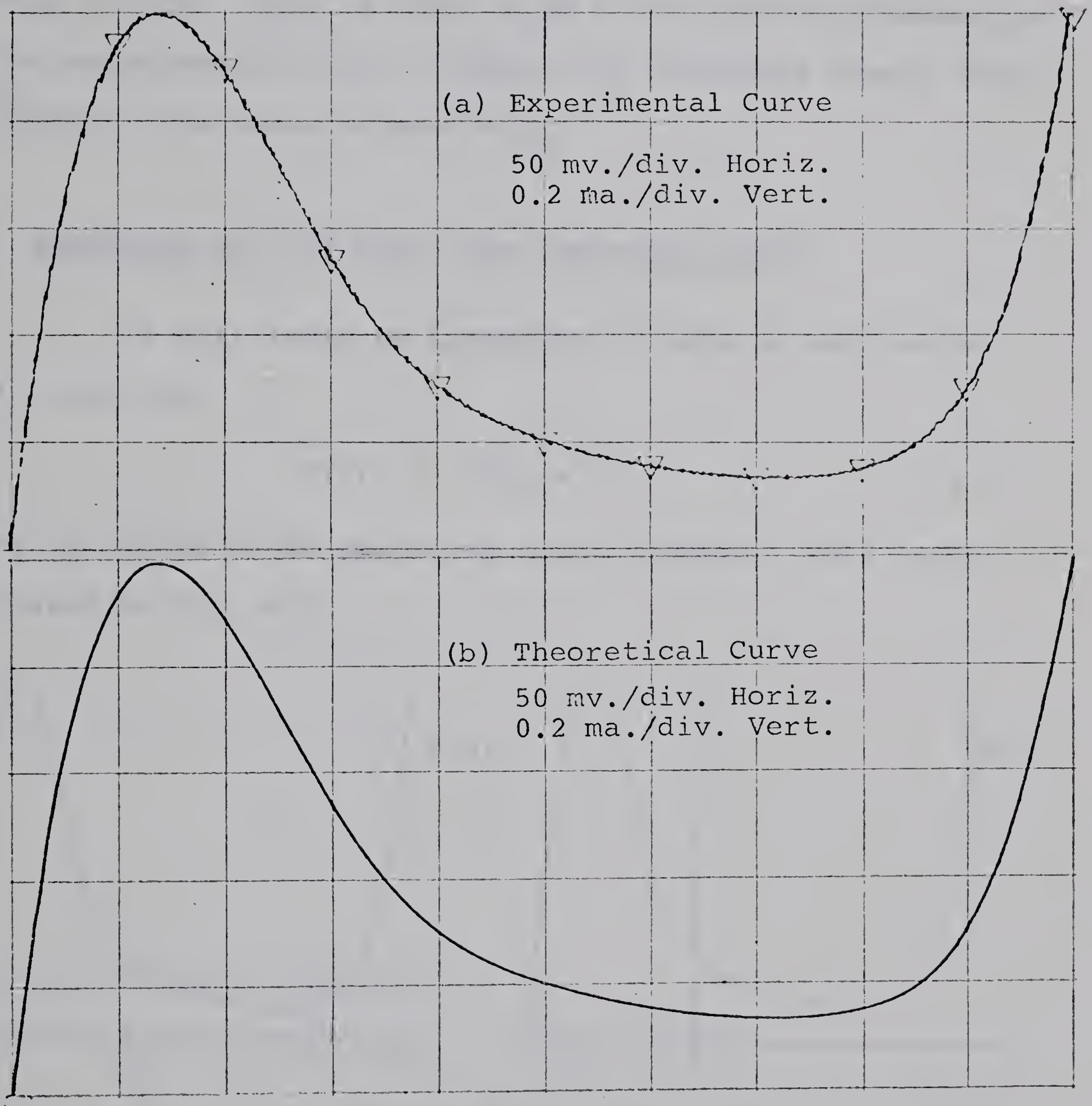

Figure 4.1
Tunnel Diode Characteristics

Using these ten coefficients, the approximate function, (4.1), was evaluated by computer, and the resulting curve is shown in Fig. 4.1(b). This is seen to be a very good approximation to the experimental curve. Hence, all following theory shall be based on the above values of h_n.

4.2 Expansion of f(V) About the Operating Point

It will later be necessary to have an expression, W(V), such that

$$W(V) = f(V_Q + V) ; \qquad (4.3)$$

where V_Q refers to an operating point voltage. This is illustrated in Fig. 4.2

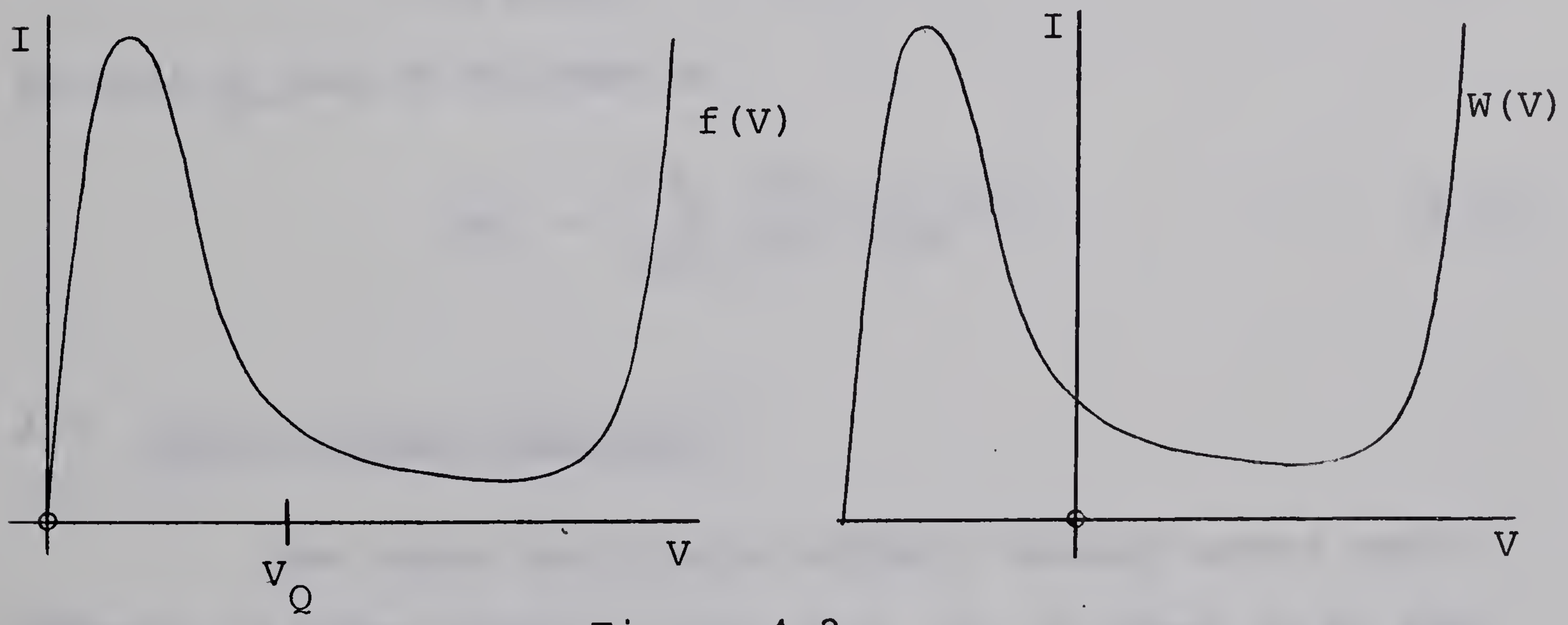

Figure 4.2
Expansion About the Operating Point

Since $f(V) = \sum_{n=1}^{K} h_n V^n$, it follows that

$$W(V) = \sum_{n=0}^{K} g_n V^n \tag{4.4}$$

where

$$g_n = \frac{f^{(n)}(V_Q)}{n!} = g_n(V_Q) \tag{4.5}$$

But $$f^{(n)}(V_Q) = \sum_{i=n}^{K} \frac{i!}{(i-n)!} h_i V_Q^{\,i-n} \tag{4.6}$$

Thus $$g_n = \sum_{i=n}^{K} \frac{i!}{n!(i-n)!} h_i V_Q^{\,i-n} \tag{4.7}$$

Also, by definition,

$$\frac{i!}{n!(i-n)!} = \binom{i}{n}, \tag{4.8}$$

so that g_n can be written as

$$g_n = \sum_{i=n}^{K} \binom{i}{n} h_i V_Q^{\,i-n} \tag{4.9}$$

4.3 Basic Circuit Equations

The basic oscillator circuit (steady-state equivalent) is shown again in Fig. 4.3. Z_T is taken to be the impedance of the primary tank circuit, and Z_B as the equivalent biasing network (Fig. 2.2).

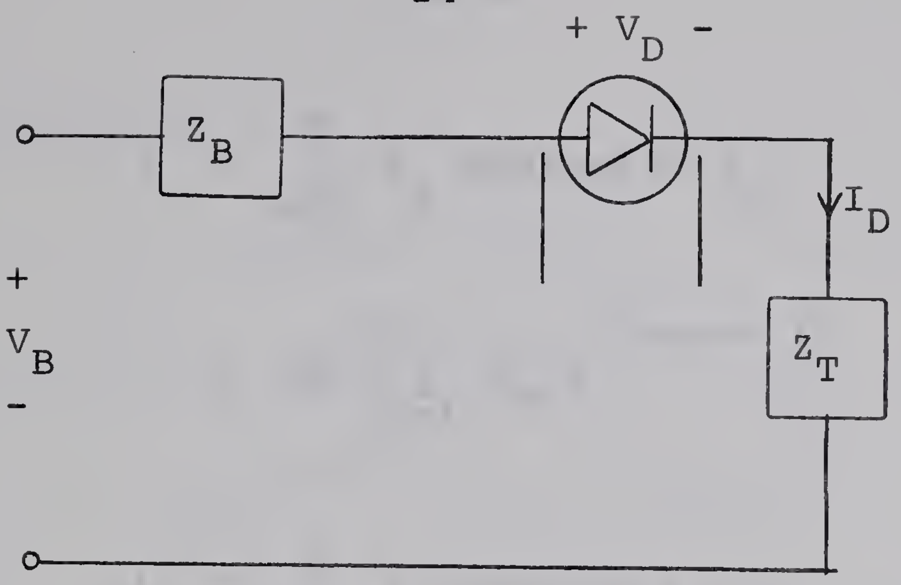

Figure 4.3
Basic Oscillator Circuit

Note that V_D and I_D denote total instantaneous values of voltage and current, and V_B is a fixed d.c. voltage. If it can be assumed that all voltages and currents are Laplace Transformable, two basic equations can be written for the circuit:

$$V_B(S) = V_D(S) + I_D(S)\left[Z_B(S) + Z_T(S)\right] \quad (4.10)$$

and

$$I_D = f(V_D) \quad (4.11)$$

Now, let

$$V_D = V_Q + v \quad (4.12)$$

and

$$I_D = I_Q + i \quad (4.13)$$

where v and i are time-dependent.

Since the circuit is known to oscillate in some manner, it can be assumed that:

$$v = \sum_{n=1}^{\infty} A_n \sin(n\omega t + \theta_n)$$

$$= \text{Im}\left[\sum_{n=1}^{\infty} A_n e^{j(n\omega t+\theta_n)}\right] \tag{4.14}$$

and

$$i = \sum_{n=1}^{\infty} I_n \sin(n\omega t + \phi_n)$$

$$= \text{Im}\left[\sum_{n=1}^{\infty} I_n e^{j(n\omega t+\phi_n)}\right] \tag{4.15}$$

For d.c., $Z_B = R_B$ and $Z_T = R_1$; and for a.c., $Z_B = 0$ and $Z_T = Z_T(jn\omega)$.

Upon substitution of the above expressions into (4.10), and letting $S = jn\omega$:

$$V_B = V_Q + \text{Im}\left[\sum_{n=1}^{\infty} A_n e^{j(n\omega t+\theta_n)}\right] + I_Q(R_B + R_1)$$

$$+ \text{Im}\left[\sum_{n=1}^{\infty} I_n e^{j(n\omega t+\phi_n)} Z_T(jn\omega)\right] \tag{4.16}$$

From this, it is seen that:

$$V_B = V_Q + I_Q(R_1 + R_B) \tag{4.17}$$

and

$$A_n e^{j\theta_n} = -I_n e^{j\phi_n} Z_T(jn\omega) \tag{4.18}$$

If the impedance of the tank circuit is sufficiently low for all harmonics of the frequency of oscillations, it

can be assumed that

$$Z_T(jn\omega) = 0 \; ; \qquad n \neq 1.$$

Then, from (4.18), it follows that

$$A_1 e^{j\theta_1} = -I_1 e^{j\phi_1} Z_T(j\omega) \; ; \tag{4.19}$$

and $A_n = 0$; $n \neq 1$. Thus, all voltage harmonics are neglected, and the analysis is confined to sinusoidal or near-sinusoidal oscillation.

For convenience, θ_1 can now be chosen as zero, and I_1 and A_1 can be denoted simply by I and A. Eq. 4.19 can thus be rewritten as

$$\frac{I}{A} = - \frac{1}{Z_T(j\omega)e^{j\phi}} \; ; \tag{4.20}$$

where ϕ now represents the phase angle between the fundamental of current and the fundamental of voltage.

It will later be seen that in neglecting all voltage harmonics, ϕ must be zero. Hence, from (4.20), $Z_T(j\omega)$ must be real, or

$$\omega = \omega_o \, , \qquad \text{and} \qquad Z_T(j\omega) = R_o \tag{4.21}$$

This is identical to the result derived from the "Feedback Oscillator Model".

Equation 4.20 can now be rewritten as

$$\frac{I}{A} = - \frac{1}{R_o} \; ; \qquad \text{and} \tag{4.22}$$

(4.17 can be rewritten as

$$I_Q = \frac{V_B - V_Q}{R_B + R_1} \tag{4.23}$$

Equations 4.22 and 4.23 are the two equations that must be simultaneously satisfied for steady-state sinusoidal oscillation.

4.4 Describing Function and Biasing Equations

Since $I_D = I_Q + i$, and $V_D = V_Q + v$, (4.11) can be rewritten as

$$(I_Q + i) = f(V_Q + v) \tag{4.24}$$

But, from (4.3), $f(V_Q + v) = W(v)$, so that

$$(I_Q + i) = W(v) = \sum_{n=0}^{K} g_n v^n \tag{4.25}$$

Now, since $v = A \sin \omega t$, and $i = I \sin \omega t$ + (Higher Harmonics), it follows that:

$$I_Q + I \sin \omega t + \text{(Higher Harmonics)}$$
$$= \sum_{n=0}^{K} g_n A^n \sin^n \omega t \; ; \tag{4.26}$$

from which:

I_Q = the d.c. component of $\sum_{n=0}^{K} g_n A^n \sin^n \omega t$, and

I = the fundamental component of $\sum_{n=0}^{K} g_n A^n \sin^n \omega t$.

The following formula is useful for the expansion of $\sin^n \omega t$. If n is odd,

$$\sin^n \omega t = \frac{(-1)^{(n-1)/2}}{2^{n-1}} \sum_{r=0}^{\frac{n-1}{2}} (-1)^r \binom{n}{r} \sin(n-2r)\omega t \quad (4.27)$$

Since 2r is even, and n is odd, n-2r must be odd. Thus, $\sin^n \omega t$ is of the form:

$$\sin^n \omega t = a_1(n) \sin \omega t + a_3(n) \sin 3\omega t + \ldots + a_n(n) \sin n\omega t. \quad (4.28)$$

Equation 4.28 indicates that if n is odd, $\sin^n \omega t$ has only a fundamental component and odd harmonics.

If n is even, n-1 will be odd, and n can be replaced by n-1 in (4.27). Hence,

$$\sin^{n-1} \omega t = \frac{(-1)^{(n-2)/2}}{2^{n-2}} \sum_{r=0}^{\frac{n-2}{2}} (-1)^r \binom{n-1}{r} \sin(n-1-2r)\omega t.$$

Then, $\sin^n \omega t = \sin^{n-1} \omega t \cdot \sin \omega t$, or

$$\sin^n \omega t = \frac{(-1)^{(n-2)/2}}{2^{n-2}} \sum_{r=0}^{\frac{n-2}{2}} (-1)^r \binom{n-1}{r} \sin(n-1-2r)\omega t \cdot \sin \omega t \quad (4.29)$$

Since n is now even, and 2r is even, n-1-2r must be odd, so that $\sin^n \omega t$ is of the form:

$$\sin^n \omega t = a_o(n) \sin^2 \omega t + a_2(n) \sin \omega t \cdot \sin 3\omega t + \ldots$$

$$+ a_{n-2}(n) \sin \omega t \cdot \sin(n-1)\omega t. \qquad (4.30)$$

This can be rewritten as

$$\sin^n \omega t = a_o(n) \frac{(1 - \cos 2\omega t)}{2} + a_2(n) \frac{(\cos 2\omega t - \cos 4\omega t)}{2}$$

$$+ \ldots + a_{n-2}(n) \frac{[\cos(n-2)\omega t - \cos n\omega t]}{2} \qquad (4.31)$$

Thus, if n is even, $\sin^n \omega t$ has only a d.c. component and even harmonics.

Referring now to Eq's. 4.28 and 4.31 it is apparent that I_Q depends only on the even coefficients g_n, and the even powers of $A^n \sin^n \omega t$; and that I depends only on the odd coefficients g_n and the odd powers of $A^n \sin^n \omega t$.

First consider the fundamental component of current, I, as given by (4.26). The general term in the expansion for $(I_Q + i)$ is $g_n A^n \sin^n \omega t$. The fundamental component due to this term (for odd values of n) will be $g_n A^n a_1(n)$, where $a_1(n)$ is the coefficient of $\sin \omega t$ in Eq. 4.27. i.e. $a_1(n) = \frac{(-1)^{(n-1)/2}}{2^{n-1}} (-1)^r \binom{n}{r}$; where $r = \frac{n-1}{2}$. Substituting $n = 2r + 1$ into the expression for $a_1(n)$;

$$a_1(r) = \frac{1}{2^{2r}} \binom{2r+1}{r} . \qquad (4.32)$$

Also, $g_n A^n \sin^n \omega t$ can be expressed as $g_{2r+1} A^{2r+1} \sin \omega t$, and the fundamental component due to this term will be

$$g_{2r+1}\ A^{2r+1}\ a_1(r) \ = \ g_{2r+1}\ A^{2r+1}\ \frac{1}{2^{2r}} \binom{2r+1}{r} \tag{4.33}$$

The smallest odd value of n is one, for which 2r+1 = 1, or r = 0. Also, if K is even, the largest odd value of n is K-1, for which 2r+1 = K-1, or r = (K-2)/2. Thus, the total fundamental component of current will be given by the equation

$$I \ = \ \sum_{r=0}^{\frac{K-2}{2}} g_{2r+1}\ A^{2r+1} \left(\frac{1}{2}\right)^{2r} \binom{2r+1}{r} \tag{4.34}$$

Dividing both sides by A;

$$\frac{I}{A} \ = \ \sum_{r=0}^{\frac{K-2}{2}} g_{2r+1} \left(\frac{A}{2}\right)^{2r} \binom{2r+1}{r} \tag{4.35}$$

Equation 4.35 is essentially a describing-function equation, as it relates the amplitude of the fundamental component of the output of a non-linear device to the amplitude of an applied sinusoidal input.

Recalling that $g_n = \sum_{i=n}^{K} \binom{i}{n} h_i V_Q^{i-n}$, it is apparent that (4.35) is a function of both A and V_Q. Furthermore, as the ratio I/A has dimensions of conductance, the summation shall be defined as

$$G_{eq}(A,V_Q) \tag{4.36}$$

Equation 4.22 can now be written as

$$G_{eq}(A,V_Q) = -\frac{1}{R_o} \tag{4.37}$$

The d.c. component of current, I_Q, must now be found. From Eq. 4.31, the d.c. component of the general term, $g_n A^n \sin^n \omega t$ (for even values of n) will be $g_n A^n \frac{a_o(n)}{2}$; where $a_o(n)$ is the coefficient of $\sin^2 \omega t$ in (4.29). i.e.

$a_o(n) = \frac{(-1)^{(n-2)/2}}{2^{n-2}} (-1)^r \binom{n-1}{r}$, where $r = \frac{n-2}{2}$. Substituting $n = 2r+2$ into the above expression,

$$a_o(r) = \frac{1}{2^{2r}} \binom{2r+1}{r}. \tag{4.38}$$

Since $n = 2r+2$, $g_n A^n \sin^n \omega t$ can be written as $g_{2r+2} A^{2r+2} \sin^{2r+2} \omega t$, and the d.c. component due to this term will be

$$g_{2r+2} A^{2r+2} \frac{a_o(r)}{2} = g_{2r+2} A^{2r+2} \left(\frac{1}{2}\right)^{2r+1} \binom{2r+1}{r} \tag{4.39}$$

The smallest even value of n in the expansion of $(I_Q + i)$ is zero. This corresponds to $r = -1$. But if $r = -1$, $2r+1 = -1$, and the expression $\binom{-1}{-1}$ is meaningless. By inspection of Eq. 4.25, it is seen, however, that the term corresponding to $n = 0$ is simply g_o, which is certainly a d.c. component. i.e.

$$g_o = \sum_{i=0}^{K} \binom{i}{0} h_i V_Q^{\,i} = \sum_{i=1}^{K} h_i V_Q^{\,i} = f(V_Q).$$

The next smallest even value of n is two, for which $r = 0$. This is valid, as the expression $\binom{1}{0}$ is meaningful. Again assuming K to be even, the largest even value of n will be K, for which $r = (k-2)/2$. Thus,

$$I_Q = g_o + \sum_{r=0}^{\frac{K-2}{2}} g_{2r+2} \left(\frac{1}{2}\right)^{2r+1} A^{2r+2} \binom{2r+1}{r} \qquad (4.40)$$

As before, g_n is a function of V_Q, so that I_Q is a function of both V_Q and A. The summation in (4.40) shall thus be defined as

$$I_Q \ (A, V_Q) \qquad (4.41)$$

Equation 4.23 can now be written as

$$I_Q(A, V_Q) = \frac{V_B - V_Q}{R_B + R_1} \qquad (4.42)$$

It is shown in Sec. 5.6 that a solution to equation 4.23 (for a specific value of A) determines V_Q and I_Q. Hence, this equation shall be referred to as the "Biasing Equation".

To summarize the results of the preceding pages, for steady-state sinusoidal oscillations, the following two relationships must be satisfied sumultaneously:

$$G_{eq}(A, V_Q) = -\frac{1}{R_o}$$

$$I_Q(A, V_Q) = \frac{V_B - V_Q}{R_B + R_1} \qquad (4.43)$$

Footnote

It was stated without proof in Sec. 4.3 that by neglecting all voltage harmonics, the phase angle between voltage and the fundamental component of current would be zero. This is true because in the expansion of $\sin^n \omega t$, for odd values of n, only sine-terms are present. A phase-shift here would require the presence of cosine-terms of the fundamental frequency.

If harmonic distortion is permitted in the voltage wave-form, it can easily be shown that such a phase shift can occur. For the sake of illustration, it will be sufficient to consider only the second harmonic, and the second term in the expansion of $(I_Q + i)$. i.e.

$$\begin{aligned} g_2 V^2 &= g_2(A_1 \sin \omega t + A_2 \sin 2\omega t)^2 \\ &= g_2(A_1^2 \sin^2 \omega t + 2A_1A_2 \sin \omega t \cdot \sin 2\omega t \\ &\quad + A_2^2 \sin^2 2\omega t). \end{aligned}$$

Now $A_1^2 \sin^2 \omega t$ contains only d.c. and second harmonic, and $A_2^2 \sin^2 2\omega t$ contains only d.c. and fourth harmonic. However, $2A_1A_2 \sin \omega t \sin 2\omega t = A_1A_2(\cos \omega t - \cos 3\omega t)$. Thus, the term $g_2A_1A_2 \cos \omega t$ has been introduced, which is a cosine-term of the fundamental frequency. This must produce a phase-shift between current fundamental and voltage fundamental.

Referring now to Eq. 4.20, ϕ will no longer be zero, so that $Z_T(j\omega)$ will no longer be real; and a shift in frequency from ω_o will occur.

It must be concluded then, that distortion of the voltage wave form, in general, may be accompanied by a departure in frequency from that indicated by the describing-function method.

V. SOLUTION TO DESCRIBING FUNCTION AND BIASING EQUATIONS

5.1 Discussion of $G_{eq}(A,V_Q)$

Because of the complexity of Eq's. 4.43, the most convenient means of finding a simultaneous solution is to develop a graphical method. The initial step shall be a rather detailed discussion of the describing-function, $G_{eq}(A,V_Q)$.

Using the ten coefficients listed in Table 4.2, the describing-function has been evaluated by means of a digital computer. Fig's. 5.1(a) and (b) show some typical curves corresponding to various ranges of V_Q.

A solution to Eq. 4.37 is now determined by the intersection of a horizontal line at $-1/R_o$ with the curve corresponding to the value of V_Q chosen. It can be seen that either one, two, or three such solutions may exist.

The function $G_{eq}(A,V_Q)$ can be expressed as

$$G_{eq}(A,V_Q) = g_1 + \frac{3}{4} g_3 A^2 + \left(\begin{matrix}\text{Higher Powers}\\ \text{of A}\end{matrix}\right) \qquad (5.1)$$

Thus,

$$\lim_{A\to 0} G_{eq}(A,V_Q) = g_1 = f'(V_Q) . \qquad (5.2)$$

Since $f'(V_Q)$ is defined as $-1/rd$, Eq. 4.37 now becomes

$-\frac{1}{rd} = -\frac{1}{R_o}$, or $R_o = rd$.

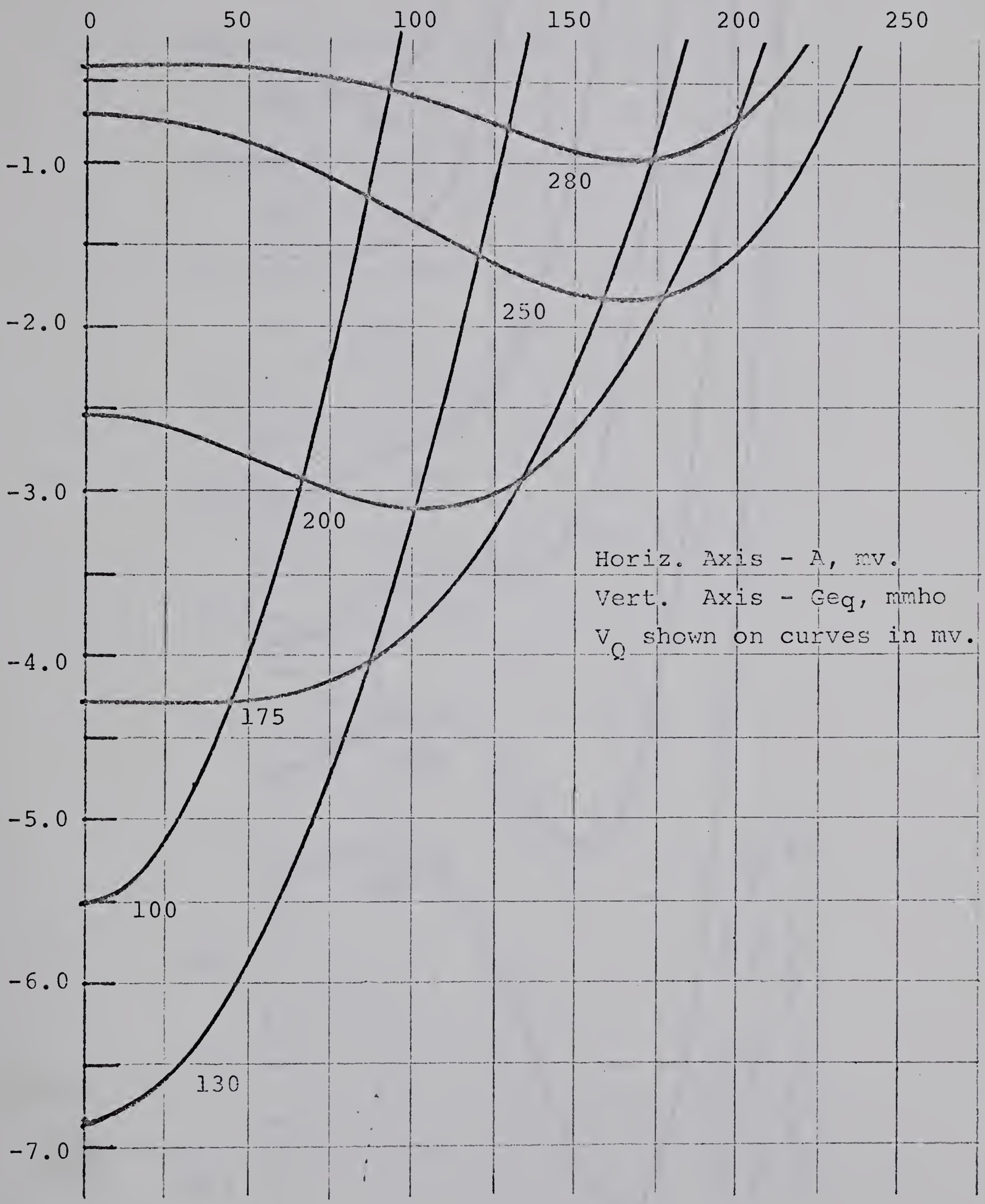

Figure 5.1(a)
Describing-Function Curves

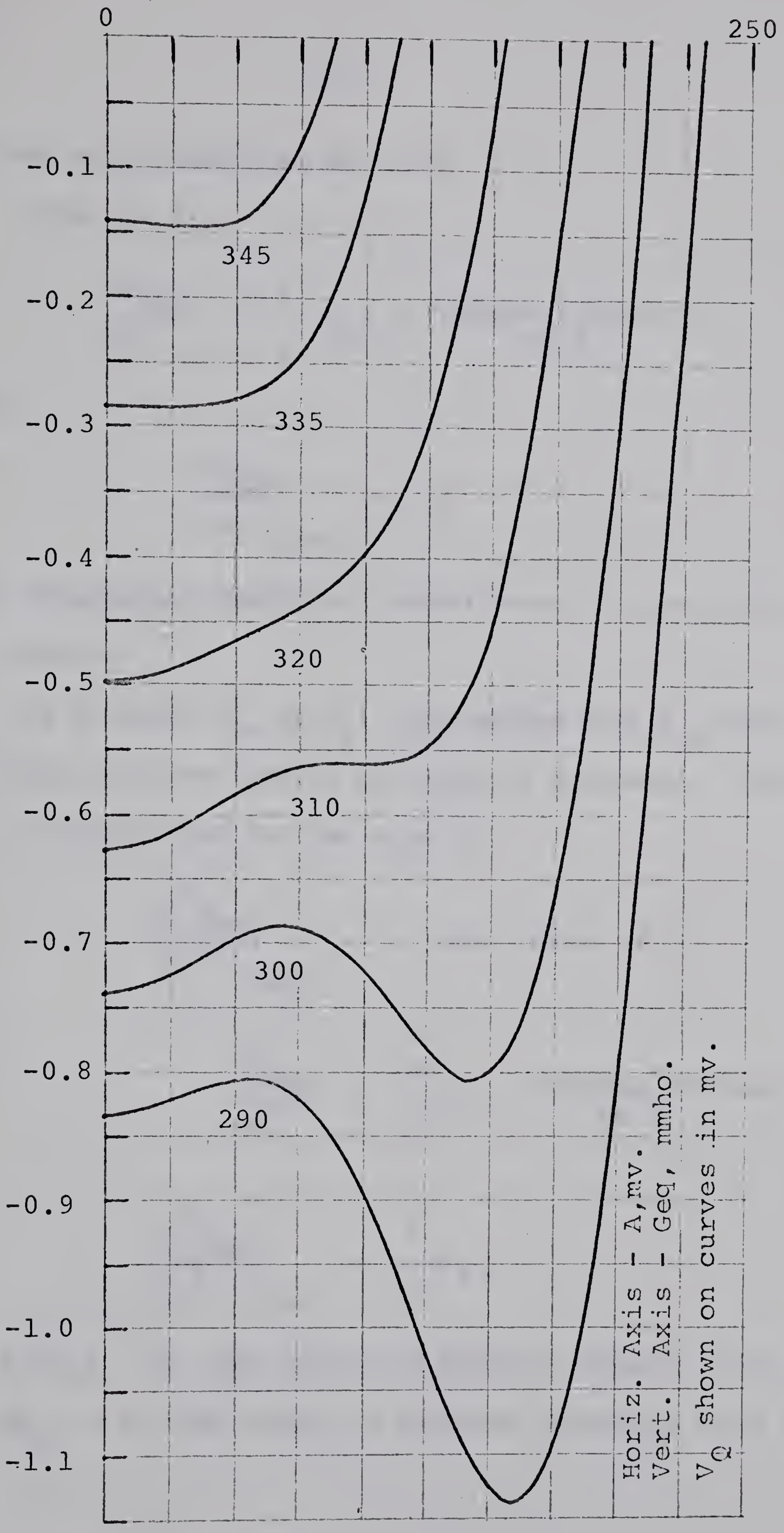

Figure 5.1(b)

Describing-Function Curves

This is the same result as Eq. 2.9.

From (5.1),

$$\frac{\partial G_{eq}}{\partial A} = \frac{3}{2} g_3 A + \left(\begin{matrix}\text{Higher Powers} \\ \text{of } A\end{matrix}\right) ; \qquad (5.3)$$

and hence,

$$\left.\frac{\partial G_{eq}}{\partial A}\right|_{A=0} = 0 \qquad (5.4)$$

Thus, all describing function curves meet the vertical axis at right angles.

As a curve $G_{eq}(A,V_Q)$ approaches the G_{eq}-axis, it can be either concave upward or concave downward. This property is determined by the sign of

$$\left.\frac{\partial^2 G_{eq}}{\partial A^2}\right|_{A=0} .$$

But from (5.3)

$$\frac{\partial^2 G_{eq}}{\partial A^2} = \frac{3}{2} g_3 + \left(\begin{matrix}\text{Higher Powers} \\ \text{of } A\end{matrix}\right); \qquad (5.5)$$

so that

$$\left.\frac{\partial^2 G_{eq}}{\partial A^2}\right|_{A=0} = \frac{3}{2} g_3 \qquad (5.6)$$

Thus, if $g_3(V_Q) > 0$, the curve is concave upward at $A = 0$; and if $g_3(V_Q) < 0$, the curve is concave downward at $A = 0$.

5.2 Radius of Curvature

By introducing the concept of the radius of curvature of f(V) at the point V_Q, a relationship between the sign of g_3 and the rate of change of the radius of curvature (with respect to arc-distance along the curve) can be derived. Note that in the VI-plane, distance will have mixed units. (i.e. $S = \sqrt{V^2 + I^2}$) Thus, all physical dimensions shall be neglected in this section.

The radius of curvature, ρ, can be defined as

$$\rho = \frac{\left[1 + f'(V_Q)^2\right]^{3/2}}{f''(V_Q)} \qquad (5.8)$$

It is shown in Sec. A1.1 that the rate of change of ρ, with respect to arc-distance, is given by

$$\frac{d\rho}{dS} = \frac{3f'(V)f''(V)^2 - \left[1 + f'(V)^2\right]f'''(V)}{f''(V)^2} \qquad (5.9)$$

The basic result obtained from the radius of curvature concept shall be simply stated here as a theorem, which is proven in Sec. A1.1.

Theorem 5.1

If {X} represents the complete set of values of V_Q for which $f'(V_Q) < 0$; and {R} represents a continuous range of values of V_Q, included by {X}, for which $\left.\frac{d\rho}{dS}\right|_{V=V_Q} \geq 0$; then {R} must be included by a

larger continuous range, {R'} for which $g_3(V_Q) < 0$. This is illustrated in Fig. 5.2.

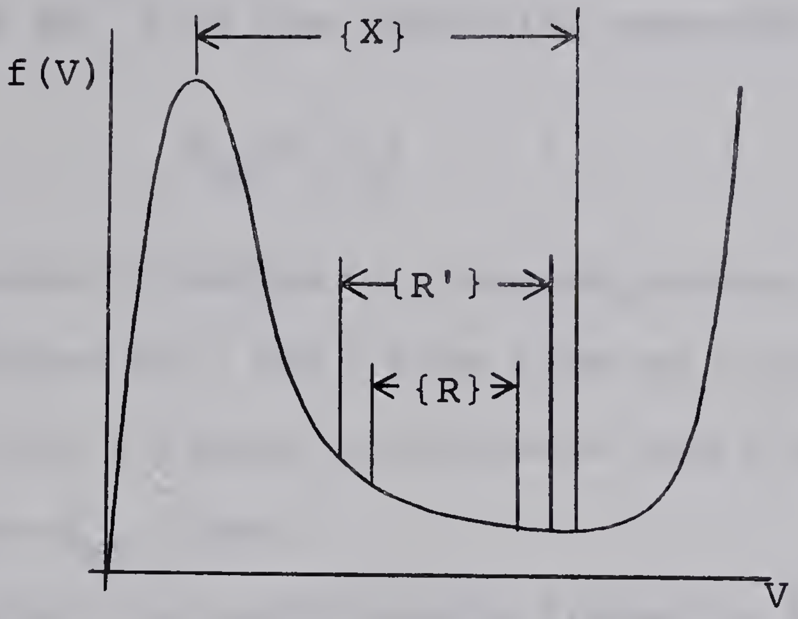

Figure 5.2
Graphical Interpretation of Theorem 5.1

It should be pointed out that if f(V) is concave downward, f''(V) will be negative, and hence ρ, as defined by Eq. 5.8, will be negative. Now, if $\rho < 0$, $d\rho/dS < 0$ means that $|\rho|$ must be increasing. This is the case in the region between the peak point and the inflection point.

As the relationship between the sign of g_3 and the concavity of the describing function curves has already been discussed, the conclusion to be drawn at this point is that if a range {R} can be identified (by inspection of the d.c. characteristic) for which $d\rho/dS \geq 0$, this range must be characterized by describing function curves which are concave downward at the G_{eq}-axis.

5.3 Constant-G_{eq} Chart

If $-\frac{1}{R_o}$ is replaced by an arbitrary negative constant, Γ, in Eq. 4.37 the resulting equation,

$$G_{eq}(A,V_Q) = \Gamma , \tag{5.10}$$

defines a locus or contour in the AV_Q-plane. Hence, choosing different values of Γ will give rise to a family of such contours. Such a family of contours shall be referred to as a Constant-G_{eq} Chart.

Using the coefficients listed in Table 4.2, a digital computer was used to numerically find a solution in A to Eq. 5.10, V_Q and Γ being specified. A sufficient number of values of V_Q and Γ were chosen as to obtain reasonable accuracy throughout the region of interest. The resulting chart is shown in Fig. 5.3.

It is now apparent that the contour $G_{eq}(A,V_Q) = \Gamma$ represents the locus of all possible solutions to Eq. 4.37, if Γ is chosen to be $-\frac{1}{R_o}$.

Note that the Constant-G_{eq} Chart depends in no way on the circuitry external to the tunnel diode itself, but only on the d.c. characteristic of the particular diode under consideration. Such a chart, if obtained, can thus be used in conjunction with any desirable type of network, providing the applied voltage is sinusoidal, or nearly so. In specifying

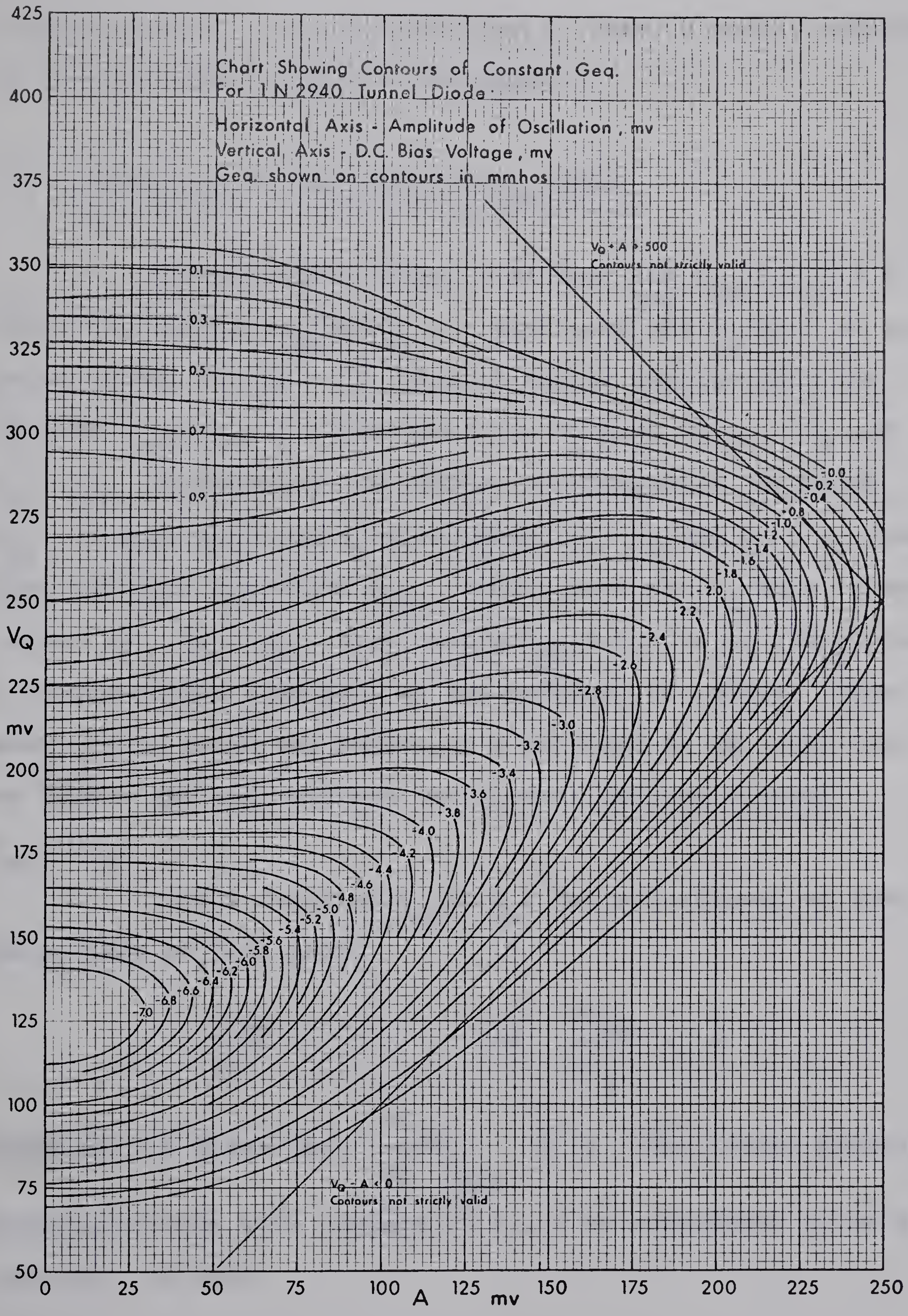

Figure 5.3
Constant-G_{eq} Chart

a tank circuit (i.e. in specifying R_o) one is merely confined to a particular contour on the chart.

5.4 Properties of the Constant-G_{eq} Chart

It was shown (by Eq. 5.2) that $\lim_{A \to 0} G_{eq}(A,V_Q) = f'(V_Q)$. Thus, the contour $G_{eq}(A,V_Q) = \Gamma$ must meet the V_Q-axis at the points where $f'(V_Q) = \Gamma$. This of course implies that the contour $G_{eq}(A,V_Q) = 0$ must meet the V_Q-axis at $V_Q = V_P$ and $V_Q = V_V$. Furthermore, it implies that contours for which $G_{eq} > 0$ must meet the V_Q-axis where $V_Q < V_P$ and $V_Q > V_V$; and that contours for which $G_{eq} < 0$ must meet the V_Q-axis in the region $V_P < V_Q < V_V$. Also, since $G_{eq}(A,V_Q)$ is at every point a single-valued function, no two contours can cross. Thus, every point which can represent a solution to Eq. 4.37 must be within the area between the V_Q-axis and the contour $G_{eq}(A,V_Q) = 0$.

If the function $G_{eq}(A,V_Q)$ has an extremum at some point,then at this point

$$\frac{\partial G_{eq}}{\partial A} = 0 , \qquad \text{and} \qquad \frac{\partial G_{eq}}{\partial V_Q} = 0 .$$

Equation 5.4 shows that $\left.\frac{\partial G_{eq}}{\partial A}\right|_{A=0} = 0$. Now, under partial differentiation with respect to V_Q, A is considered to be a constant, so that

$$\left.\frac{\partial G_{eq}}{\partial V_Q}\right|_{A=0} = \frac{\partial}{\partial V_Q} G_{eq}(0,V_Q).$$

But by (5.2), $G_{eq}(0,V_Q) = f'(V_Q)$. Hence, $\left.\frac{\partial G_{eq}}{\partial V_Q}\right|_{A=0} = 0$ implies that $f''(V_Q) = 0$, or $V_Q = V_I$. Thus, the point $(0,V_I)$ is an extremum of $G_{eq}(A,V_Q)$.

Also, $G_{eq}(0,V_I) = f'(V_I)$, which is defined as $-G_d$, by Eq. 1.2. This is the minimum value of $f'(V_Q)$. Thus, it follows that no point can exist for which G_{eq} is less than $-G_d$, as the contour through such a point would have to meet the V_Q-axis where $f'(V_Q)$ were less than $-G_d$. Hence, the point $(0,V_I)$ must be an absolute minimum of $G_{eq}(A,V_Q)$.

It can now be concluded that all contours for which $G_{eq} < 0$ must enclose the point $(0,V_I)$, and must in turn be enclosed by the contour $G_{eq} = 0$.

It was pointed out earlier that for certain values of V_Q and R_o, more than one solution to the equation $G_{eq}(A,V_Q) = -\frac{1}{R_o}$ can exist. This is clearly evident from the Constant-G_{eq} Chart as well.

It is shown in Sec. A1.2 that the contours immediately surrounding the inflection point are approximately elliptic; with centres at $(0,V_I)$, major axis of

$$4\sqrt{\frac{G_d + \Gamma}{3g_3(V_I)}}, \tag{5.11}$$

and minor axis of

$$2\sqrt{\frac{G_d + \Gamma}{3g_3(V_I)}} \quad . \tag{5.12}$$

The major axis is parallel to the A-axis. Γ is the value of G_{eq} on the contour, and is of course negative;

$$g_3(V_I) = \frac{f'''(V_I)}{3!} \quad ; \quad \text{and} \quad G_d = -f'(V_I) .$$

For the diode under consideration, G_d and $g_3(V_I)$ have been evaluated, and are approximately 7.36×10^{-3} A/V and 0.545 A/V^3 respectively. For the smallest contour shown in Fig. 5.3, $\Gamma = -7.0 \times 10^{-3}$, so that the minor axis should be

$$2\sqrt{\frac{(7.36 - 7.0) \times 10^{-3}}{3(0.545)}} \simeq 29.7 \text{ mv.}$$

This can be easily verified by inspection of Fig. 5.3.

There are two other properties of the Constant-G_{eq} Chart that shall be stated here as theorems, and are proven in Sec's. A1.4 and A1.5.

Theorem 5.2

All contours $G_{eq}(A,V_Q) = \Gamma$ meet the V_Q-axis at right angles.

Theorem 5.3

If a contour $G_{eq} = \Gamma$ meets the V_Q-axis at a value of V_Q within a continuous range, $\{V_Q\}$, for which all curves $G_{eq}(A,V_Q)$ have the same direction of concavity at A = 0, then the direction of concavity

of the contour (at A = 0) will be:

1) the opposite to that of the curves $G_{eq}(A,V_Q)$, if $V_Q > V_I$; and

2) the same as that of the curves $G_{eq}(A,V_Q)$ if $V_Q < V_I$.

This is illustrated in Fig. 5.4. In Fig. 5.4(a), V_{Q_1} and V_{Q_2} belong to the ranges $\{V_{Q_1}\}$ and $\{V_{Q_2}\}$ respectively, as shown in Fig. 5.4(b).

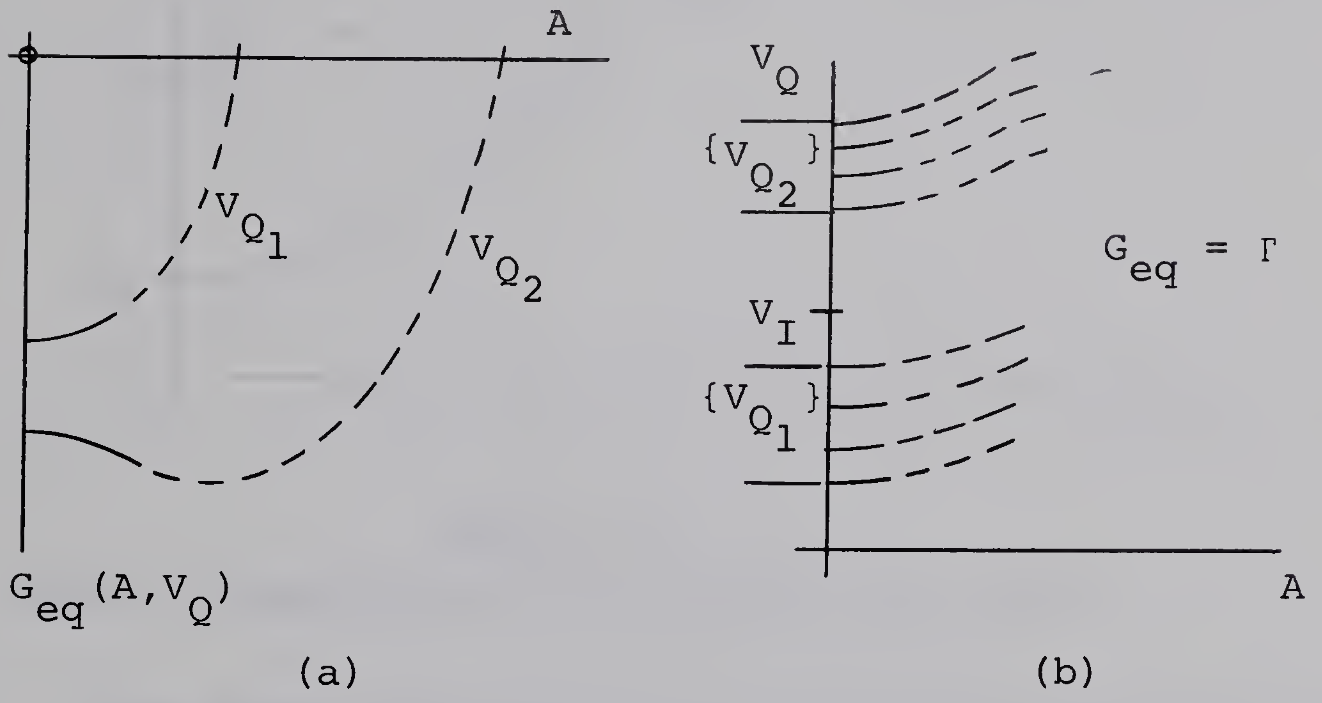

Figure 5.4
Graphical Interpretation of Theorem 5.3

Since relationships between the radius of curvature of f(V), $g_3(V_Q)$, and the direction of concavity of the describing-function curves have already been established, it follows that these relationships can be extended to the Constant-G_{eq} Chart. Hence, the ranges {R} and {R'}, as shown in Fig. 5.2, would be characterized by contours being concave

upward at the V_Q-axis.

Figure 5.5 illustrates the basic properties of the Constant-G_{eq} Chart that have been discussed in this section.

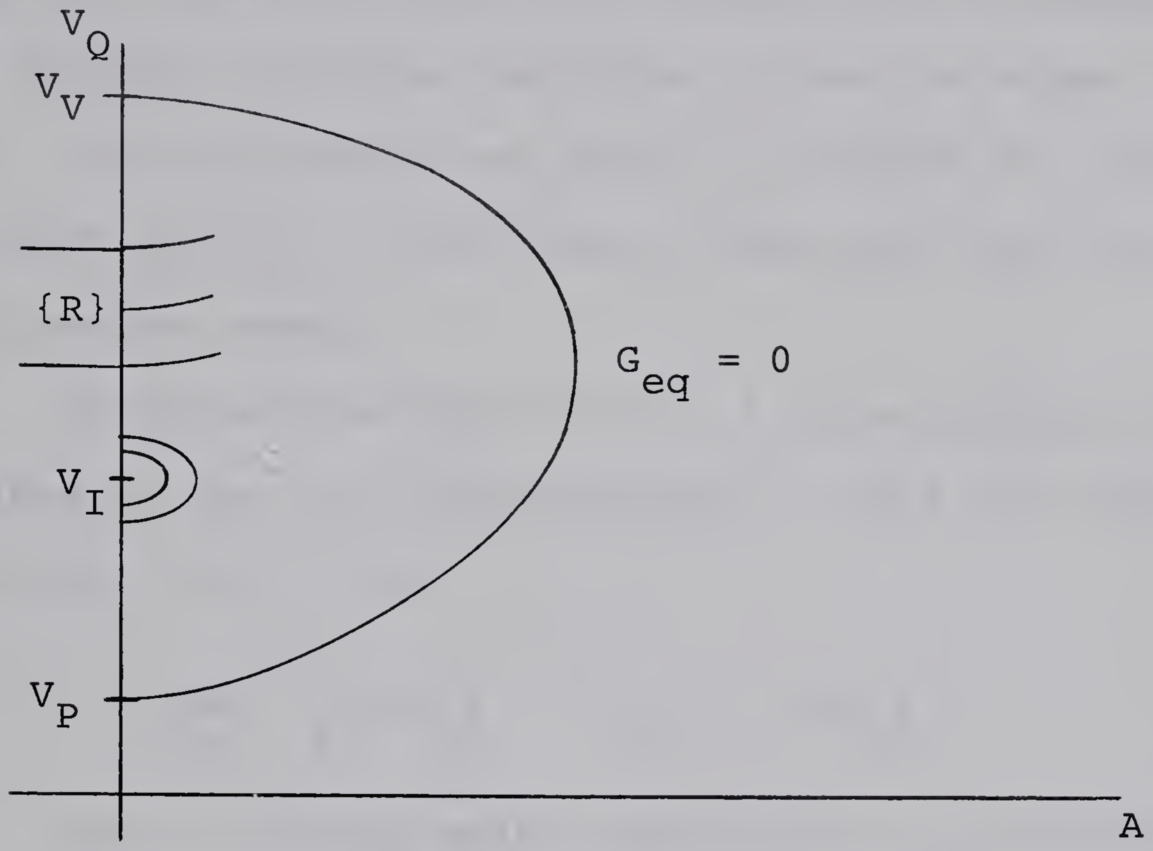

Figure 5.5
Basic Properties of the Constant-G_{eq} Chart

One minor limitation of the Constant-G_{eq} Chart as derived for the IN2940 tunnel diode should be pointed out. Referring to Fig. 4.1, it is seen that the d.c. characteristic based on the coefficients listed in Table 4.2 is known to be accurate only in the voltage range $0 \leq V \leq 500$ mv. Thus, for the method of analysis to be strictly valid, the diode voltage must at all times be confined to this range. This means, that on the Constant-G_{eq} Chart, portions of contours within the regions where $V_Q + A > 500$ mv, and $V_Q - A < 0$ will probably be less accurate than those outside these regions. These regions are indicated in Fig. 5.3.

5.5 Discussion of the Biasing Function

The biasing function, $I_Q(A,V_Q)$, based on the ten coefficients listed in Table 4.2 has been evaluated using a digital computer, and the resulting curves are shown in Fig. 5.6. The evaluation was done only within the range of V_Q for which $g_1(V_Q) < 0$, as this is the only range for which oscillations may occur.

It is noticed that for $A = 0$, the biasing function degenerates to the d.c. characteristic. This can easily be seen from Eq. 4.40. i.e.

$$\lim_{A \to 0} I_Q(A,V_Q) = g_o = f(V_Q) .$$

Also, for very small values of A, I_Q can be approximated by the first two terms of Eq. 4.40, or

$$I_Q(A,V_Q) \simeq g_o + \tfrac{1}{2} g_2 A^2 \tag{5.13}$$

Now, it is known that:

1. if $V_Q < V_I$, $g_2 < 0$; $f(V_Q)$ is concave downward
2. if $V_Q = V_I$, $g_2 = 0$; $f(V_Q)$ has an inflection point
3. if $V_Q > V_I$, $g_2 > 0$; $f(V_Q)$ is concave upward.

Hence, from (5.13), it follows that the biasing curves corresponding to very small values of A will be beneath $f(V_Q)$ if $V_Q < V_I$; will cross $f(V_Q)$ at $V_Q \simeq V_I$; and will be above $f(V_Q)$ if $V_Q > V_I$. The above can easily be verified by inspection of Fig. 5.6.

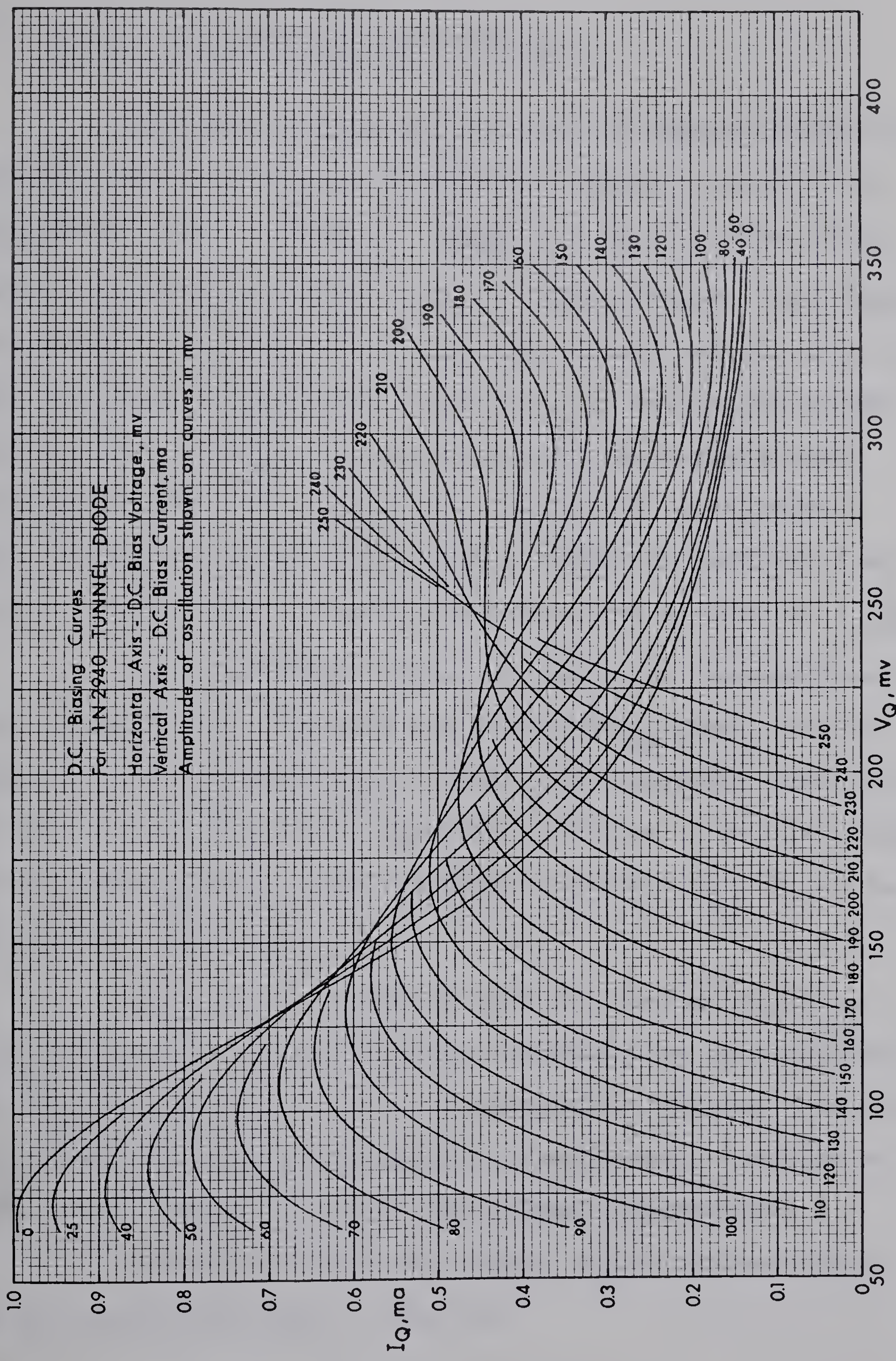

Figure 5.6

Biasing Curves

5.6 Unique Determination of A and V_Q

Referring now to Eq. 4.42, it is apparent that the quantity $(V_B-V_Q)/(R_1+R_B)$ represents a straight line in the V_QI_Q-plane; with a slope of $-\frac{1}{R_1+R_B}$, a V_Q-intercept of V_B, and an I_Q-intercept of $V_B/(R_1+R_B)$. This straight line shall be referred to as the d.c. load-line. Thus, the solution to Eq. 4.42, for a particular value of A, is determined by the intersection of the d.c. load-line with the biasing curve corresponding to that value of A. Fig. 4.7 illustrates a set of biasing curves, along with a number of possible load-lines. Note that all load-lines shown have a slope of $-\frac{1}{125\Omega}$.

If a sufficient number of points of intersection are now obtained and plotted on the Constant-G_{eq} Chart, the resulting curve represents the locus of all possible solutions to Eq. 4.42. Since for a specific load-line, A can be thought of as determining V_Q, the functional notation $V_Q = V_Q(A)$ can be used for this locus.

If it is now recalled that the contour $G_{eq}(A,V_Q) = -\frac{1}{R_o}$ is the locus of all possible solutions to this equation, it is apparent that a point of intersection between this contour and the curve $V_Q(A)$ must be a simultaneous solution to Eq's. 4.43. Hence, V_Q and A are uniquely determined.

Figure 5.8 shows the curves, $V_Q(A)$ corresponding to the load-lines shown in Fig. 5.7

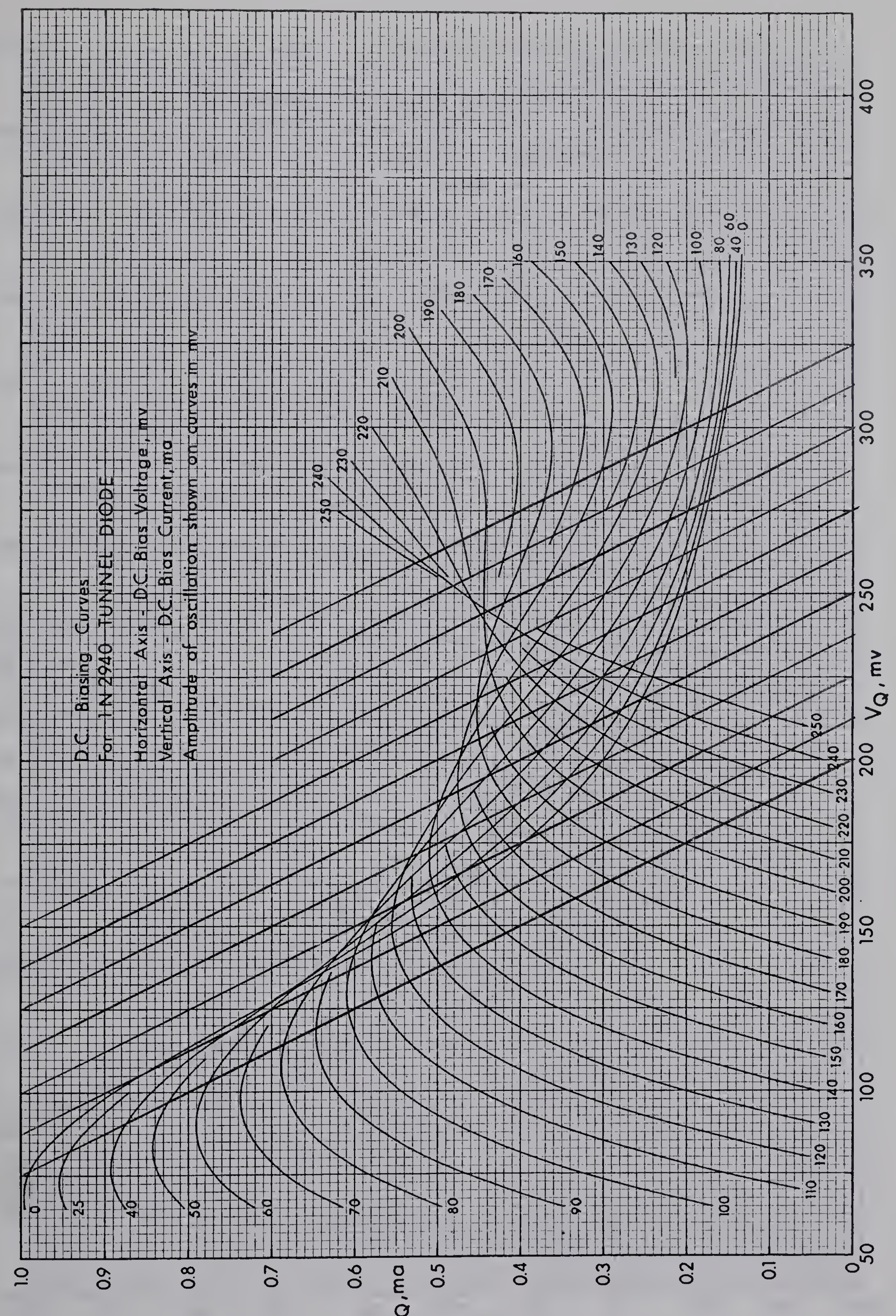

Figure 5.7

Biasing Curves and Load-Lines

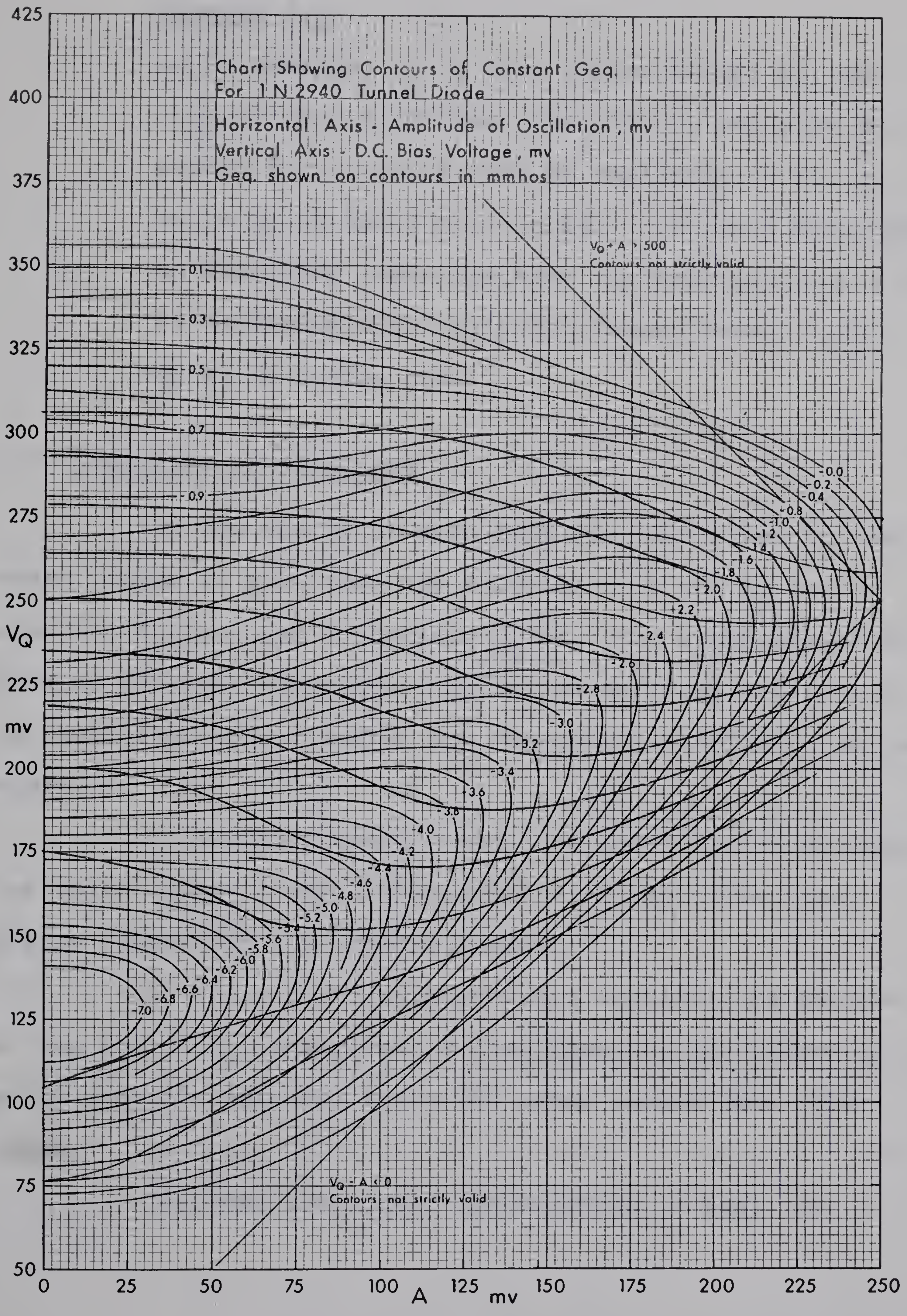

Figure 5.8

Constant-G_{eq} Chart and Loci

Example 5.1

As an example, if V_B were chosen as 225 mv, and $-\frac{1}{R_o}$ as -4.0×10^{-3}mho, the circuit could be expected to oscillate with an amplitude of 111 mv., and a V_Q of 152.5 mv. In Fig. 5.7, this corresponds to the third load-line from the left and in Fig. 5.8 it corresponds to the third lowest curve, $V_Q(A)$. R_o is of course 250Ω.

5.7 Stability of Solutions

It can easily be seen from Fig. 5.8, that in many cases, there is more than one solution in A and V_Q for a specific contour and a specific $V_Q(A)$. The stability of the various possible solutions will now be analysed and it will be shown that both "stable" and "unstable" solutions are possible.

A "stable" solution shall be defined as a solution for which, under a small displacement in amplitude, the system returns to its original state.

An "unstable" solution shall similarly be defined as one for which, under such a displacement, the system departs from its original state and tends toward some other state.

Consider the linear system shown in Fig. 5.9.

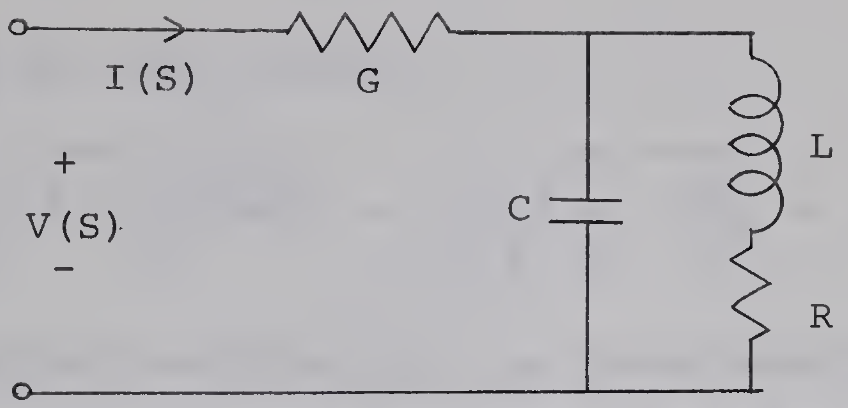

Figure 5.9
Comparative Linear System

For this system

$$Z_T(S) = \frac{R + SL}{S^2LC + SCR + 1} \; ; \quad \text{and}$$

$$Z(S) = \frac{1}{G} + Z_T(S)$$

$$= \frac{(R + SL)G + S^2LC + SCR + 1}{G(S^2LC + SCR + 1)}$$

Thus,

$$\frac{I(S)}{V(S)} = \frac{G(S^2LC + SCR + 1)}{S^2LC + S(CR + GL) + (1 + RG)} \; .$$

The Characteristic Equation is

$S^2LC + S(CR + GL) + (1 + RG) = 0$, and its roots are

$$S = -\frac{(CR + GL)}{2LC} \pm j\sqrt{\frac{(1+RG)}{LC} - \frac{(CR+GL)^2}{4L^2C^2}} \qquad (5.14)$$

Now, for sinusoidal oscillation, the roots of the Characteristic Equation must be imaginary, or $(CR + GL) = 0$. From this,

$$G = -\frac{CR}{L} = -\frac{1}{R_o} \; . \qquad (5.15)$$

Substituting (5.15) into (5.14),

$$S = \pm j\sqrt{\frac{1 - (R^2C/L)}{LC}} = \pm j\sqrt{\frac{1}{LC} - \frac{R^2}{L^2}} = \pm j\omega_o \quad (5.16)$$

Thus, for sinusoidal oscillation, the describing-function model of the non-linear system can be compared to the linear system having a negative conductance, G, equal to G_{eq} for the non-linear system.

Referring again to the linear system, if $G < \frac{-1}{R_o}$, $-(CR+GL) > 0$, or the roots of the Characteristic Equation are in the right-hand side of the S-plane. This will correspond to increasing amplitude of oscillation. Similarily, if $G > \frac{-1}{R_o}$, $-(CR+GL) < 0$, and the amplitude will decrease.

Since at a solution for sinusoidal oscillation, the describing function model is known to behave in a similar manner to the linear system, it can be assumed that the same will be true for a differential displacement, δA, from such a solution. In the AV_Q-plane, the displacement δA, corresponds to displacement along the curve $V_Q(A)$, from P_1 to P_2. This is shown in Fig. 5.10.

The displacement δA will be accompanied by an incremental change in G_{eq}, given by

$$\delta G_{eq} = \frac{dG_{eq}}{dA}\,\delta A \quad . \qquad (5.17)$$

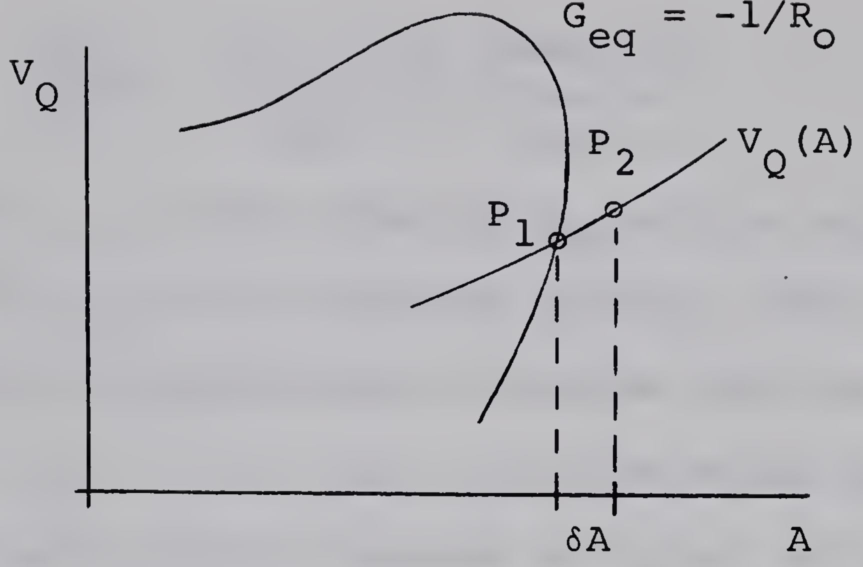

Figure 5.10
Differential Displacement from a Solution

Since P_1 is a solution for sinusoidal oscillation, at P_1, $G_{eq} = \frac{-1}{R_o}$. Hence, at P_2, $G_{eq} = -\frac{1}{R_o} + \frac{dG_{eq}}{dA}\delta A$. If it is now assumed that dG_{eq}/dA is positive at P_1, and δA is taken as positive, then at P_2, G_{eq} must be greater than $-\frac{1}{R_o}$, and the amplitude should decrease. Taking δA as negative, and dG_{eq}/dA as positive would result in G_{eq} being less than $-\frac{1}{R_o}$, and the amplitude should thus increase. Therefore, it is concluded that any solution for which

$$\frac{dG_{eq}}{dA} > 0 \qquad (5.18)$$

is a stable solution. A similar argument shows that any solution for which

$$\frac{dG_{eq}}{dA} < 0 \qquad (5.19)$$

is an unstable solution.

It is shown in Sec. A1.3 that at the point P_1,

$$\frac{dG_{eq}}{dA} \simeq \frac{(\Gamma_2 - \Gamma_1)}{|\Delta S|} \; \frac{\cos(\alpha-\beta)}{\cos\beta} \qquad (5.20)$$

In Eq. 5.20, Γ_1 is the value of G_{eq} at the solution, Γ_2 is the value of G_{eq} on an adjacent contour, such that $\Gamma_2 > \Gamma_1$; and $|\Delta S|$ is the perpendicular distance from the solution to the contour $G_{eq} = \Gamma_2$. Also, β is the acute angle between the horizontal axis and the tangent to $V_Q(A)$, at the solution; and α is the angle between the horizontal axis and a vector parallel to the line $|\Delta S|$, in the direction of increasing G_{eq}. This is shown in Fig. 5.11.

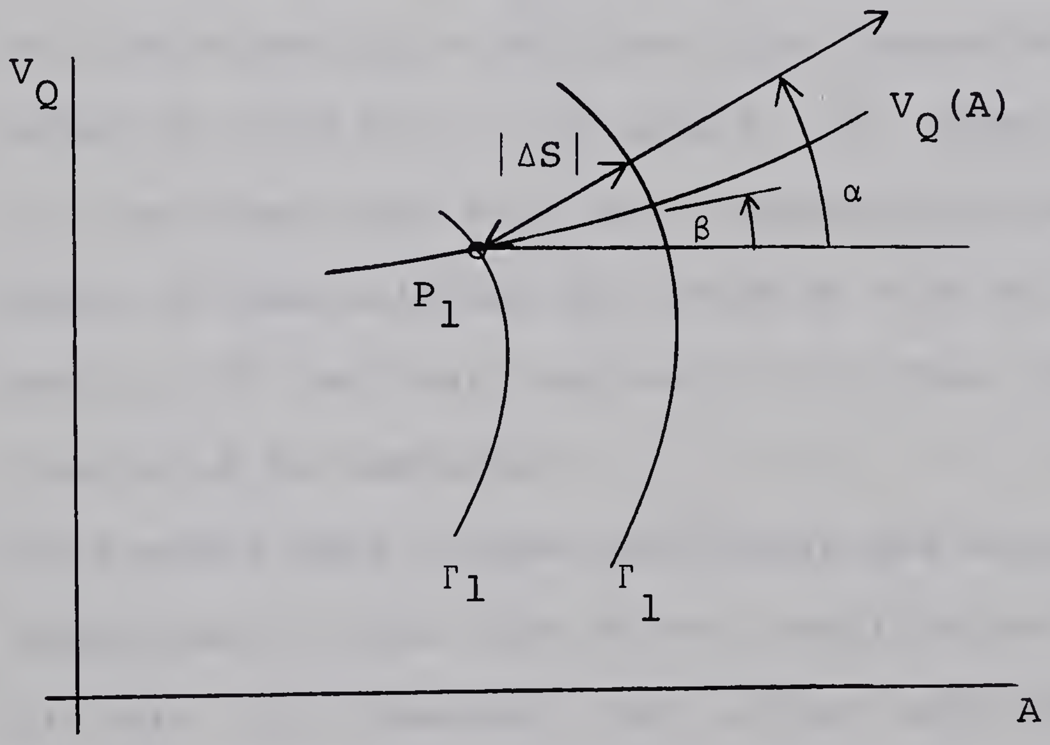

Figure 5.11
Determination of Stability

Now, $(\Gamma_2-\Gamma_1)/|\Delta S|$ is by definition positive, and since $-90^\circ \leq \beta \leq 90^\circ$, $\cos\beta$ must be positive or zero. Thus, the sign of dG_{eq}/dA will be the same as the sign of $\cos(\alpha-\beta)$.

Note that if $(\alpha-\beta) = \pm 90^{\circ}$, $dG_{eq}/dA = 0$. This corresponds to a displacement parallel to the contour $G_{eq} = \Gamma_1$. Also if $\beta = \pm 90^{\circ}$, $dG_{eq}/dA = \infty$. This corresponds to a vertical displacement, so that $dA = 0$.

Example 5.2

Consider now an example where there are known to be two solutions. Referring to Fig's. 5.7 and 5.8, this could correspond to $V_B = 237.5$ mv, $R_1+R_B = 125\Omega$, and $R_o = 250\Omega$. There is seen to be one solution for $A = 116$ mv and $V_Q = 171$ mv, and another for $A = 58$ mv and $V_Q = 188.5$ mv. At the solution for which $A = 116$ mv, $\alpha \simeq 0$, and $\beta \simeq 0$. Thus, $\cos(\alpha-\beta) \simeq 1$, so that this will be a stable solution. However, at the solution for which $A = 58$ mv, $\alpha > 90^{\circ}$, and $\beta < 0^{\circ}$, so that $\cos(\alpha-\beta) < 0$. Thus, this solution will be unstable.

This means that if the oscillator had an initial amplitude of less than 58 mv, oscillations would die out. If, however, the initial amplitude were greater than 58 mv, oscillations would build up until the stable solution were reached, at 116 mv. It can also be seen from Fig's. 5.7 and 5.8, that if V_B were now increased to 250 mv, there would be no solution; and that for some value of V_B between 237.5 mv and 250 mv, the stable and unstable

solutions would converge to the same point. This point will thus determine a minimum amplitude for sustained oscillation. For this example, the minimum amplitude is seen to be approximately 105 mv. Note that oscillation with this minimum amplitude can be realized only by gradually increasing V_B from a smaller value, so that A is always larger than that for the unstable solution.

A similar situation would occur if V_B were decreased to somewhat less than 200 mv. The minimum amplitude in this case would be about 65 mv.

From the preceding discussion, it is apparent that in order for oscillations to build up from zero, the solution occurring for the lowest value of A must be stable (if more than one solution exists). It is interesting to note that for $V_B = 312.5$ mv, $R_1+R_B = 125\Omega$, and $-\frac{1}{R_o} = -0.8$ mmho, there are three solutions. The first and the third are stable, and the second is unstable.

5.8 Relative Stability

Referring once more to the linear system of Fig. 5.9 it is well-known that the rate of growth (or decay) of amplitude is determined by the magnitude of the real part of the root S. i.e. the magnitude of (CR+GL)/2LC. If this is also assumed to be true for the describing-function model under

the virtual displacement δA, it then follows that the magnitude of $\frac{(\Gamma_2-\Gamma_1)}{|\Delta S|}\frac{\cos(\alpha-\beta)}{\cos\beta}$ will determine the rate with which the system tends toward (or away from) its initial state. Thus, the quantity $\frac{(\Gamma_2-\Gamma_1)}{|\Delta S|}\frac{\cos(\alpha-\beta)}{\cos\beta}$ can be thought of as an "Amplitude Stability Factor", and solutions for which this quantity is relatively large can be termed "relatively stable".

5.9 Further Comments on Distortion

Inherent to the describing-function method is the assumption that voltage across the diode is purely sinusoidal. It is quite obvious, however, that the current waveform can have a very high harmonic content, and since the tank circuit does have finite impedance at any frequency, the assumption of sinusoidal voltage can never be met exactly. It was also pointed out earlier, that for large degrees of voltage distortion, a departure in the frequency of oscillation from the resonant frequency of the tank circuit can be expected. Although a detailed analysis of distortion would be too difficult and lengthy to be practical,it would certainly be worthwhile to determine the primary factors governing distortion.

Consider once more the "Feedback Amplifier Model" of the oscillator, as shown in Fig. 2.3(b). It will be recalled that an equivalent open-loop gain, $A_V = -Z_T/rd$, can be defined. This is valid for very small signals only.

It was also shown in the discussion of the tank circuit, that for large Q_1, the impedance to the n^{th} harmonic above resonance is given approximately by

$$|Z_T(jn\omega_o)| \simeq \sqrt{\frac{L_1}{C_1}}\ \frac{n}{(n^2-1)} \quad .$$

Thus, the open-loop, small-signal gain, at a frequency of $n\ _o$, will be given by

$$|A_V(jn\omega_o)| \simeq \sqrt{\frac{L_1}{C_1}}\ \frac{n}{(n^2-1)\,rd} \quad .$$

From this it is apparent that if $(1/rd)\sqrt{L_1/C_1} > (n^2-1)/n$, the open-loop gain for the n^{th} harmonic will be greater than one. Thus, upon closing the loop, a harmonic initially present in the voltage wave-form would in effect be amplified and fed back to the input. Hence, it must be concluded that if the n^{th} voltage harmonic is to be negligible, $(1/rd)\sqrt{L_1/C_1}$ must be much less than $(n^2-1)/n$.

If the second harmonic, and the minimum value of rd (i.e. $1/G_d$) are considered, the resulting relationship is that

$$G_d\sqrt{\frac{L_1}{C_1}} << \frac{3}{2} \tag{5.21}$$

It is to be expected that voltage distortion will be decreased as amplitude is decreased, as the harmonic content of the current wave-form will be decreased. Thus, for small values of amplitude, near-linear oscillation may be realized

even though (5.21) is not satisfied.

Referring now to Fig. 3.1, it has been shown that if $\sqrt{L_1/C_1}$ is increased:

1. Q_1 will be increased;
2. the impedance to all harmonics will be increased; and
3. R_o will be increased.

In general, increasing R_o will result in an increase in amplitude, and thus an increase in the harmonic content of the current wave-form. Now since the impedance to all harmonics will be simultaneously increased, it follows that an increase in voltage distortion may occur, in spite of the fact that Q_1 will have been increased.

It is of interest to note that for a tank circuit having $R_1 = 0$, both Q_1 and R_o would be infinite. Thus, varying $\sqrt{L_1/C_1}$ would do nothing more than produce different degrees of voltage distortion and frequency departure. Since an infinite-Q tank circuit can easily be simulated on an analogue computer, this suggests an interesting means of experimentally verifying the previous conclusions. (See Sec. A2.3)

5.10 Effect of Self-Oscillation

It was stated in Sec. 1.3 that normally a tunnel diode, when used in a circuit, will have associated with it parasitic circuit elements, R_s, L_s, and C_s; and an equivalent circuit for a real tunnel diode was suggested. This

is shown again in Fig. 5.12.

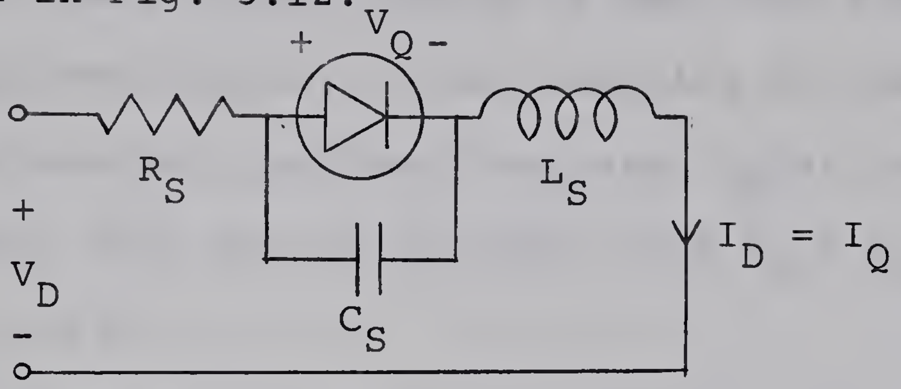

Figure 5.12
Equivalent Circuit for a Real Tunnel Diode

If at some instant a d.c. voltage appears across the terminals of the real diode, as shown in Fig. 5.12, then for high frequencies, the two terminals are essentially connected together. Thus, the ideal diode is connected across a parallel resonant circuit. It then follows that if the resonant resistance, L_s/R_sC_s, is larger than 1/Gd for the ideal diode, self-oscillation will occur whenever V_D is such that the ideal diode is appropriately biased. If R_s is quite small, it can be neglected for d.c., so that the d.c. voltage across the ideal diode, V_Q, will be the d.c. voltage, V_D.

If it is assumed that self-oscillation of amplitude A_1 does occur for some value of V_D (say V_{D_1}) the d.c. current through the real diode, I_{Q_1}, can be found directly from the Biasing Curves, by taking V_Q as V_{D_1} and A as A_1.

If some value is assumed for the parasitic resonant resistance, L_s/R_sC_s, the contour $G_{eq} = -R_sC_s/L_s$ will determine the amplitude of self-oscillation for any d.c. voltage,

V_Q, across the ideal diode. Since it has been assumed that R_s can be neglected for d.c., the load-line for the ideal diode will be vertical, so that the curve $V_Q(A)$, on the Constant-G_{eq} Chart, will be the straight line $V_Q = V_D$. This is shown in Fig. 5.13.

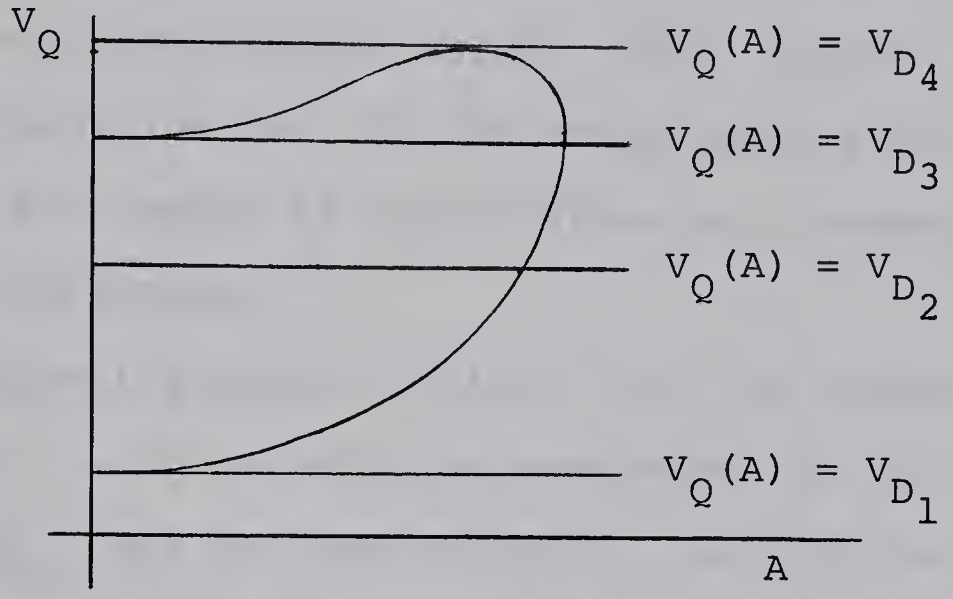

Figure 5.13
Derivation of the Modified D.C. Characteristic

For a contour such as that shown in Fig. 5.13 there can again be two solutions. As before, the one for the smaller value of A will be unstable, and the other one will be stable. Thus, if V_D were increased from V_{D_1} to V_{D_4}, A would increase from zero to a maximum, and then decrease until V_{D_4} were reached. At this point, oscillation would of course cease completely. If V_D were now decreased, oscillation would not re-occur until V_{D_3} were reached, and the amplitude would then vary continuously until V_{D_1} were again reached.

It is now apparent that if a number of points on the contour $G_{eq} = -L_sC_s/R_s$ are plotted on the Biasing Curves

a "Modified D.C. Characteristic" will result. This modified characteristic is analagous to that defined in the Dual Input Describing-Function method*, with the exception that the self-oscillation is present only for a certain range of values of V_D, and within this range varies in amplitude between zero and some maximum value. Thus, the d.c. characteristic will be modified only in the range where self-oscillation occurs, and the degree of modification will depend on the amplitude of oscillation.

Referring again to Fig. 5.13, for increasing V_D, the characteristic will be modified everywhere in the range $V_{D_1} < V_D < V_{D_4}$; and for decreasing V_D, it will be modified in the range $V_{D_1} < V_D < V_{D_3}$. Thus, the modified d.c. characteristic will exhibit hysteresis.

Assuming a parasitic resonant conductance of 3.0×10^{-3} mho, a modified d.c. characteristic has been derived, and is shown in Fig. 5.14. This form of characteristic is often seen when a tunnel diode characteristic is displayed on a conventional curve tracer (see Ref. 3, page 67).

Consider now the real tunnel diode used in conjunction with an external tank circuit and biasing network as shown in Fig. 5.15

---

* See Ref. 1, page 408.

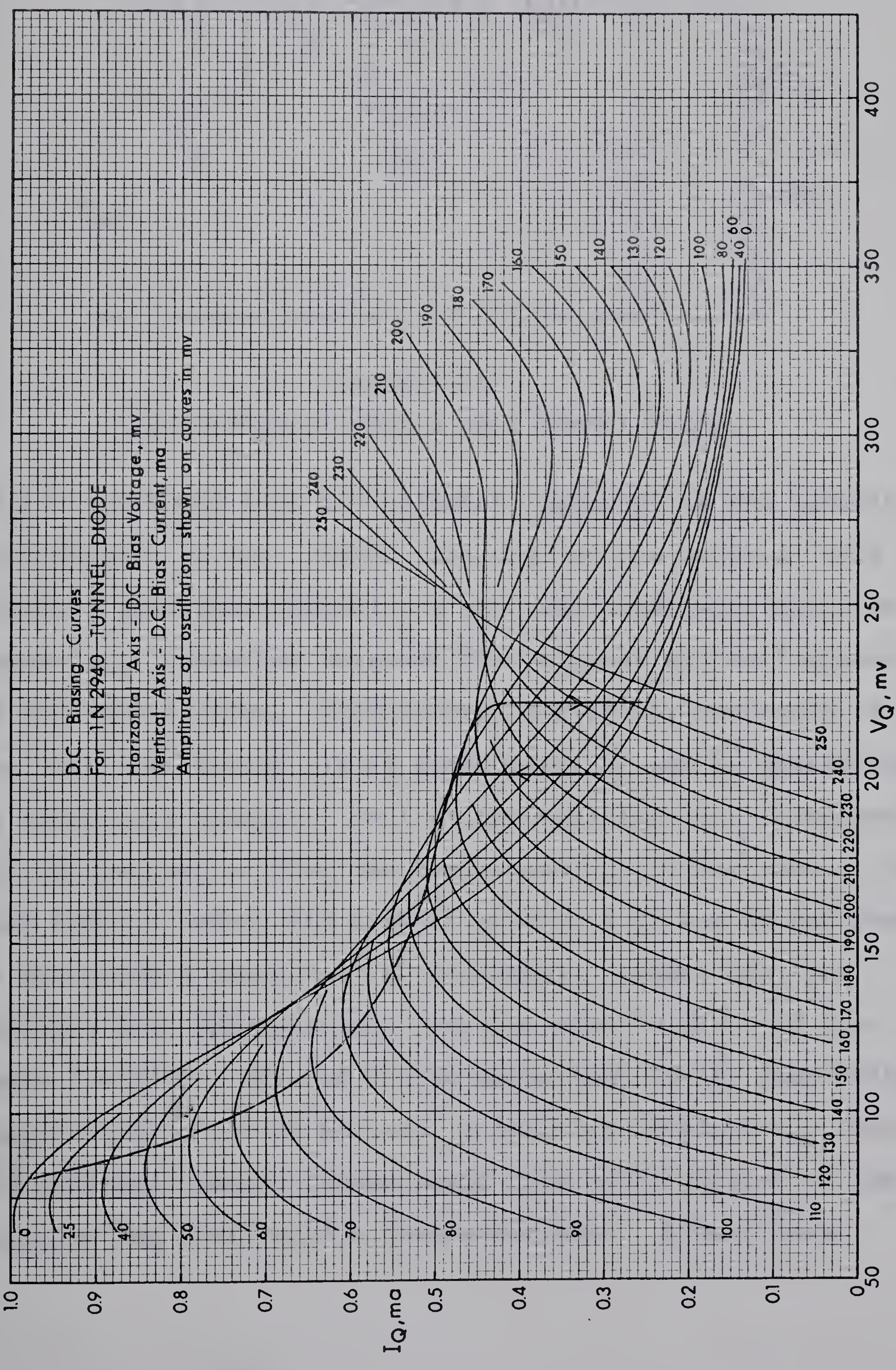

Figure 5.14

Modified D.C. Characteristic

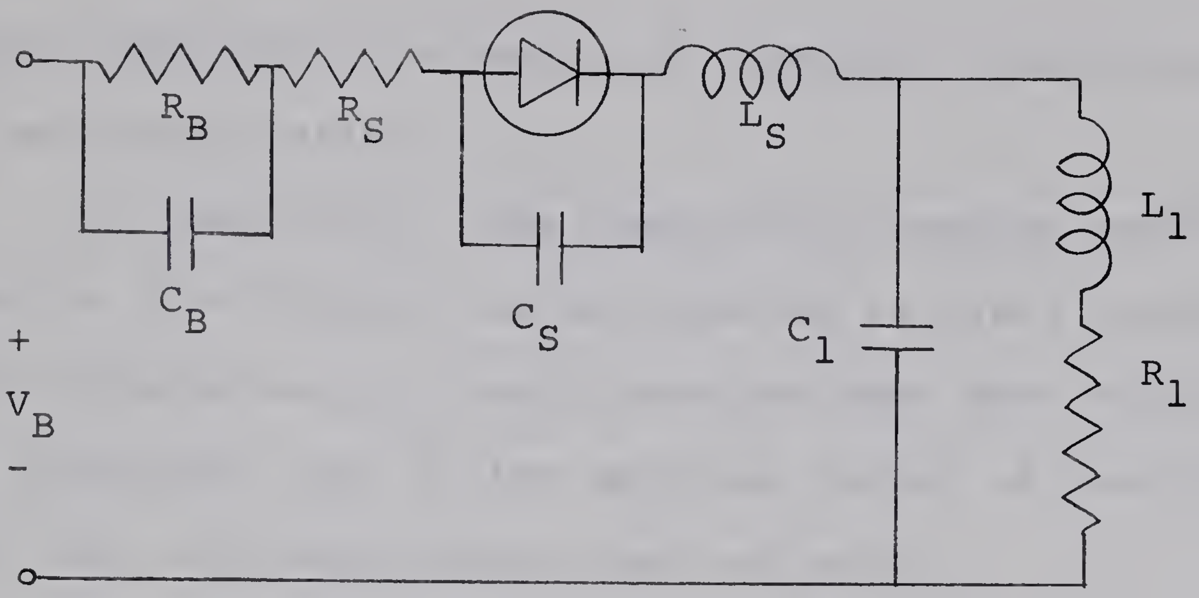

Figure 5.15
An Oscillator Using a Real Tunnel Diode

If it is assumed that the resonant frequency of the parasitic tank circuit is much higher than that of the external tank circuit, then the terminals of the real diode will again be essentially connected together for voltages at the frequency of self-oscillation. Furthermore, during any one cycle of the self-oscillation (if it does occur) V_D can be considered as relatively constant, so that the modified d.c. characteristic can be used to find the corresponding current through the real diode. Hence, the circuit of Fig. 5.15 can be analysed by the methods discussed in this thesis, except that the modified d.c. characteristic must be used in place of the curve $I = f(V)$. This of course means that if the describing-function method is to be used, a modified Constant-G_{eq} Chart and modified Biasing Curves would have to be derived on the basis of the modified d.c. characteristic. A much more

practical approach is to avoid, if possible, conditions leading to self-oscillation.

In conclusion , the describing-function method, as outlined in this thesis, can be expected to yield reasonably accurate results only if conditions are such that voltage is nearly sinusoidal, and if the physical layout of the circuitry is such that self-oscillation does not occur.

VI. Effect of Second Tuned Circuit

It has been established that the circuit shown in Fig. 1.4(a) can be made to oscillate with frequency ω_o, such that Im $\{Z_T(j\omega_o)\} = 0$, providing a stable solution to Eq's. 4.43 can be found. Furthermore, aside from the Biasing Curves and Constant-G_{eq} Chart, which pertain only to a particular tunnel diode, the determination of a solution to Eq's. 4.43 requires only the specification of the d.c. load-line, and the resonant resistance of the tank circuit. Since mutually coupling a second tank circuit cannot alter the d.c. load-line, it follows that analysis of this system will require only additional knowledge concerning its resonant states.

6.1 Resonant Frequencies

In the following analysis, $Z_T(S)$ shall refer to the impedance of the mutually coupled tank circuits, as shown in Fig. 6.1; or

$$Z_T(S) = \frac{V(S)}{I(S)} . \tag{6.1}$$

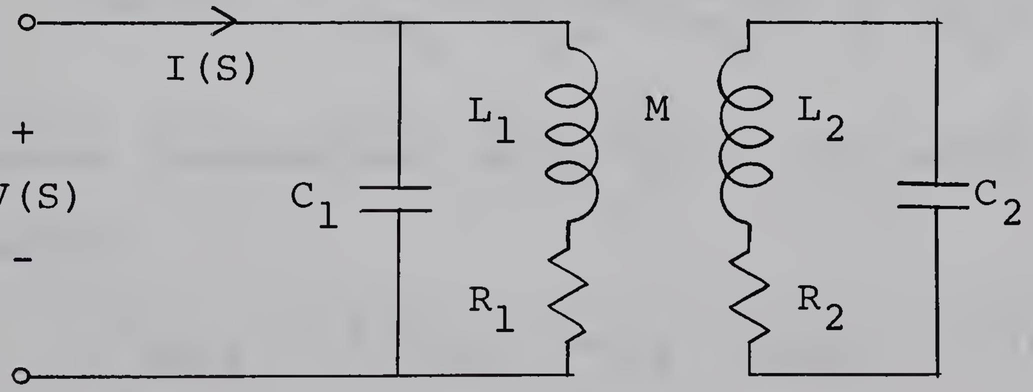

Figure 6.1
Mutually Coupled Tank Circuits

It is not difficult to show that

$$Z_T(S) = \frac{a_3S^3 + a_2S^2 + a_1S + a_o}{b_4S^4 + b_3S^3 + b_2S^2 + b_1S + b_o} , \qquad (6.2)$$

where

$$\begin{aligned}
a_o &= R_1 \\
a_1 &= L_1 + R_1R_2C_2 \\
a_2 &= R_1L_2C_2 + L_1R_2C_2 \\
a_3 &= L_1L_2C_2(1 - K^2) \\
b_o &= 1 \qquad (6.3) \\
b_1 &= R_1C_1 + R_2C_2 \\
b_2 &= L_1C_1 + L_2C_2 + R_1R_2C_1C_2 \\
b_3 &= R_1L_2C_1C_2 + L_1R_2C_1C_2 \\
b_4 &= L_1L_2C_1C_2(1 - K^2) ,
\end{aligned}$$

and

$$K^2 = \frac{M^2}{L_1L_2} \text{ . Note that } 0 \leq K^2 \leq 1 . \qquad (6.4)$$

Letting $S = j\omega$,

$$Z_T(j\omega) = \frac{(a_o - a_2\omega^2) + j(a_1\omega - a_3\omega^3)}{(b_o - b_2\omega^2 + b_4\omega^4) + j(b_1\omega - b_3\omega^3)} \qquad (6.5)$$

For resonant frequencies, $\text{Im}\{Z_T(j\omega)\} = 0$, which results in the equation:

$$\omega^6a_3b_4 + \omega^4(b_3a_2 - a_3b_2 - a_1b_4) + \omega^2(a_3b_o + a_1b_2 - b_1a_2 - b_3a_o) + (a_ob_1 - a_1b_o) = 0 \qquad (6.6)$$

Equation 6.6 is a cubic in ω^2, and cannot readily be solved without loss of generality. However, it may have either one, two, or three real solutions in ω^2.

Note that if $(a_o b_1 - a_1 b_o) = 0$, a trivial solution to (6.6) is $\omega^2 = 0$. Substituting the values of a_o, b_1, a_1, and b_o into the above, the result is that $Q_1{}^2 = 1$. i.e.

$$a_o b_1 = R_1(R_1C_1 + R_2C_2) = R_1{}^2C_1 + R_1R_2C_2 \quad ; \text{ and}$$

$$a_1 b_o = L_1 + R_1R_2C_2 \;, \quad \text{so that}$$

$$R_1{}^2C_1 = L_1 \;, \quad \text{or} \quad \frac{L_1}{R_1{}^2C_1} = Q_1{}^2 = 1.$$

Since for a single tank circuit, $\omega_o{}^2 = \dfrac{1}{L_1C_1}\left(1 - \dfrac{1}{Q_1{}^2}\right)$, the above corresponds to the case where the primary circuit is not resonant.

Because of the inconvenience that would be involved in analytically solving Eq. 6.6, a numerical means of determining the resonant frequencies will now be developed. This method will also permit a certain amount of optimization of the resonant states if it be desired.

Consider the circuit shown in Fig. 6.2(a), where

$$Z_1(S) = \frac{V_1(S)}{I_1(S)} \tag{6.7}$$

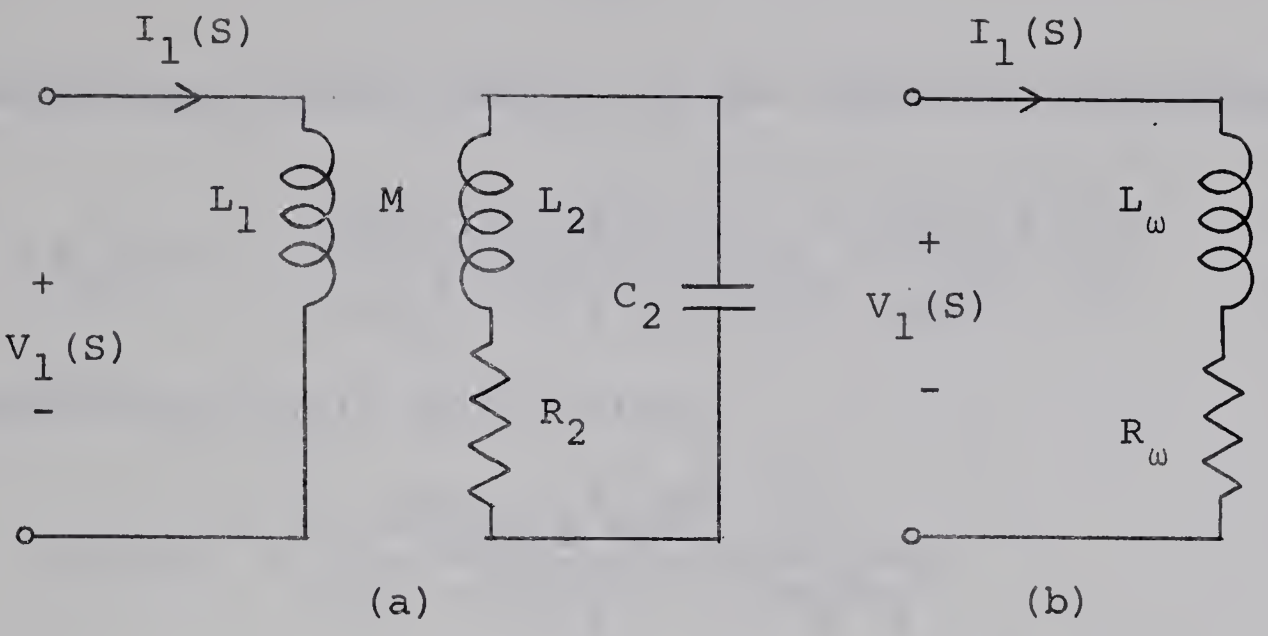

Figure 6.2
Equivalent Circuits

Analysis shows that

$$Z_1(S) = SL_1 \frac{\{S^2L_2C_2(1-K^2) + SR_2C_2 + 1\}}{(S^2L_2C_2 + SR_2C_2 + 1)} \qquad (6.8)$$

and

$$Z_1(j\omega) = j\omega L_1 \frac{\{1 - \omega^2L_2C_2(1-K^2) + j\omega R_2C_2\}}{(1 - \omega^2L_2C_2) + j\omega R_2C_2} \qquad (6.9)$$

Equation 6.9 can be written as

$$Z_1(j\omega) = j\omega L_1 \frac{(\alpha_1 + j\beta)}{(\alpha_2 + j\beta)}\ , \qquad (6.10)$$

where

$$\alpha_1 = 1 - \omega^2L_2C_2(1-K^2)$$
$$\alpha_2 = 1 - \omega^2L_2C_2\ , \quad \text{and} \qquad (6.11)$$
$$\beta = \omega R_2C_2\ .$$

Rationalizing (6.10) results in the following expression:

$$Z_1(j\omega) = \frac{\omega L_1 \beta(\alpha_1 - \alpha_2)}{(\alpha_2^2 + \beta^2)} + j\omega L_1 \frac{(\alpha_1\alpha_2 + \beta^2)}{(\alpha_2^2 + \beta^2)} \quad . \qquad (6.12)$$

Substituting (6.11) into (6.12);

$$Z_1(j\omega) = \frac{\omega^4 L_1 L_2 C_2{}^2 R_2 K^2}{(1 - \omega^2 L_2 C_2)^2 + \omega^2 R_2{}^2 C_2{}^2}$$

$$+ \frac{j\omega L_1 \left[(1-\omega^2 L_2 C_2)\{1-\omega^2 L_2 C_2(1-K^2)\} + \omega^2 R_2{}^2 C_2{}^2\right]}{(1 - \omega^2 L_2 C_2)^2 + \omega^2 R_2{}^2 C_2{}^2} \qquad (6.13)$$

If Im $\{Z_1(j\omega)\}$ is defined as $j\omega L_\omega$, and Re$\{Z_1(j\omega)\}$ as R_ω, (6.13) can be written as

$$Z_1(j\omega) = R_\omega + j\omega L_\omega \ . \qquad (6.14)$$

Thus, it can be concluded that the two circuits in Fig. 6.2 will have identical impedances.

Normalized frequency, u, can now be defined such that

$$u^2 = \omega^2 L_2 C_2 \ ; \qquad (6.15)$$

and Q_2 such that

$$Q_2{}^2 = \frac{L_2}{R_2{}^2 C_2} \ . \qquad (6.16)$$

Note that u, as defined above, has a different meaning than in Eq. 3.5.

Also, let $R_n = \dfrac{R_\omega}{R_1}$, and (6.17)

$$L_n = \frac{L_\omega}{L_1} \qquad (6.18)$$

Substituting (6.15) and (6.16) into (6.14), the results are:

$$L_n = \frac{L_\omega}{L_1} = \frac{\left[(1-u^2)\{1-u^2(1-K^2)\} + \frac{u^2}{{Q_2}^2}\right]}{\{(1-u^2)^2 + u^2/{Q_2}^2\}} \; ; \qquad (6.19)$$

and

$$R_n = \frac{R_\omega}{R_1} = \frac{u^4K^2\left(\frac{L_1}{L_2}\frac{R_2}{R_1}\right)}{\{(1-u^2)^2 + u^2/{Q_2}^2\}} \qquad (6.20)$$

The quantity F_f shall now be defined as

$$F_f = \sqrt{\frac{L_2C_2}{L_1C_1}} \qquad (6.21)$$

This is approximately the ratio of the resonant frequency of the primary tank circuit to that of the secondary. Also Q_e shall be defined as

$$Q_e = \frac{Q_1}{F_f} \qquad (6.22)$$

Consider now the ratio Q_e/Q_2, as given by (6.22), (6.21) and (6.16).

$$\frac{Q_e}{Q_2} = \frac{Q_1}{Q_2F_f} = \frac{1}{R_1}\sqrt{\frac{L_1}{C_1}} \cdot R_2\sqrt{\frac{C_2}{L_2}} \cdot \sqrt{\frac{L_1C_1}{L_2C_2}}$$

$$= \frac{R_2}{R_1}\frac{L_1}{L_2} . \qquad (6.23)$$

Now, by (6.23),(6.20) can be written as

$$R_n = \frac{u^4K^2(Q_e/Q_2)}{(1-u^2)^2 + u^2/{Q_2}^2} \qquad (6.24)$$

If all previous definitions are kept in mind, the circuit of Fig. 6.1 can now be represented by the one shown in Fig. 6.3.

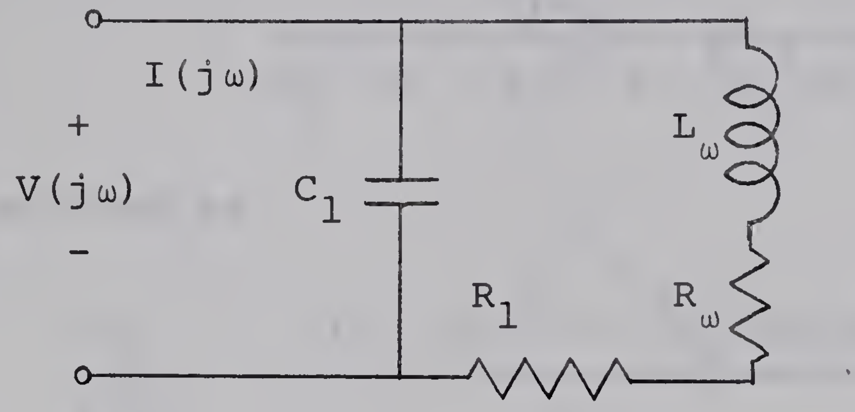

Figure 6.3
Equivalent Circuit for Mutually Coupled Tank Circuits

For this circuit,

$$Y_T(j\omega) = \frac{1}{Z_T(j\omega)}$$

$$= j\omega C_1 + \frac{1}{(R_1 + R_\omega) + j\omega L_\omega}$$

$$= j\omega C_1 + \frac{(R_1 + R\ ) - j\omega L_\omega}{(R_1 + R_\omega)^2 + \omega^2 L_\omega^2} \ . \qquad (6.25)$$

For resonance, $\text{Im}\{Y_T(j\omega)\} = 0$, or

$$C_1 = \frac{L_\omega}{(R_1 + R_\omega)^2 + \omega^2 L_\omega^2} \qquad (6.26)$$

But $L_\omega = L_1 L_n$, and $R_\omega = R_1 R_n$, so that (6.26) can be written as

$$C_1 = \frac{L_1 L_n}{R_1^2(1 + R_n)^2 + \omega^2 L_1^2 L_n^2}$$

$$= \frac{L_1 L_n}{R_1^2\{(1 + R_n)^2 + \omega^2 L_n^2 (L_1/R_1)^2\}}$$

This can be written as

$$\frac{L_1}{R_1^2 C_1} = \frac{(1 + R_n)^2 + \omega^2 L_n^2 (L_1/R_1)^2}{L_n} .$$

But

$$\frac{L_1}{R_1^2 C_1} = Q_1^2 \quad , \quad \text{so that}$$

$$Q_1^2 = \frac{(1 + R_n)^2 + \omega^2 L_n^2 (L_1/R_1)^2}{L_n} \qquad (6.27)$$

By Eq. 6.12, the term $\omega^2 (L_1/R_1)^2$ can be expressed as $(u^2/L_2C_2)(L_1/R_1)^2$.

Consider now the ratio Q_1^2/F_f^2. Since $Q_1^2 = L_1/R_1^2C_1$, and $F_f^2 = L_2C_2/L_1C_1$,

$$\frac{Q_1^2}{F_f^2} = \frac{L_1}{R_1^2 C_1} \cdot \frac{L_1 C_1}{L_2 C_2} = \frac{1}{L_2 C_2} \left(\frac{L_1}{R_1}\right)^2 .$$

Thus,

$$\omega^2 \left(\frac{L_1}{R_1}\right)^2 = u^2 \frac{Q_1^2}{F_f^2} . \quad \text{But from (6.22)}$$

$Q_1^2/F_f^2 = Q_e^2$, so that (6.27) can now be written as

$$Q_1^{\ 2} = \frac{(1 + R_n)^2 + u^2 Q_e^{\ 2} L_n^{\ 2}}{L_n} \qquad (6.28)$$

Substituting (6.19) and (6.24) into (6.28), the resulting equation is

$$Q_1^{\ 2} = \frac{\{(1-u^2)^2 + \frac{u^2}{Q_2^{\ 2}} + u^4 K^2 \frac{Q_e}{Q_2}\}^2 + u^2 Q_e^{\ 2}\{(1-u^2)\{1-u^2(1-K^2)\} + \frac{u^2}{Q_2^{\ 2}}\}^2}{\{(1-u^2)^2 + \frac{u^2}{Q_2^{\ 2}}\}\{(1-u^2)\{1-u^2(1-K^2)\} + \frac{u^2}{Q_2^{\ 2}}\}} \qquad (6.29)$$

The solution to Eq. 6.29 now determines the resonant frequencies to the circuit shown in Fig. 6.1.

The right-hand-side of Eq. 6.29 shall be defined as $F(u^2,K^2)$, so that (6.29) can be written as

$$Q_1^{\ 2} = F(u^2,K^2) \qquad (6.30)$$

It should now be pointed out that there are only two independent parameters in $F(u^2,K^2)$. i.e. Q_2 and Q_e. If Q_2 and Q_e are specified, and the function is evaluated and plotted, u^2, (for resonance) will be determined by the intersections of the line at $Q_1^{\ 2}$ with the function. Thus, in varying $Q_1^{\ 2}$, the solutions can be shifted one way or the other as desired. It must be kept in mind, however, that in varying Q_1, Q_e must remain constant, and since $Q_e = Q_1/F_f$, it follows that F_f must be varied correspondingly.

6.2 Discussion of $F(u^2,K^2)$

Since Eq. 6.30 determines the resonant frequencies for any value of K^2, it must also apply for $K^2 = 0$, which corresponds to a single tuned circuit. Letting $K^2 = 0$,

$$F(u^2,0) = 1 + Q_e^2 u^2 \tag{6.31}$$

Thus, from (6.30),

$$1 + Q_e^2 u^2 = Q_1^2$$

or

$$u^2 = \frac{Q_1^2 - 1}{Q_e^2} . \quad \text{But } Q_e^2 = \frac{Q_1^2}{F_f^2} ,$$

so that $u^2 = \dfrac{(Q_1^2 - 1)F_f^2}{Q_1^2} = F_f^2(1 - \dfrac{1}{Q_1^2})$ (6.32)

Now $u^2 = \omega^2 L_2 C_2$, and $F_f^2 = \dfrac{L_2 C_2}{L_1 C_1}$. Thus, (6.32) can be expressed as

$$\omega^2 L_2 C_2 = \frac{L_2 C_2}{L_1 C_1} (1 - \frac{1}{Q_1^2}) , \quad \text{or}$$

$$\omega = \frac{1}{\sqrt{L_1 C_1}} \sqrt{1 - \frac{1}{Q_1^2}} .$$

This is the resonant frequency for a single tank circuit.

In the following discussion, only positive values of u^2 are considered.

Referring again to Eq. 6.31, it is seen that for $K^2 = 0$, $F(u^2,K^2)$ is a straight line, with a vertical intercept

of one, and a slope of Q_e^2. Also, it can be shown that $\lim_{u^2 \to 0} F(u^2,K^2) = 1$, and $\lim_{u^2 \to \infty} F(u^2,K^2) = \infty$.

Further inspection of (6.29) indicates that the numerator of $F(u^2,K^2)$ must always be greater than zero, because the first term must always be positive, and the second term must always be positive or zero. Furthermore, the first term in the denominator must always be positive. Hence, the sign of $F(u^2,K^2)$ will be the same as that of the second term in the denominator, and $F(u^2,K^2)$ will have vertical as~~s~~ymptotes wherever this term is zero; or

$$(1 - u^2)\left[1 - u^2(1 - K^2)\right] + \frac{u^2}{Q_2^2} = 0 \qquad (6.33)$$

Equation 6.33 can be rewritten as

$$u^4(1 - K^2) - u^2(2 - K^2 - \frac{1}{Q_2^2}) + 1 = 0 \qquad (6.34)$$

The roots of this are

$$u^2 = \frac{(2 - K^2 - \frac{1}{Q_2^2}) \pm \sqrt{(2-K^2 - 1/Q_2^2)^2 - 4(1-K^2)}}{2(1 - K^2)} \qquad (6.35)$$

Consider first the case for which there is only one as~~s~~ymptote, or one root to (6.34). i.e. $(2 - K^2 - \frac{1}{Q_2^2})^2 = 4(1 - K^2)$; which can be written as

$$K^4 + 2\frac{K^2}{Q_2^2} - (\frac{4}{Q_2^2} - \frac{1}{Q_2^4}) = 0$$

From this,

$$K^2 = \frac{-\frac{2}{Q_2{}^2} \pm \sqrt{\frac{4}{Q_2{}^4} + 4\left(\frac{4}{Q_2{}^2} - \frac{1}{Q_2{}^4}\right)}}{2}$$

$$= -\frac{1}{Q_2{}^2} \pm \frac{2}{Q_2} \; ; \quad \text{or}$$

$$K^2 = \frac{2}{Q_2} - \frac{1}{Q_2{}^2} \; . \qquad (6.36)$$

Substituting (6.36) into (6.35)

$$u^2 = \frac{2 - \frac{2}{Q_2} + \frac{1}{Q_2{}^2} - \frac{1}{Q_2{}^2}}{2\left(1 - \frac{2}{Q_2} + \frac{1}{Q_2{}^2}\right)} \text{ , which simplifies}$$

to

$$u^2 = \frac{Q_2}{Q_2 - 1} \; . \qquad (6.37)$$

The final location of the two as~~s~~ymptotes, as $K_2 \rightarrow 1$, can easily be found. Equation 6.35 can be written as

$$u^2 = \frac{N_1(K^2)}{D(K^2)} \text{ , or } \quad u^2 = \frac{N_2(K^2)}{D(K^2)} \text{ ; where:}$$

(1) $\lim\limits_{K^2 \rightarrow 1} N_1(K^2) = \left(1 - \frac{1}{Q_2{}^2}\right) + \left(1 - \frac{1}{Q_2{}^2}\right) = 2\left(1 - \frac{1}{Q_2{}^2}\right)$;

(2) $\lim\limits_{K^2 \rightarrow 1} N_2(K^2) = \left(1 - \frac{1}{Q_2{}^2}\right) - \left(1 - \frac{1}{Q_2{}^2}\right) = 0$; and

(3) $\lim\limits_{K^2 \rightarrow 1} D(K^2) = 0$.

Thus,

$$\lim_{K^2\to 1} \frac{N_1(K^2)}{D(K^2)} = \infty \; . \tag{6.38}$$

By the application of l'Hospital's Rule,

$$\lim_{K^2\to 1} \frac{N_2(K^2)}{D(K^2)} = \lim_{K^2\to 1} \frac{N_2'(K^2)}{D'(K^2)} \; .$$

$$N_2'(K^2) = \frac{d}{dK^2}\left[(2 - K^2 - \frac{1}{Q_2^{\,2}}) - \sqrt{(2 - K^2 - 1/Q_2^{\,2})^2 - 4(1-K^2)}\right]$$

$$= -1 - \frac{-2(2 - K^2 - 1/Q_2^{\,2}) + 4}{2\sqrt{(2-K^2-1/Q_2^{\,2})^2 - 4(1-K^2)}} \; .$$

Similarly

$$D'(K^2) = \frac{d}{dK^2}\left[2(1-K^2)\right] = -2$$

Thus,

$$\frac{N_2'(K^2)}{D'(K^2)} = \frac{1}{2} + \frac{1}{4}\,\frac{-2(2 - K^2 - \frac{1}{Q_2^{\,2}}) + 4}{\sqrt{(2-K^2-1/Q_2^{\,2})^2 - 4(1-K^2)}}$$

Letting $K^2 = 1$, and simplifying,

$$\lim_{K^2\to 1} \frac{N_2'(K^2)}{D'(K^2)} = u^2 = \frac{Q_2^{\,2}}{Q_2^{\,2} - 1} \tag{6.39}$$

The preceding discussion can now be summarized by the following properties:

(1) $$\lim_{K^2\to 0} F(u^2,K^2) = 1 + Q_e^{\,2}u^2 \;;$$

(2) $$\lim_{u^2\to 0} F(u^2,K^2) = 1 \;;$$

(3) $$\lim_{u^2\to \infty} F(u^2,K^2) = \infty \;;$$

(4) if $K^2 < \dfrac{2}{Q_2} - \dfrac{1}{Q_2^{\,2}}$; $F(u^2,K^2)$ is positive and continuous;

(5) if $K^2 = \dfrac{2}{Q_2} - \dfrac{1}{Q_2^{\,2}}$; $F(u^2,K^2)$ is positive and has one vertical as~~s~~ymptote at $u^2 = \dfrac{Q_2}{Q_2 - 1}$;

(6) if $K^2 > \dfrac{2}{Q_2} - \dfrac{1}{Q_2^{\,2}}$; $F(u^2,K^2)$ has two vertical as~~s~~ymptotes (given by Eq. 6.35) between which it is negative. Everywhere else it is positive; and

(7) as $K^2 \to 1$, these as~~s~~ymptotes approach $+\infty$ and $\dfrac{Q_2^{\,2}}{Q_2^{\,2} - 1}$.

Properties (2) and (3) are sufficient conditions for the existence of one resonant frequency, for any K^2, provided that $Q_1^{\,2} > 1$. Note that $Q_1^{\,2} = 1$ corresponds to the case where the primary circuit is non-resonant, as was discussed in Sec. 6.1.

Properties (2), (5), (6), and (7) are sufficient conditions (if $Q_1^{\,2} > 1$) for the existence of one resonant frequency in the region $0 < u^2 < \dfrac{Q_2}{Q_2 - 1}$, provided that

$$K^2 \geq \frac{2}{Q_2} - \frac{1}{Q_2^{\,2}}$$

Property (6) is a sufficient condition that no resonant frequency can exist in the region between the two as~~s~~ymptotes.

Properties (6) and (7) are sufficient conditions that, for $K^2 = 1$, no resonant frequency can exist for which

$$u^2 \geq \frac{Q_2^{\,2}}{Q_2^{\,2} - 1} \quad .$$

Since for every finite value of u^2 beyond the second as~~s~~ymptote, $F(u^2,K^2)$ is positive and finite, properties (3) and (6) are sufficient conditions for the existence of two resonant frequencies in this region, providing $Q_1^{\,2}$ is sufficiently large.

A sketch of $F(u^2,K^2)$, corresponding to the range $\frac{2}{Q_2} - \frac{1}{Q_2^{\,2}} < K^2 < 1$, is shown in Fig. 6.4. The portions of the curve represented by dashed lines indicate that the exact nature of the function in these regions is not known. It is only known that the function must be continuous and of fixed sign, so that the possibility of relative extrema has not been excluded.

The exact nature of $F(u^2,K^2)$ for $K^2 < \frac{2}{Q_2} - \frac{1}{Q_2^{\,2}}$, is very difficult to determine. If the function is differentiated

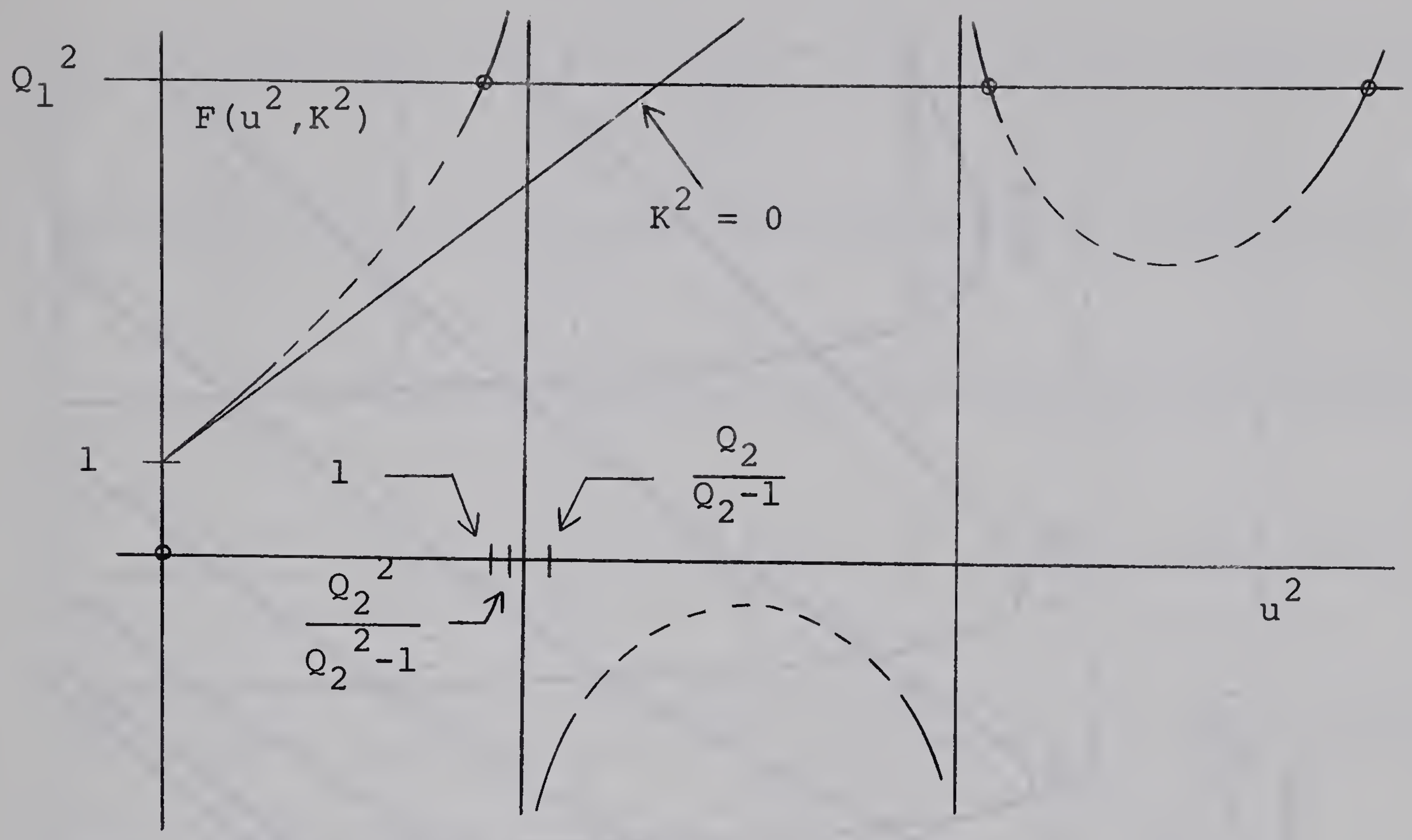

Figure 6.4
Approximate Form of $F(u^2,K^2)$

and equated to zero, the resulting equation is considerably more complex than the original cubic in ω^2 (Eq. 6.6). Thus, such an undertaking is impractical.

Assuming Q_2 as 50 and Q_e as $\sqrt{50}$, $F(u^2,K^2)$ has been evaluated by means of a digital computer, and the resulting curves (corresponding to different values of K^2) are shown in Fig. 6.5. Only positive values of the function are shown, and only positive values of u^2 are considered. The curves are seen to agree qualitatively with the sketch in Fig. 6.4.

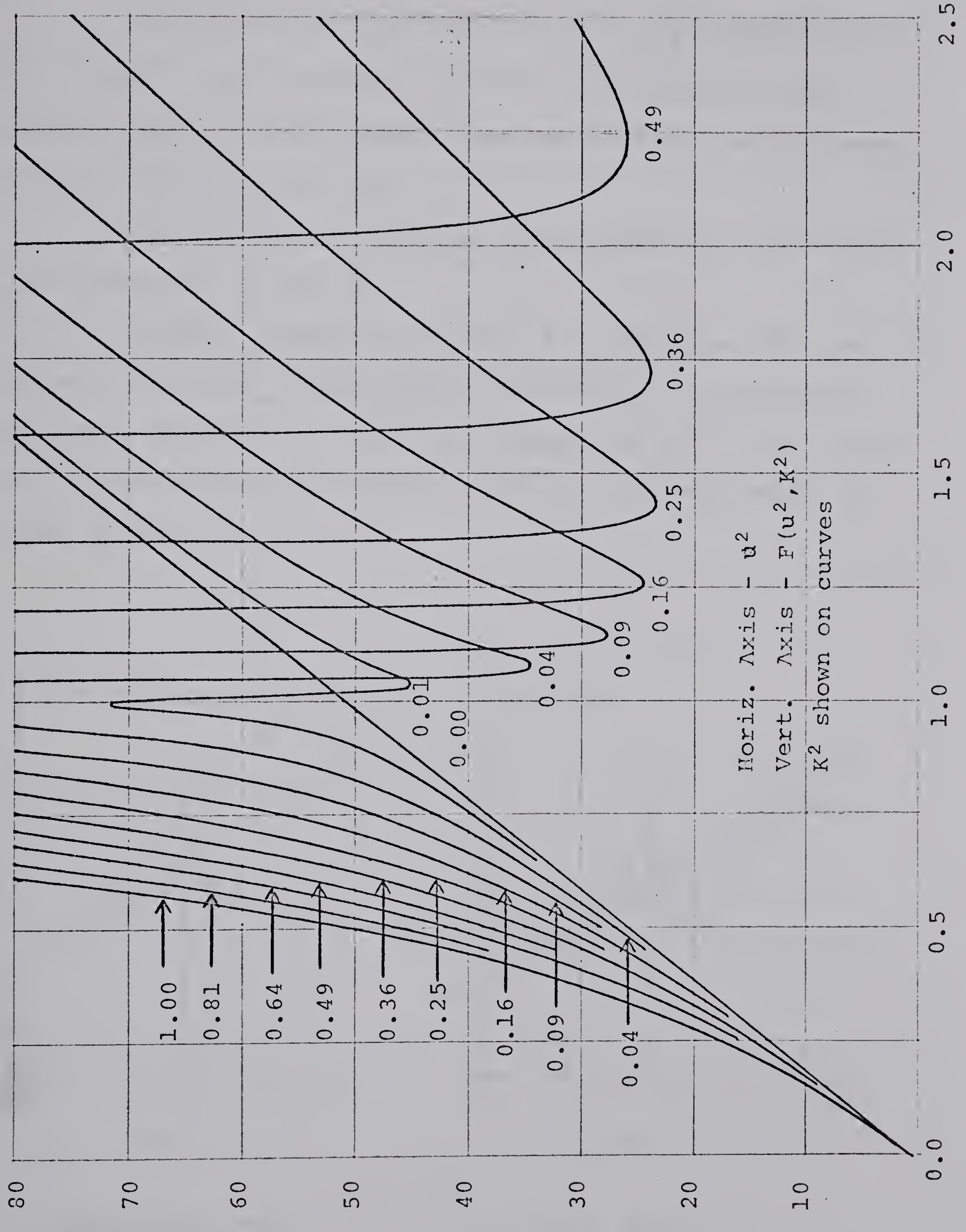

Figure 6.5
Graph of F (u^2, K^2)

Note that for $Q_2 = 50$, $K^2 = \frac{2}{Q_2} - \frac{1}{Q_2^{\,2}}$ corresponds to $K^2 = 0.0396$. Thus the curve for $K^2 = 0.01$ should be continuous, and all others should have two vertical as~~s~~ymptotes. This is seen to be the case.

The reason for choosing Q_2 considerably larger than Q_e is discussed in Sec. 6.7.

Careful inspection of Fig. 6.5 indicates that two uniquely different situations can occur as K^2 is increased from zero, depending on the value chosen for $Q_1^{\,2}$. Fig. 6.6(a) and (b) illustrate the nature of $F(u^2,K^2)$ for very small K^2, as can be seen in Fig. 6.5.

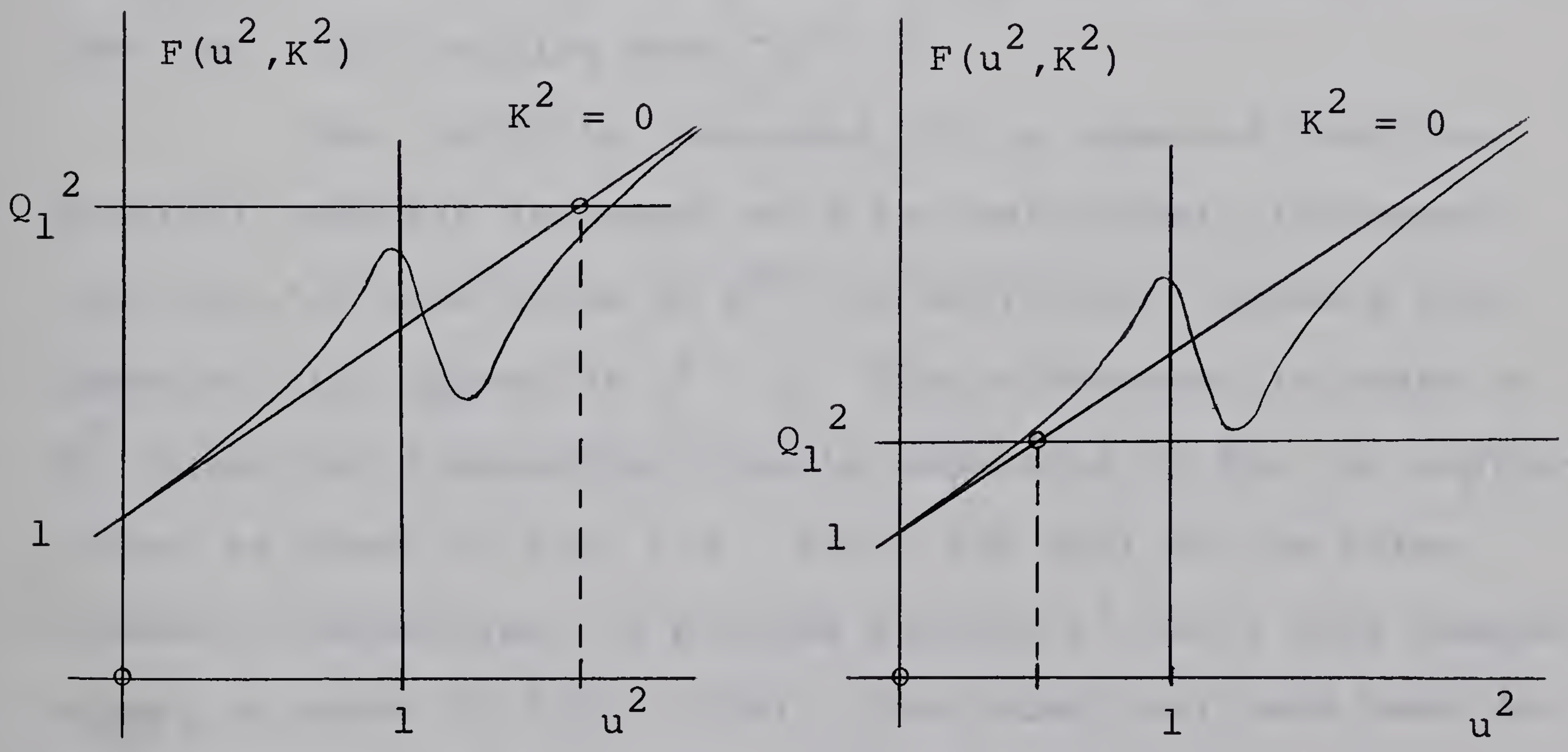

(a) (b)

Figure 6.6

Approximate Form of $F(u^2,K^2)$ for Very Small K^2

Note that the relative maximum appears to occur for u^2 slightly less than one. This is approximately the same place as the as~~s~~ymptotes first appear.

Consider first Fig. 6.6(a). With reference to Fig. 6.5, this could correspond to $Q_1^2 \simeq 80$. It is apparent that for $K^2 = 0$, u^2 (for resonance) is considerably larger than one. Since for $K^2 = 0$, $F(u^2,K^2) = 1 + Q_e^2u^2$, this value of u^2 is determined by the equation

$$1 + Q_e^2u^2 = Q_1^2 \quad , \qquad \text{or} \qquad u^2 = \frac{Q_1^2 - 1}{Q_e^2}$$

$$= F_f^2\left(1 - \frac{1}{Q_1^2}\right). \quad \text{(From 6.31)}$$

If $Q_1^2 >> 1$, $u^2 \simeq F_f^2$. But since u^2 is considerably larger than one, this implies that $F_f^2 > 1$.

Now, as K^2 is increased, it is apparent that the original resonant frequency will be continuously increased, and that for some value of K^2, two additional resonant frequencies will appear at $u^2 \simeq 1$. Upon subsequent increase of K^2, these two frequencies will be separated by the two as~~s~~ymptotes, as shown in Fig. 6.4. Thus, the loci of the three resonant frequencies, if plotted against K^2, will look approximately as shown in Fig. 6.7(a). The three loci have been designated as State (1), State (2), and State (3).

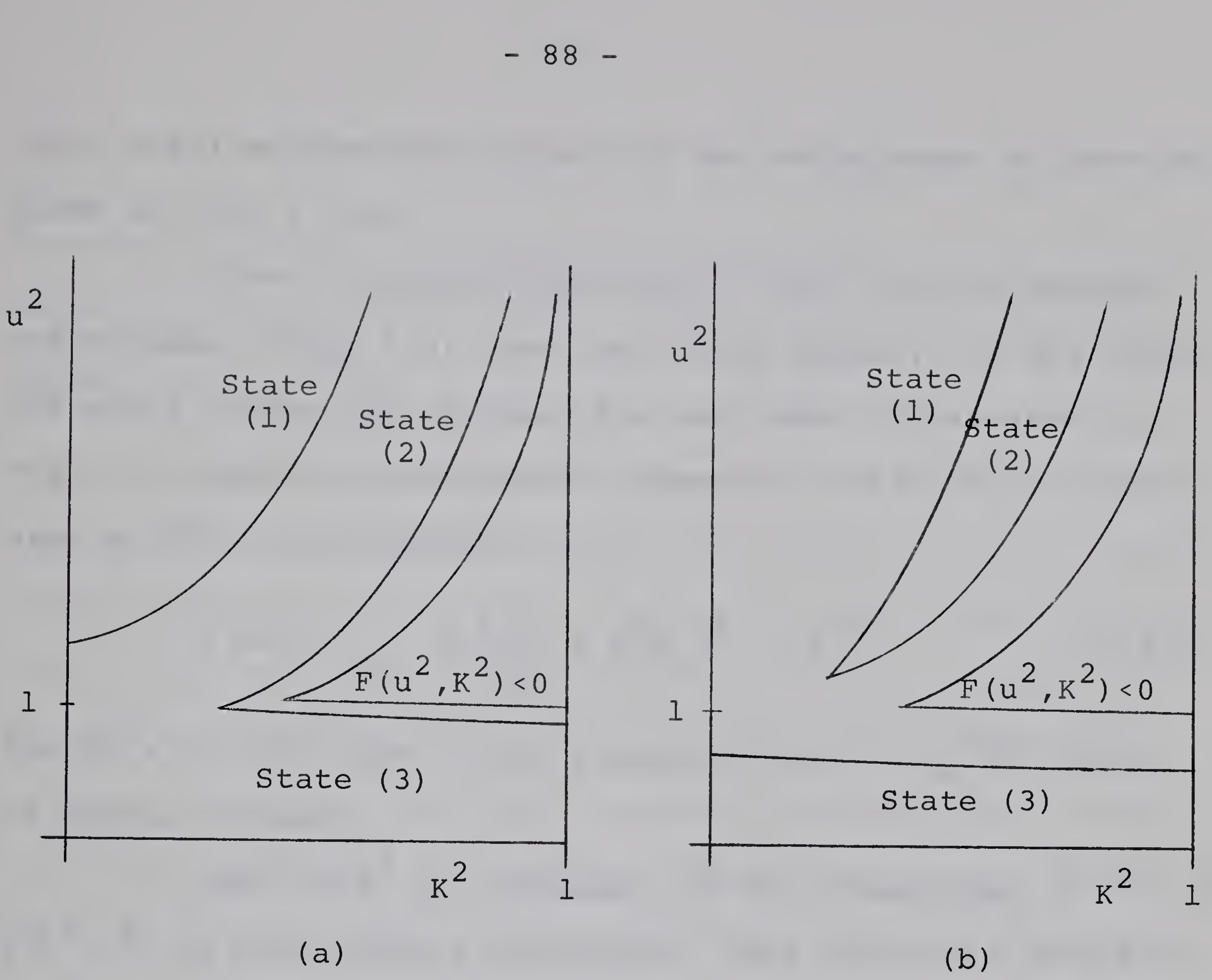

(a) (b)

Figure 6.7
Resonant Frequency Loci

Now consider the second situation, as shown in Fig. 6.6(b). This could correspond to $Q_1^{\,2} \simeq 40$. In this case, for $K^2 = 0$, u^2 is seen to be less than one. Again, for $K^2 = 0$, $u^2 \simeq F_f^{\,2}$ (if $Q_1^{\,2} >> 1$), so that $F_f^{\,2}$ must clearly be less than one.

As K^2 is now increased, the original resonant frequency is decreased, and two additional resonances will be introduced for u^2 somewhat greater than one. Again, the two lower frequencies will be separated by the two as~~s~~ymptotes

(Fig. 6.4); so that the three loci can be expected to look as shown in Fig. 6.7(b).

Since the exact locations of the relative maximum and minimum, (Fig. 6.6) when they first appear, are not known, the exact border-line between the two cases illustrated in Fig. 6.7 cannot be determined. However, if $F(u^2,K^2)$ is evaluated at $u^2 = 1$, the result is

$$F(1,K^2) = Q_2^{\,2}\left(\frac{1}{Q_2} + K^2Q_e\right)^2 + Q_e^{\,2} \qquad (6.40)$$

For $K^2 = 0$, this lies on the straight line $1 + Q_e^{\,2}u^2$, which of course it must.

Now, as K^2 is increased, (6.40) shows that at $u^2 = 1$, $F(u^2,K^2)$ is continuously increased. This indicates that the relative minimum (Fig. 6.6) must lie to the right of $u^2 = 1$. Furthermore, a solution, for $K^2 = 0$, at $u^2 = 1$, must be initially pushed to the left as K^2 is increased, and must therefore correspond to the situation shown in Fig. 6.7(b). For such a solution,

$$1 + Q_e^{\,2} = Q_1^{\,2}\,; \quad \text{(from Eq. 6.31)}$$

or

$$1 + \frac{Q_1^{\,2}}{F_f^{\,2}} = Q_1^{\,2}\,, \quad \text{from which}$$

$$F_f^{\,2} = \frac{Q_1^{\,2}}{Q_1^{\,2} - 1} \qquad (6.41)$$

Thus, it can be concluded that if $F_f^2 \leq \dfrac{Q_1^2}{Q_1^2 - 1}$, the resonant frequency loci must correspond to those shown in Fig. 6.7(b); and for the loci shown in Fig. 6.7(a), F_f^2 must be somewhat larger than $\dfrac{Q_1^2}{Q_1^2 - 1}$.

It is now noticed that State (1) and State (3) of Fig. 6.7(a) qualitatively resemble the experimentally observed pattern shown in Fig. 1.5(a). Also, the above conclusions concerning the magnitude of F_f^2 agree with the experimental observation mentioned in Sec. 1.4. It will in fact be shown (in Sec. 6.5) that the above situation can give rise to the switching phenomenon discussed in Sec. 1.4. However, before this can be done, the resonant resistance loci, corresponding to States (1), (2), and (3) must be determined.

6.3 Resistance at Resonance

Assuming that a numerical (or graphical) solution to Eq. 6.30 has been found, the impedance at the resulting resonant frequencies must now be determined.

R_o' shall be defined as the resistance of any resonant state, as determined by Eq. 6.30. Thus, for $K^2 = 0$, $R_o' = R_o$. Also, G_o' shall be defined as $1/R_o'$.

Referring now to Eq. 6.25, at resonance

$$Y_T(j\omega) = G_o' = \frac{(R_1 + R_\omega)}{(R_1 + R_\omega)^2 + \omega^2 L_\omega^2} \qquad (6.42)$$

Also, from (6.26),

$$C_1 = \frac{L_\omega}{(R_1 + R_\omega)^2 + \omega^2 L_\omega^{\ 2}} \quad ; \quad \text{which can}$$

be rearranged as

$$\omega^2 L_\omega^{\ 2} = \frac{L_\omega}{C_1} - (R_1 + R_\omega)^2 \qquad (6.43)$$

Substituting (6.43) into (6.42),

$$G_o' = \frac{(R_1 + R_\omega)}{(R_1 + R_\omega)^2 + \frac{L_\omega}{C_1} - (R_1 + R_\omega)^2}$$

$$= \frac{(R_1 + R_\omega)C_1}{L_\omega} \quad ; \qquad \text{or}$$

$$R_o' = \frac{L_\omega}{(R_1 + R_\omega)C_1} \quad . \qquad (6.44)$$

Recalling the definition of L_n and R_n (Eq's. 6.17 and 6.18), (6.44) can be written as

$$R_o' = \frac{L_1 L_n}{C_1 R_1 (1 + R_n)} \quad .$$

But $\frac{L_1}{R_1 C_L} = R_o$, so that $R_o' = R_o \frac{L_n}{1 + R_n}$, or

$$\frac{R_o'}{R_o} = \frac{L_n}{1 + R_n} \qquad (6.45)$$

Substituting (6.19) and (6.24) into (6.45),

$$\frac{R_o'}{R_o} = \frac{(1 - u^2)\left[1 - u^2(1 - K^2)\right] + \dfrac{u^2}{{Q_2}^2}}{(1 - u^2)^2 + \dfrac{u^2}{{Q_2}^2} + u^4K^2\dfrac{Q_e}{Q_2}} \qquad (6.46)$$

It must be kept in mind that Eq. 6.46 is valid only for values of u^2 as determined by Eq. 6.30.

6.4 Discussion of the Function R_o'/R_o

It should first be pointed out that only the same two parameters, Q_2 and Q_e, appear in this function as in $F(u^2,K^2)$. This is very important with respect to optimization, as it implies that both functions can be evaluated for a specified Q_e and Q_2. Furthermore, if Q_1 (and F_f) are varied, the corresponding variations, both in resonant frequencies and in resonant resistances, can be studied simultaneously.

It can easily be seen from (6.46) that $\lim\limits_{K^2\to 0} \dfrac{R_o'}{R_o} = 1$. This of course corresponds to a single tank circuit. Also

$$\lim_{u^2\to 0} \frac{R_o'}{R_o} = 1 \text{ , and} \qquad (6.47)$$

$$\lim_{u^2\to\infty} \frac{R_o'}{R_o} = \frac{1 - K^2}{1 + K^2\dfrac{Q_e}{Q_2}} \qquad (6.48)$$

Equation 6.48 represents a horizontal as~~s~~ymptote, which must lie between zero and one, for $0 < K^2 < 1$.

Since the denominator of R_o'/R_o must always be positive, and the numerator is the second factor in the denominator of $F(u^2,K^2)$, R_o'/R_o must have the same sign as $F(u^2,K^2)$, and must be zero where $F(u^2,K^2)$ has vertical as~~s~~ymptotes. Thus, at any solution to Eq. 6.30, R_o'/R_o must be greater than zero.

If R_o'/R_o is equated to one, the resulting equation is

$$(1-u^2)\left[1-u^2(1-K^2)\right] + \frac{u^2}{Q_2{}^2} = (1-u^2)^2 + \frac{u^2}{Q_2{}^2} + u^4K^2\frac{Q_e}{Q_2}$$

Upon simplification, this can be expressed as

$$u^2\left[1 - u^2(1 + \frac{Q_e}{Q_2})\right] = 0; \qquad \text{for } K^2 \neq 0 .$$

Thus,

$$u^2 = 0 \qquad \text{or} \qquad u^2 = \frac{1}{1 + \frac{Q_e}{Q_2}} . \tag{6.49}$$

Since there are only two points for which $R_o'/R_o = 1$, and since

$$\lim_{u^2\to\infty} \frac{R_o'}{R_o} = \frac{1 - K^2}{1 + K^2\frac{Q_e}{Q_2}}$$

, it follows that

$$\text{if} \quad 0 < u^2 < \frac{1}{1 + \frac{Q_e}{Q_2}}, \text{ then } \frac{R_o'}{R_o} > 1; \text{ and}$$

$$\text{if} \quad u^2 > \frac{1}{1 + \frac{Q_e}{Q_2}}, \text{ then } \frac{R_o'}{R_o} < 1. \tag{6.50}$$

Referring now to Fig. 6.4, (6.50) implies that for the two possible solutions to the right of the second asymptote, R_o'/R_o must be less than one, and for the solution to the left of the first asymptote, R_o'/R_o can be either greater or less than one.

It is also of interest to evaluate the function R_o'/R_o at $u^2 = 1$. The result is seen to be

$$\left.\frac{R_o'}{R_o}\right|_{u^2=1} = \frac{1}{1 + k^2 Q_e Q_2} \tag{6.51}$$

Figure 6.8 illustrates the general nature of R_o'/R_o (as concluded from the previous discussion) for $K^2 > \frac{2}{Q_2} - \frac{1}{Q_2^2}$. The relationship to the function $F(u^2, K^2)$ is also shown. The dashed lines again indicate regions of relative uncertainty as to the exact nature of the functions.

It is apparent from Fig. 6.8, that R_o'/R_o must have an absolute maximum in the region $0 < u^2 < \frac{1}{1 + Q_e/Q_2}$; and

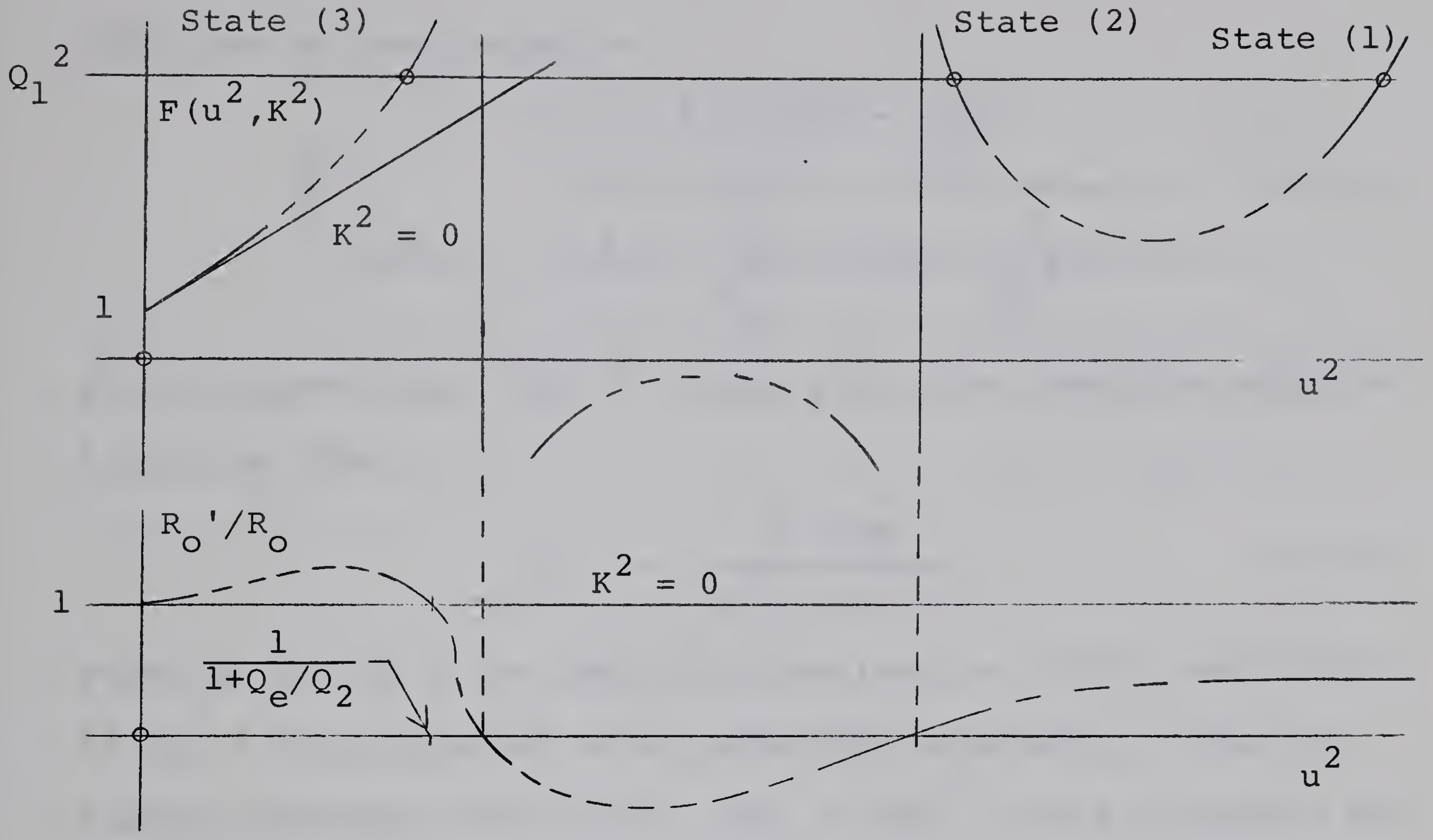

Figure 6.8
Approximate Form of R_o'/R_o and
its Relationship to $F(u^2,K^2)$

an absolute minimum in the region where the function is negative (for $K^2 > \frac{2}{Q_2} - \frac{1}{Q_2^{\,2}}$). The ordinate values of these extrema can quite easily be found for $K^2 = 1$. This will be of further assistance from the point of view of optimization. Letting $K^2 = 1$,

$$\left.\frac{R_o'}{R_o}\right|_{K^2=1} = \frac{(1-u^2) + \frac{u^2}{Q_2^{\,2}}}{(1-u^2)^2 + \frac{u^2}{Q_2^{\,2}} + \frac{u^4 Q_e}{Q_2}} \quad ;$$

which can be rearranged as

$$\left.\frac{R_o'}{R_o}\right|_{K^2=1} = \frac{1 - u^2(1 - \frac{1}{Q_2^{\,2}})}{u^4(1 + \frac{Q_e}{Q_2}) - u^2(2 - \frac{1}{Q_2^{\,2}}) + 1} \qquad (6.52)$$

If x is substituted for u^2 in Eq. 6.52, the resulting equation is of the form

$$y(x) = \frac{1 - ax}{bx^2 - cx + 1} \qquad (6.53)$$

where a, b, and c are implicitly defined by (6.53) and (6.52). If Eq. 6.53 is equated to an arbitrary constant, λ, the resulting equation will be $(1 - ax) = \lambda(bx^2 - cx + 1)$; which can be expressed as

$$x^2\lambda b - x(\lambda c - a) + (\lambda - 1) = 0 \qquad (6.54)$$

If Λ is now taken to represent an extreme value of R_o'/R_o, there can be only one solution to the equation

$x^2\Lambda b - x(\Lambda c - a) + (\Lambda - 1) = 0$; from which

$(\Lambda c - a)^2 = 4\Lambda b(\Lambda - 1)$. This can be rearranged

as

$$\Lambda^2(c^2 - 4b) + \Lambda(4b - 2ca) + a^2 = 0 . \qquad (6.55)$$

The two roots to (6.55) are

$$\Lambda = \frac{-(4b - 2ca) \pm \sqrt{(4b - 2ca)^2 - 4a^2(c^2 - 4b)}}{2(c^2 - 4b)}$$

which simplify to

$$\Lambda = \frac{(ca - 2b) \pm 2\sqrt{b^2 - abc + a^2b}}{c^2 - 4\,ab} \qquad (6.56)$$

If the values of a, b, and c are now substituted into Eq. 6.56 an exact expression for Λ can be obtained. However, if $Q_2^{\,2} >> 1$, then $a \simeq 1$, and $c \simeq 2$. No such approximation can be made for b, so that $b = 1 + Q_e/Q_2$. Substituting these values into (6.56) and simplifying,

$$\Lambda \simeq \frac{1}{2}\left(1 \pm \sqrt{1 + Q_2/Q_e}\right) \qquad (6.57)$$

Equation 6.57 indicates that the maximum possible resonant resistance is determined primarily by the ratio Q_2/Q_e.

The function R_o'/R_o has been evaluated for $Q_2 = 50$ and $Q_e = \sqrt{50}$, and is shown in Fig. 6.9. Substituting the above values into (6.57), $\Lambda \simeq 1.92$ and -0.92. These are seen to agree with the peaks shown in Fig. 6.9 (for $K^2=1$).

The resonant resistance loci, corresponding to the three resonant states shown in Fig. 6.7(a), can now be qualitatively determined. Consider first the locus designated as State (1). Since for this state, u^2 is always greater than one, it is apparent from Fig. 6.9, that for $K^2 > 0$, $R_o'/R_o < 1$. Also, as $K^2 \rightarrow 1$, $u^2 \rightarrow \infty$; and as $u^2 \rightarrow \infty$, $R_o'/R_o \rightarrow \dfrac{1 - K^2}{1+K^2\ Q_e/Q_2}$. This approaches zero as K^2 approaches one. Thus, the locus

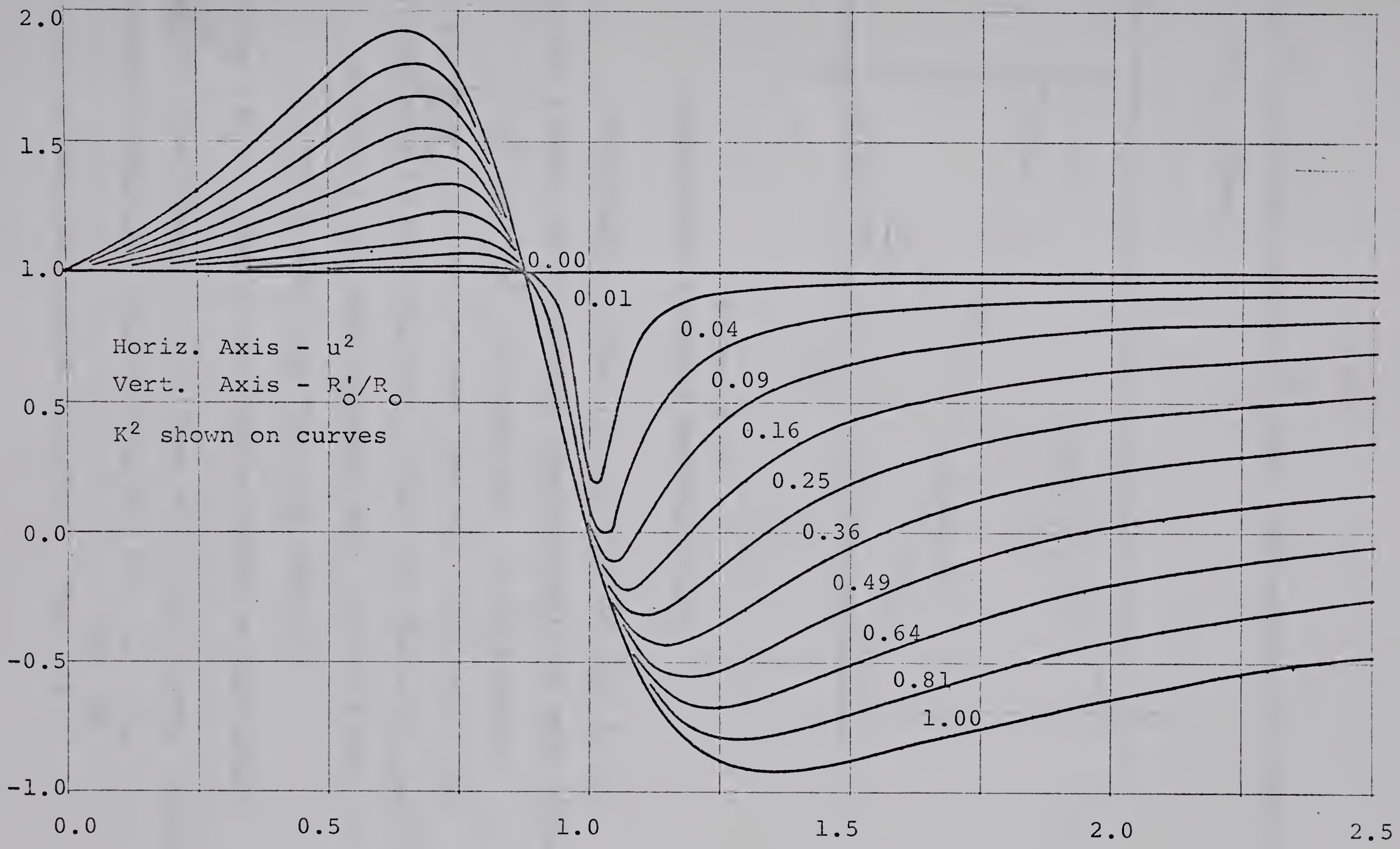

Figure 6.9

Graph of R'_o/R_o

of R_o'/R_o, plotted against K^2, must look somewhat as shown in Fig. 6.10, State (1) .

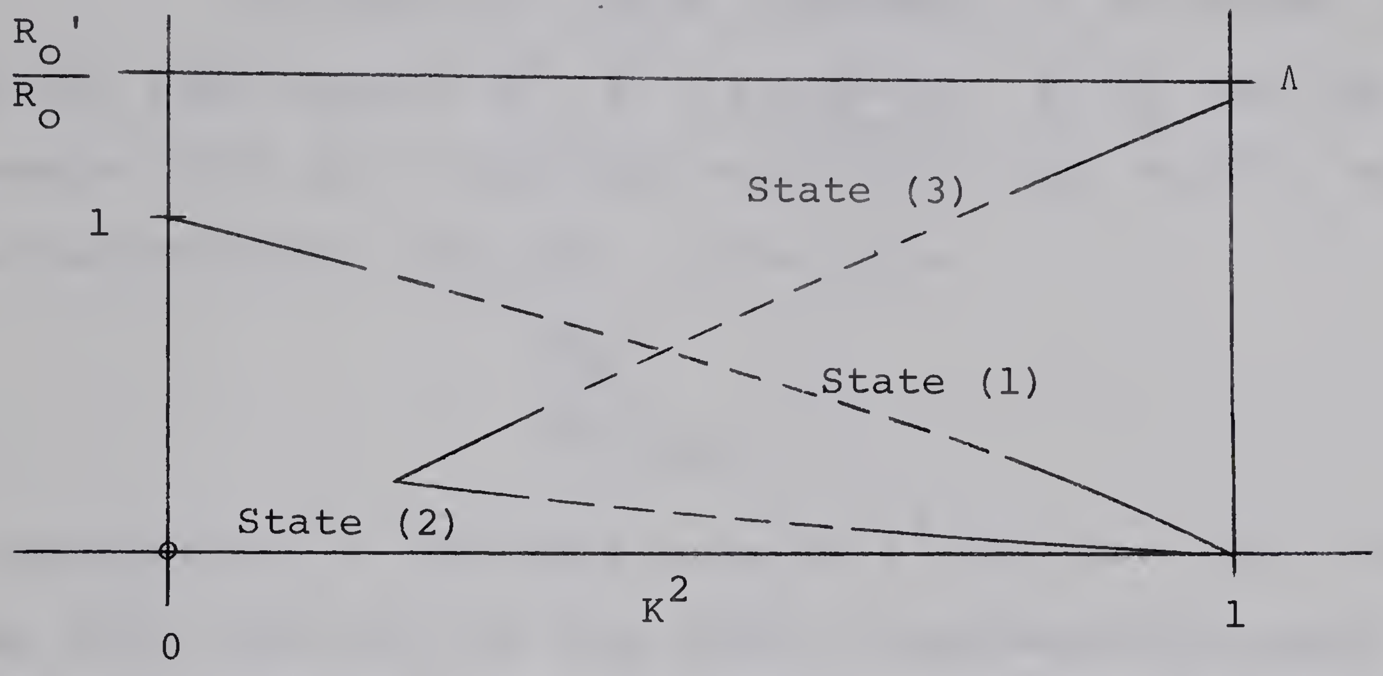

Figure 6.10
Approximate Resonant Resistant Loci

Now consider States (2) and (3), of Fig. 6.7(a). These two states are introduced simultaneously at some value of u^2. If $Q_1^{\ 2}$ (and $F_f^{\ 2}$) are such that, at this point, $u^2 > \dfrac{1}{1 + Q_e/Q_2}$, it can be seen from Fig. 6.8 that R_o'/R_o must initially be less than one. Also, for State (2), as $K^2 \to 1$, $u^2 \to \infty$, so that R_o'/R_o must approach zero, as for State (1).

It can be seen from Fig. 6.8, that if $\dfrac{2}{Q_2} - \dfrac{1}{Q_2^{\ 2}} < K^2 < 1$, State (2) will be closer to the second asymptote than State (1), and thus will have a lower resonant resistance. This will also be true for $K^2 < \dfrac{2}{Q_2} - \dfrac{1}{Q_2^{\ 2}}$ if State (2) is near the minimum of R_o'/R_o (Fig. 6.9).

Thus, the locus of R_o'/R_o for State (2) must be approximately as shown in Fig. 6.10.

For State (3), as K^2 increases, u^2 decreases. Hence, if for some value of K^2, $u^2 < \frac{1}{1 + Q_e/Q_2}$, R_o'/R_o must be greater than one. The final value of R_o'/R_o, as $K^2 \rightarrow 1$, will be determined by the point on the curve

$$\left. \frac{R_o'}{R_o} \right|_{K^2=1} ,$$

corresponding to the final value of u^2 for State (3). From Eq. 6.57, this must be less than, or approximately equal to $\frac{1}{2}(1 + \sqrt{1 + Q_2/Q_e})$. The approximate shape of the locus R_o'/R_o for State (3) is shown in Fig. 6.10.

By careful inspection of Fig's. 6.5 and 6.9, it can be seen that the general forms of loci indicated in Fig's. 6.7(a) and 6.10 can be realized if Q_1^2 is chosen as 70. Since $F_f^2 = Q_1^2/Q_e^2$, and $Q_e^2 = 50$, this implies that $F_f^2 = 70/50 = 1.4$.

Using $Q_2 = 50$, $Q_e = \sqrt{50}$, and $Q_1 = \sqrt{70}$, a digital computer has been used to numerically solve Eq. 6.30 (for different values of K^2), and subsequently to evaluate R_o'/R_o. The resulting resonant frequency and resonant resistance loci are shown in Fig's. 6.11 and 6.12. Note that R_o'/R_o is much less for State (2) than for State (3).

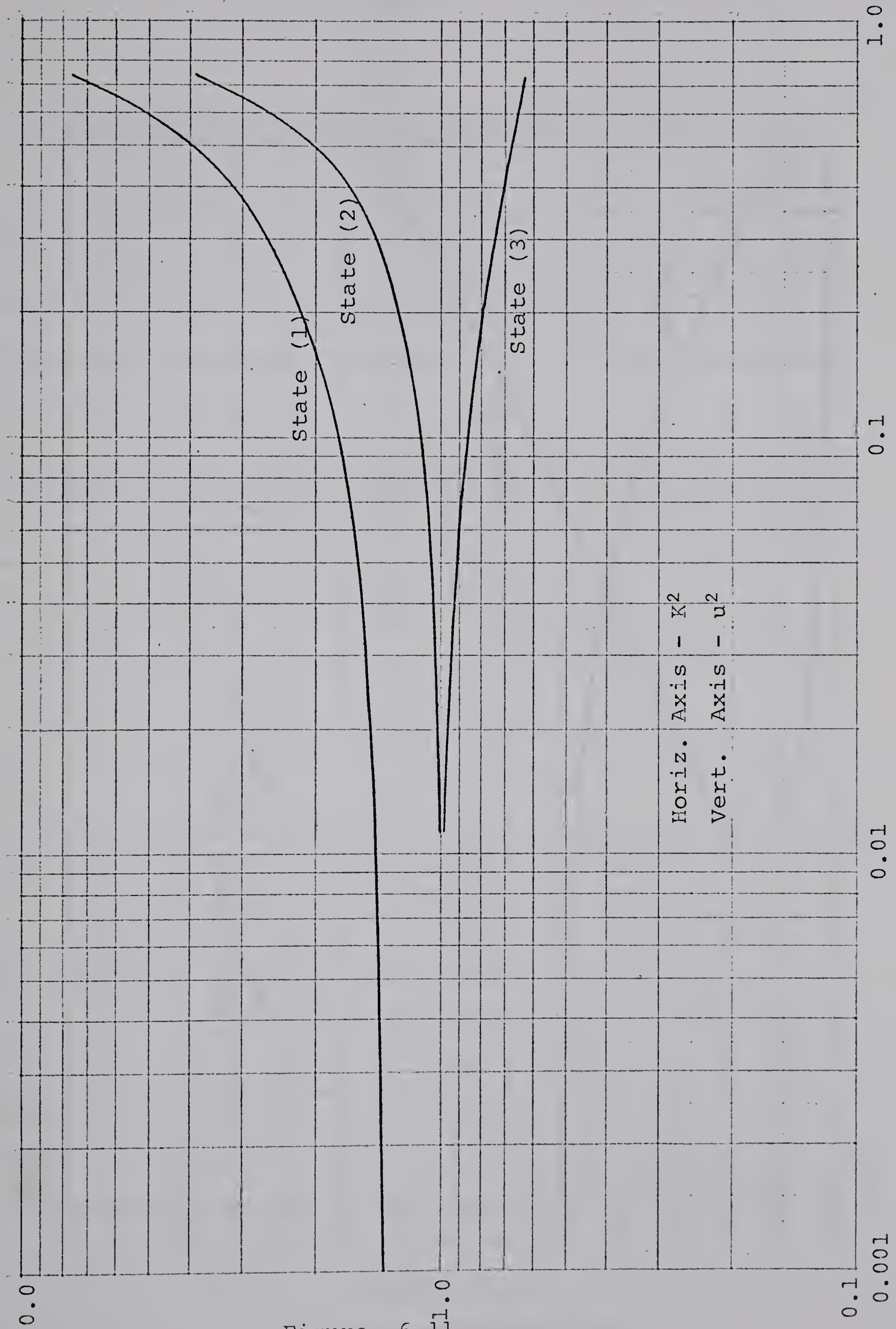

Figure 6.11

Resonant Frequency Loci

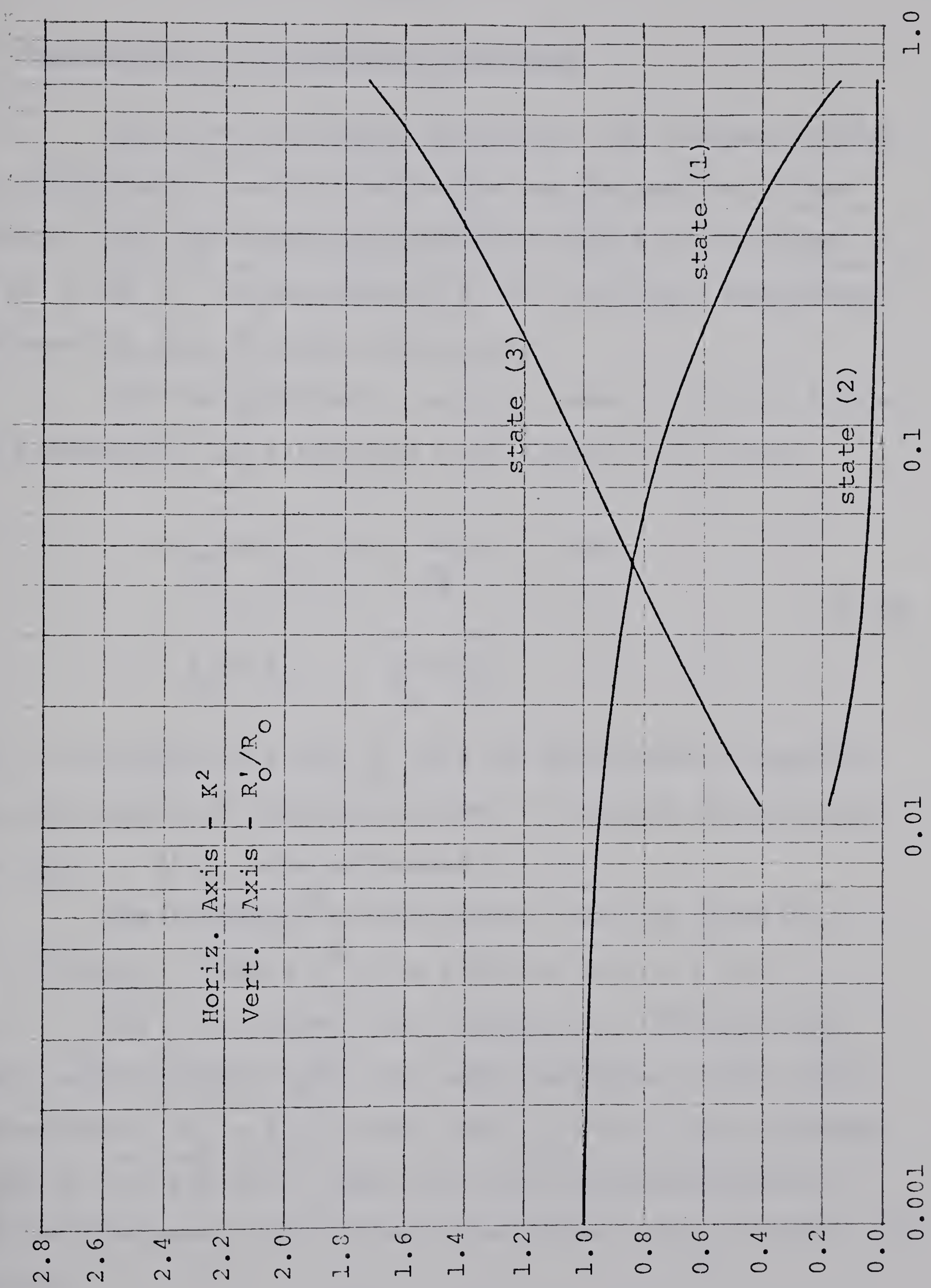

Figure 6.12

Resonant Resistance Loci

6.5 Explanation of Switching Phenomenon

The previous theory concerning the resonant states for the mutually tuned circuits can now be applied in conjunction with the describing function method as developed in Sec's. 4 and 5. An explanation of the switching phenomenon, discussed in Sec. 1.4 will thus result.

For the oscillator circuit shown in Fig. 1.4, the basic equations for sinusoidal oscillation will now be

$$\begin{aligned} G_{eq}(A,V_Q) &= -\frac{1}{R_o'}, \quad \text{and} \\ I_Q(A,V_Q) &= \frac{V_B - V_Q}{R_B + R_1}. \end{aligned} \tag{6.38}$$

Thus, a solution in A and V_Q will be determined in exactly the same manner as described in Sec. 5, except that the contour $G_{eq} = -1/R_o'$ must be chosen.

The frequency of oscillation will be given by $\omega_o^2 = u^2/L_2C_2$; where u^2 is a solution to Eq. 6.30.

Fig. 6.13 shows four contours on a Constant-G_{eq} Chart, and the curve $V_Q(A)$ for some load-line. This could correspond to $(R_1 + R_B) = 125\Omega$, and $V_B = 237.5$ mv, as shown in Fig's. 5.7 and 5.8. Also, Fig. 6.14 illustrates the resonant frequency and resonant resistance loci of Fig's. 6.11 and 6.12.

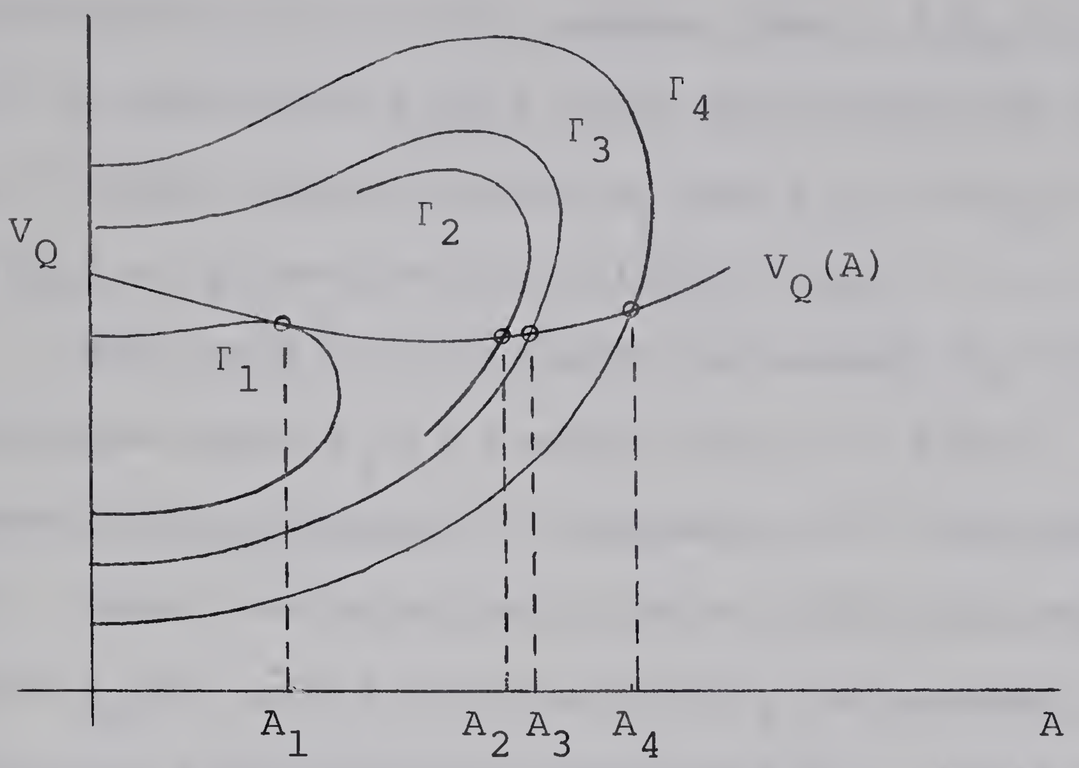

Figure 6.13
Constant-G_{eq} Chart and Locus

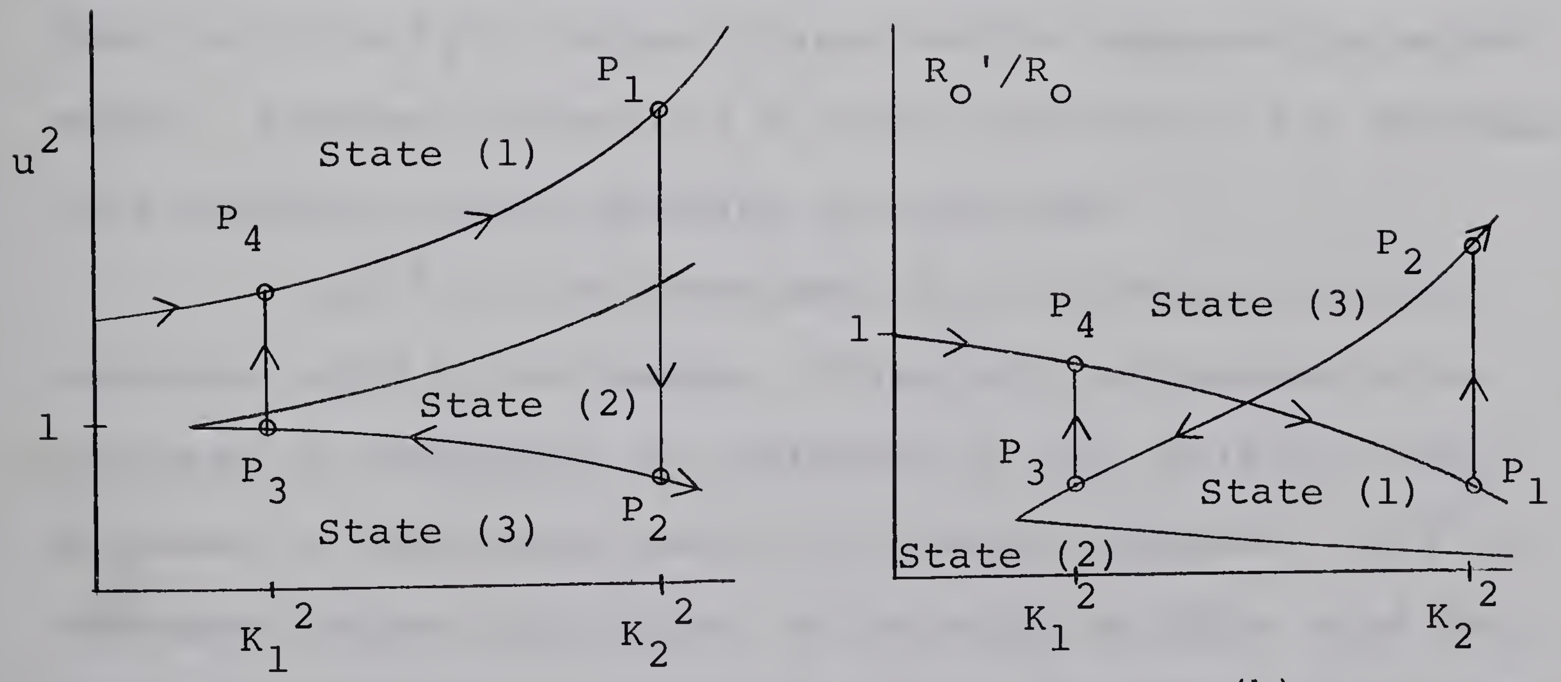

(a) (b)

Figure 6.14
Resonant Frequency and Resonant Resistance Loci

[illegible]

[illegible]

[illegible]

[illegible]

With reference to Fig. 6.13, assume that $- 1/R_o = \Gamma_3$. Thus, for $K^2 = 0$, oscillation will occur with amplitude A_3. Also in Fig. 6.14(b) assume that at P_1 and P_3, $- 1/R_o' = \Gamma_1$; at P_2, $- 1/R_o' = \Gamma_4$; and at P_4, $- 1/R_o' = \Gamma_2$.

Now, as K^2 is initially increased, R_o' for State (1) will decrease until P_1 is reached (Fig. 6.14(B)). This will correspond to an increase in frequency, as indicated by Fig. 6.14(a). Also, the solution to Eq's. 6.58 will move along the curve $V_Q(A)$, until the countour Γ_1 is reached; which will correspond to oscillation of amplitude A_1. It is apparent that upon subsequent increase of K^2, no solution to Eq's. 6.58 can exist for the value of R_o' corresponding to State (1). However, for this value of K^2, $-1/R_o'$, for State (3), is equal to Γ_4, so that oscillation may take place with amplitude A_4; and frequency as determined by P_2, Fig. 6.14(a). Thus, at $K^2 = K_2^2$, the oscillator can be expected to switch modes. Further increase in K^2 will now result in a decrease in frequency, and an increase in amplitude.

If K^2 is now decreased, R_o' for State (3) will decrease until P_3 is reached. This will correspond to an increase in frequency, as indicated by Fig. 6.14(a); and a decrease in amplitude, until A_1 is again reached. If K^2 is decreased beyond this point, no solution to Eq's. 6.58 for State (3) can exist. However, $- 1/R_o'$ for State (1) is now equal to Γ_2, so that oscillation of amplitude A_2 may occur.

Thus, the oscillator can be expected to switch back to its original mode at $K^2 = K_1^2$.

It should be pointed out that for State (2), R_o' is always less than the minimum value for sustained oscillation. (i.e. the value at P_1 and P_3). Thus, oscillation in State (2) can never occur.

Example 6.1

Fig's. 5.7, 5.8, and 6.12 can now be used to design a system which should exhibit the switching phenomenon. Referring to Fig. 5.7, $R_1 + R_B$ can be chosen as 125Ω, and V_B as 237.5 mv, so that all solutions in A and V_Q will be on the fourth lowest curve, $V_Q(A)$. (Fig. 5.8).

If R_o is chosen as $1/1.8(10^3)\Omega$, so that $-1/R_o =$ -1.8 mmho, then for $K^2 = 0$, the circuit can be expected to oscillate with A = 177.5 mv and $V_Q =$ 185 mv.

It can be seen from Fig. 5.8 that the minimum value of R_o' for sustained oscillation corresponds to $G_{eq} \approx -4.5$ mmho, for which $R_o' = 1/4.5(10^3)\Omega$. Hence, $R_o'/R_o = 1.8/4.5 = 0.4$. Referring to Fig. 6.12, for State (1), this occurs for $K^2 \approx 0.37$. From Fig. 5.8, the minimum amplitude is seen to be approximately 82.5 mv.

Now from Fig. 6.12, State (3), for $K^2 = 0.37$,

$R_o'/R_o \simeq 1.44$, so that $-1/R_o' = -1.8/1.44$ mmho - -1.25 mmho. Thus, from Fig. 5.8, oscillation in State (3) may occur, with $A \simeq 195$ mv and $V_Q \simeq 192.5$ mv.

If K^2 is now decreased, oscillation in State (3) will continue until R_o'/R_o for State (3) reaches 0.4, so that the minimum amplitude (82.5 mv) is again reached. From Fig. 6.12, this corresponds to $K^2 \simeq 0.011$. At this point, R_o'/R_o for State (1) is approximately 0.95 so that

$$-\frac{1}{R_o'} \simeq \frac{-1.8}{0.95} \text{ mmho} = -1.9 \text{ mmho.}$$

Hence, from Fig. 5.8, State (1) oscillation may occur with $A \simeq 172$ mv and $V_Q \simeq 184$ mv.

The normalized frequencies at the switching points can now be found from Fig. 6.11. For $K^2 = 0.37$, u^2 for State (1) is about 3.0, and u^2 for State(3) is about 0.715.

For $K^2 = 0.011$, u^2 for State (1) is about 1.43, and u^2 for State (3) is about 0.98. The actual frequencies corresponding to the above values of u^2 can be found from Eq. 6.62.

It is of interest to consider what would happen if the oscillator discussed in Example 6.1 were stopped at a time when K^2 were somewhere between the two switching points.

It can be seen from Fig. 5.8 that for any contour for which $G_{eq} < -3.0$ mmho, there will be either two solutions (which may coincide)or no solution. It has been shown in Sec. 5.7 that when there are two solutions, the one occurring for the smallest amplitude is unstable, and the other one is stable. Now for $- 1/R_o' = -3.0$ mmho, $R_o' = 333\Omega$. Therefore, whenever $R_o' < 333\Omega$, for either State (1) or State (3), that state will be characterized by an unstable and a stable solution (or no solution at all). For $R_o' = 333\Omega$, $R_o'/R_o = 1.8/3.0 = 0.6$. Referring to Fig. 6.11, for State (1) this corresponds to $K^2 \simeq 0.17$, and for State (3), it corresponds to $K^2 \simeq 0.02$. Thus, if $0.02 < K^2 < 0.17$, R_o'/R_o for both State (1) and State (3) will be greater than 0.6, and only stable solutions will exist. This implies that if the oscillator were stopped and permitted to start again, the mode of oscillation could not be predicted.

If $K^2 > 0.17$, there will be only one (stable) solution for State (3), and an unstable and a stable solution for State (1) (or no solution). Hence, in this case, if the oscillator were allowed to start, oscillations would occur in State (3). Similarly, if $K^2 < 0.02$, oscillations would spontaneously occur in State (1).

It is conceivable, that under certain conditions, oscillation in both modes may occur simultaneously. If the two frequencies were fairly close together, a beat-frequency

phenomenon would thus be exhibited. Analysis of the system under such circumstances would require the simultaneous solution of three equations in V_Q, A_1, and A_2; where A_1 and A_2 represent the fundamental amplitudes of the two voltage components. Such an analysis will not be undertaken in this thesis, as it would be much too complex to be feasible.

6.6 Limitations of the Method of Analysis

Because the describing-function method is valid only for steady-state sinusoidal oscillations, no information has been obtained regarding transient response. Also, nothing has been learned about the exact nature of the switch from one mode to another. However, it seems logical to assume that transients of some form would occur during the switching process.

It has also been observed that some very non-sinusoidal modes of oscillation can occur, particularly when both tuned circuits are used. The describing-function method is of course inadequate for analysis of such modes.

In order for the assumption of sinusoidal oscillation to be nearly met, it has been shown (in Sec. 5.9) that the impedance to the harmonics of the frequency of oscillation should be as small as possible compared to r_d for the tunnel diode. For one tuned circuit alone, this is not difficult to achieve. However, when two coupled circuits are

used, the frequency response of the impedance function is known to vary drastically as coupling is varied. Thus, under certain circumstances, it is to be expected that varying the degree of coupling will vary the distortion, and thus, the frequency departure. As an example, if the circuit were oscillating in State (3), (Fig. 6.12), and K^2 were somewhat larger than the value required for the circuit to switch to State (1), the resonant resistance for State (1) would be larger than that for State (3). If the resonant frequency of State (1) were approximately twice that for State (3), the impedance to the second harmonic would be considerably larger than the impedance to the fundamental. Thus, considerable distortion would probably result.

6.7 Summary

The switching phenomenon, as predicted by the describing-function method, is seen to depend on a combination of circumstances involving both the linear and the non-linear portions of the system. Regarding the non-linear portion, such a switch can be predicted only when conditions are such that a stable and an unstable solution in A and V_Q may occur, so that there will be a minimum amplitude for sustained oscillation. Thus, the curvature of the contours $G_{eq} = \Gamma$, and of the loci $V_Q(A)$ are of primary importance.

In general, two solutions may occur in any bias range for which the contours $G_{eq} = \Gamma$ are concave upward at $A = 0$ (if $V_Q > V_I$). In Sec. 5.4, this range has been identified as the range for which $g_3(V_Q) < 0$. Also, by Theorem 5.1, $g_3(V_Q) < 0$ in any range of V_Q for which $d\rho/dS \geq 0$.

If the d.c. load-line intersects the d.c. characteristic slightly to the right of the inflection point, the curvatures of the contours and of the curves $V_Q(A)$ are both conducive to the appearance of two solutions.

For the linear portion of the system, the first requirement for the switching phenomenon to occur is that the resonant frequency loci for the mutually coupled circuits must resemble those shown in Fig. 6.7(a). It has been shown in Sec. 6.2 (Eq. 6.41) that a necessary condition for this is that F_f^2 be somewhat larger than $Q_1^2/(Q_1^2-1)$.

A second requirement is that as K^2 is increased (or decreased) the second mode must be available before the first mode becomes unavailable. If this were not so, upon increasing (or decreasing) K^2, at some point oscillation would cease entirely, and would re-occur, in the second mode when some other point were reached. Referring to Fig. 5.12, this requirement means that R_o'/R_o for State (1) should initially decrease as slowly as possible; and R_o'/R_o for State (3) should increase as rapidly as possible. It has been shown in Sec. 6.4 (Eq. 6.57) that for State (3), $R_o'/R_o \lesseqgtr \frac{1}{2}(1 + \sqrt{1 + Q_2/Q_e})$.

Also, from Fig. 6.8, it is seen that for State (3), u^2 must be less than $\frac{1}{1 + Q_e/Q_2}$, in order that R_o'/R_o be greater than one. Thus, R_o'/R_o will increase most rapidly, and have the largest value for $K^2 = 1$, when Q_2/Q_e is made as large as possible. Further optimization in this respect can be obtained by choosing $Q_1^{\,2}$ (and $F_f^{\,2}$) so that the solutions to Eq. 6.30, for State (3), be approximately on the peaks shown in Fig. 6.9. This is the basis on which Q_2, Q_1, and F_f were chosen for Fig's. 6.5, 6.9, 6.11, and 6.12.

VII. EXPERIMENTAL VERIFICATION

An analogue computer can easily be used to simulate a tunnel diode oscillator, and thus provides a convenient means of testing the previous theory. Since the frequency of oscillation is irrelevant to the nature of the solution, the computer simulation can be designed to oscillate at any desirable frequency. Thus, the time-domain solution can be effectively slowed down so that transient response can be observed. Furthermore, the actual switching process can be studied.

A further advantage to the analogue computer simulation is that the coupling coefficient, K^2, can accurately be adjusted to any value by adjusting a single pot. This is shown in Sec. A2.4.

The analogue computer simulation can of course be used to study non-sinusoidal modes as well, if this be desired.

7.1 Basic Computer Set-Up

Consider the block-diagram of the hypothetical control system shown in Fig. 7.1. Two basic equations can be written for this system;

$$x_2 = f(x_1), \quad \text{and} \tag{7.1}$$

$$x_1(S) = R(S) - x_2(S)\{H_1(S) + H_2(S)\} \tag{7.2}$$

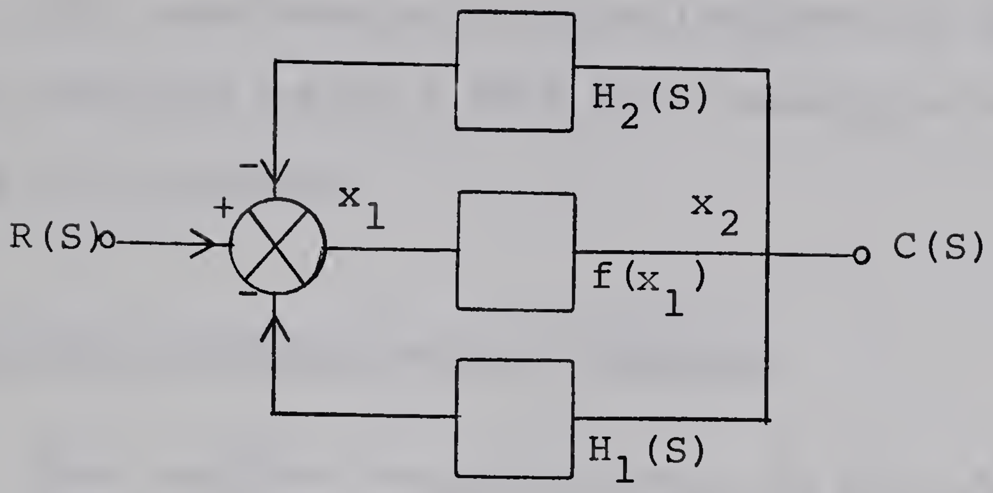

Figure 7.1
Block Diagram of Computer Simulation

Equations (7.1) and (7.2) are identical to Eq's. (4.11) and (4.10), if:

$$R(S) = V_B(S); \quad x_1(S) = V_D(S); \quad x_2(S) = I_D(S);$$
$$H_1(S) = Z_T(S); \quad \text{and} \quad H_2(S) = Z_B(S).$$

Thus, accurate simulation of the circuit shown in Fig. 4.3 requires only a non-linear function generator which will produce the d.c. characteristic for the tunnel diode; a transfer function mathematically equal to the impedance function of the tank circuit; and a transfer function mathematically equal to the impedance function of the biasing network. When mutual coupling is included, $H_1(S)$ must of course be equal to $Z_T(S)$, as shown in Fig. 6.1.

Detailed computer schematics for the above system components are derived in Sec. A2.

All experimental results included in this section have been obtained using a PACE 231-R analogue computer and an 1100-E X-Y recorder.

7.2 Oscillator Without Mutual Coupling

The computer schematic shown in Fig. A2.8 can be used to investigate any aspect of the describing-function theory, as well as the various non-sinusoidal modes of oscillation that may occur.

The circuit discussed in Example 5.1 shall first be simulated. For this circuit, $R_o = 250\Omega$, and $(R_1 + R_B) = 125\Omega$. The other circuit parameters can be chosen as desired.

Choosing

$$Q_1 = 10 \quad , \text{ and} \tag{7.3}$$

$$\frac{1}{\sqrt{L_1C_1}} = 2\pi \quad , \tag{7.4}$$

$$\omega_o = 2\pi\sqrt{1 - 1/100} \; ; \quad \text{or } f_o \simeq .995 \text{ Hz.}$$

From Eq's. 3.4 and 3.7

$$\frac{R_o}{Q_1} = \sqrt{L_1/C_1} \quad , \text{ or}$$

$$\sqrt{L_1/C_1} = 25\Omega. \tag{7.5}$$

From (7.4) and (7.5), $C_1 = 1/50\pi$, and $L_1 = 100/8\pi$.

Also, from Eq. 3.7, $R_1 = \frac{1}{Q_1}\sqrt{L_1/C_1}$, from which $R_1 = 2.5\Omega$. Since $(R_1 + R_B) = 125\Omega$, $R_B = 122.5\Omega$. The impedance of C_B can be neglected if

$$\frac{1}{\omega C_B} = .01\ R_o, \qquad \text{or}$$

$$C_B = \frac{100}{\omega_o R_o} \simeq \frac{100}{2\pi \times 250} = \frac{1}{5\pi} .$$

Note that $G_d \sqrt{L_1/C_1} \simeq 7 \times 10^{-3} \times 25 = .175$, so that near sinusoidal oscillation can be expected to occur. (see Sec's. 5.9 and 7.3.)

If the current scale is chosen as 1 ma = 1 V, $f(V_D)$ will be multiplied by $10^3\Omega$, so that all linear impedances must be divided by $10^3\Omega$. Hence, for the computer schematic,

$$R_1 = .025$$

$$L_1 = \frac{1}{80\pi}$$

$$C_1 = \frac{20}{\pi}$$

$$R_B = .1225, \qquad \text{and}$$

$$C_B = \frac{200}{\pi} .$$

Using the above values, the tracings shown in Fig's. 7.2 and 7.3 have been obtained. Fig. 7.2 shows the

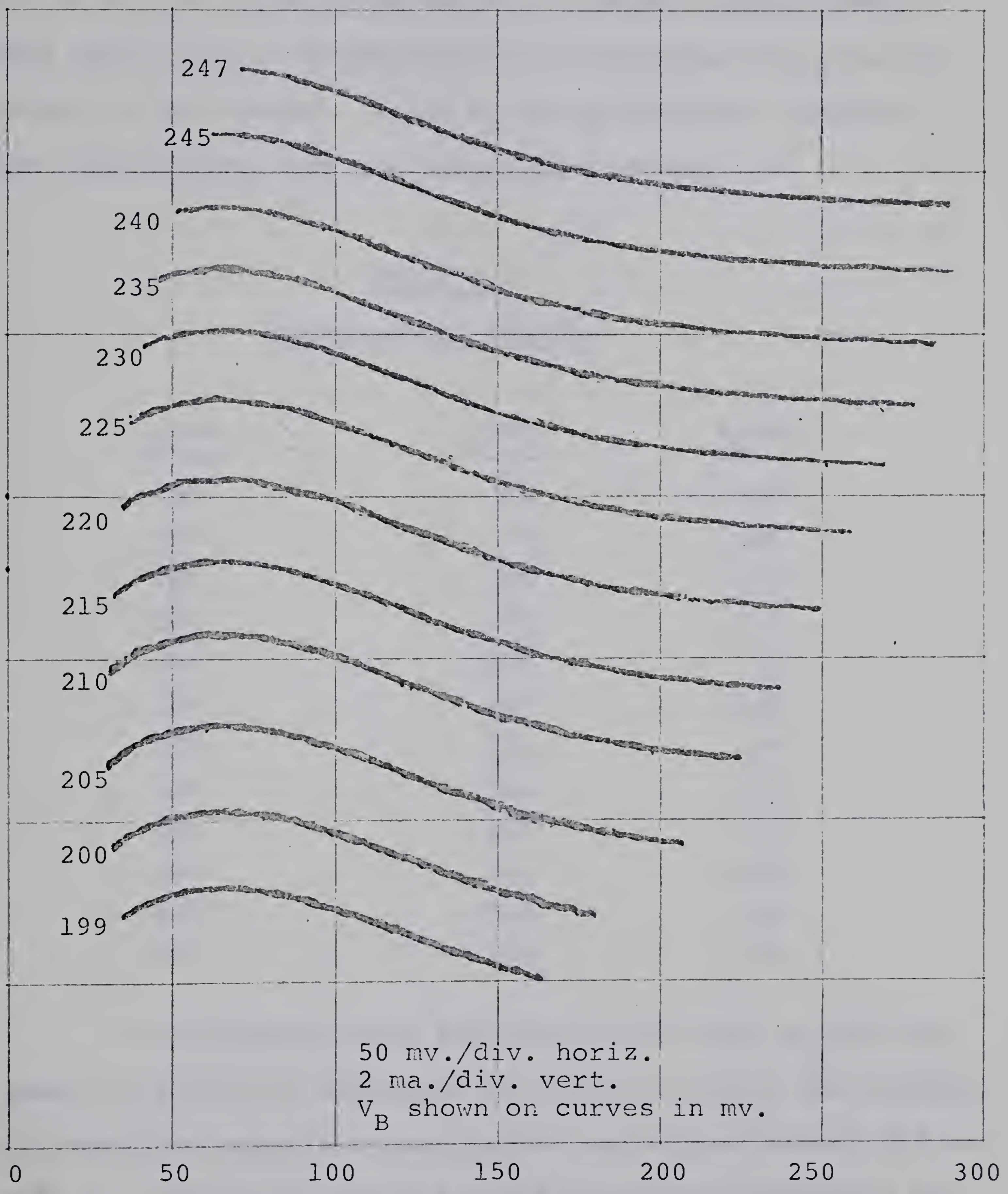

Figure 7.2

Portions of Diode Characteristic Covered During Steady-State Oscillation

portion of the diode characteristic covered during steady-state oscillation, corresponding to the values of V_B as indicated on the curves. A and V_Q can be obtained directly from these curves, and are tabulated in Table 7.1

Table 7.1

Experimental Results

V_B(mv)	A(mv)	V_Q(mv)
199	65	100
200	74	106
205	89	119
210	98	127
215	102	137
220	107	142
225	111	149
230	114	155
235	117	162
240	117	168
245	113	176
247	109	180

Oscillations were seen to die out when V_B was increased to 248 mv or decreased to 198 mv, so that the minimum amplitudes for sustained oscillation are approximately 109 mv and 65 mv. The above results agree with the predictions of the describing-function method. (See Example 5.1 and 5.2)

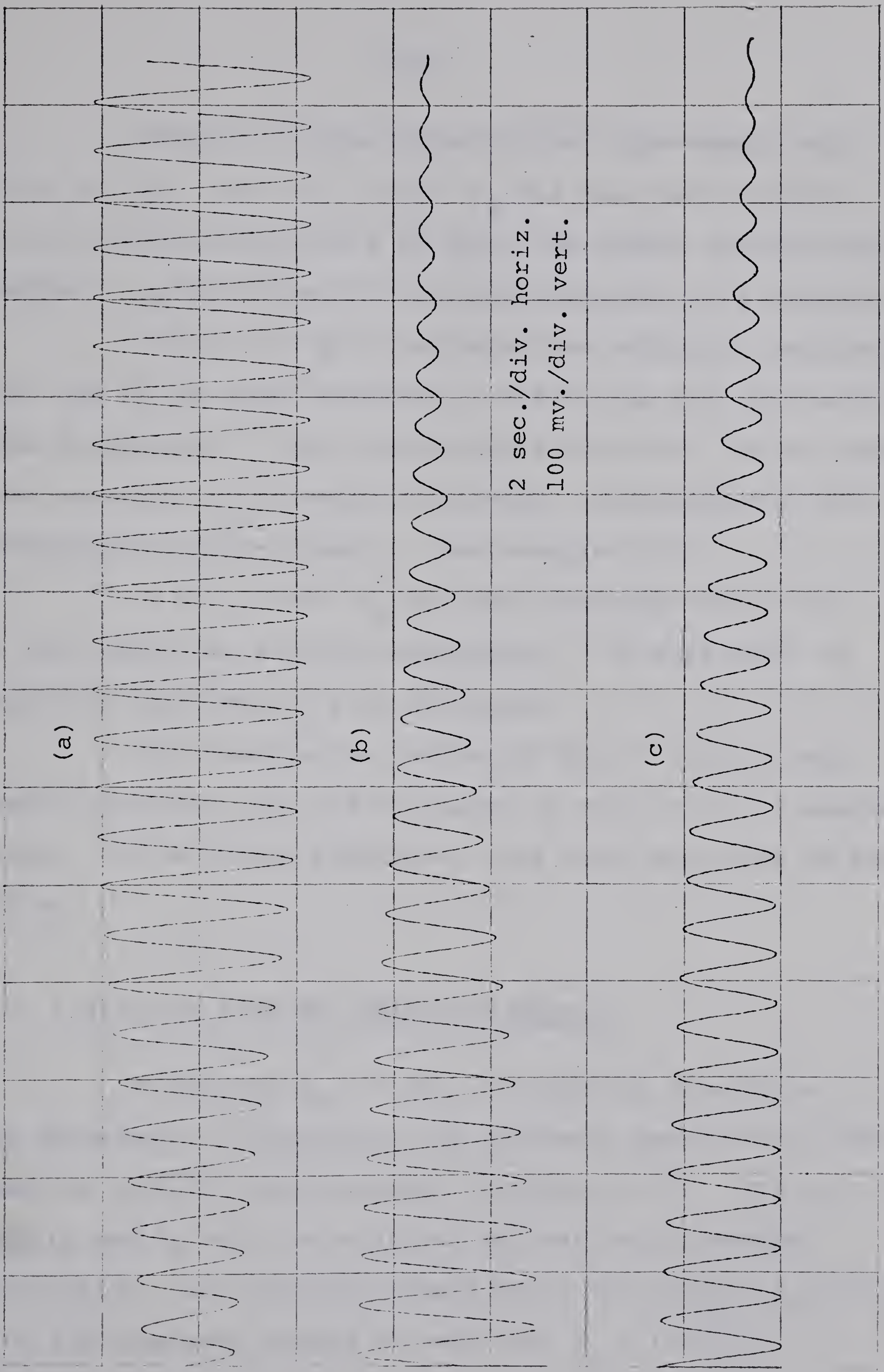

Figure 7.3
Typical Solutions

Figure 7.3 shows three typical time-domain solutions for V_D. For Fig. 7.3(a), V_B has been set at 225 mv, so that oscillations built up until the stable solution was reached. V_Q can be seen to decrease slightly as A increases.

In Fig. 7.3(b), the system was initially oscillating, and V_B was then increased to 250 mv, so that the solution disappeared. Thus, oscillations died out. As the amplitude decreases V_Q is seen to increase, as predicted by the describing-function theory. (See Example 5.2)

In Fig. 7.3(c) V_B has been decreased to 190 mv, so that again the solution disappeared. In this case, as amplitude decreases V_Q also decreases.

The steady-state portion of Fig. 7.3(a) is very nearly sinusoidal and the frequency of oscillation is approximately .995 Hz as was predicted. The final amplitude is about 112 mv.

7.3 Distortion With an Infinite-Q Circuit

By letting $R_1 = 0$ for the computer simulation, the dependence of distortion and frequency departure on the quantity $G_d\sqrt{L_1/C_1}$ can be studied (see Sec. 5.9). For $R_1 = 0$, both Q_1 and R_o will be infinite, so that for sinusoidal oscillation, all solutions should be on the contour $G_{eq}(A,V_Q) = 0$; and frequency should be such that $\omega_o = 1/\sqrt{L_1C_1}$.

Also, in this case, the biasing network can be neglected, so that $V_Q = V_B$.

In varying $G_d\sqrt{L_1/C_1}$, it is desirable that ω_o remain constant, so that the frequency departure can easily be observed. This can be conveniently achieved by multiplying $f(V_D)$ by different values, which corresponds to varying the gain in the forward loop of the computer simulation.

Using $L_1 = 1/80\pi$, $C_1 = 20/\pi$, and $V_B = V_Q = 250$ mv, the tracings shown in Fig. 7.4 have been obtained. The current scale 1 ma = 1v has again been used. For these values of L_1 and C_1, $\omega_o = 2\pi$, or $f_o = 1.0$ H_Z. Also, from the Constant-G_{eq} Chart, for $V_Q = 250$ mv and $R_o = \infty$, the amplitude should be slightly larger than 250 mv (for sinusoidal oscillation).

The curves in Fig. 7.4 are the steady-state time-domain solutions for V_D, corresponding to the values of $G_d\sqrt{L_1/C_1}$ as indicated.

It can be seen that for $G_d\sqrt{L_1/C_1} = .175$, the waveform is very nearly sinusoidal, with frequency of about 1.0 Hz, and amplitude of about 260 mv. These values are in good agreement with the describing-function theory.

It is also seen that for $G_d\sqrt{L_1/C_1} \geqq 1.0$, quite a large degree of distortion is present, and the frequency of oscillation is considerably less than the resonant frequency of the tank circuit.

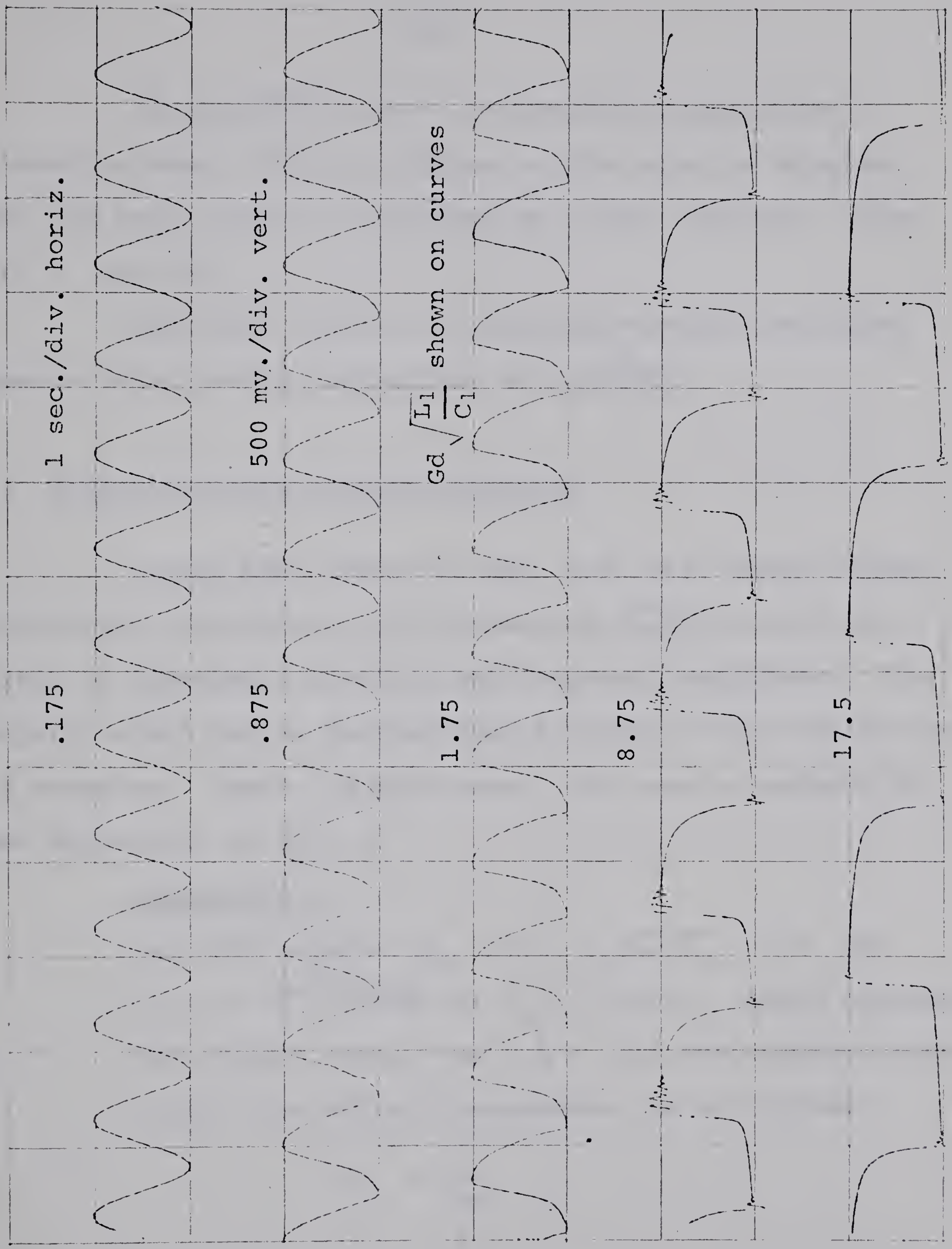

Figure 7.4
Waveforms Using an Infinite-Q Tank Circuit

For $G_d\sqrt{L_1/C_1} \gtrsim 10.0$, the solution approaches a relaxation mode. This is similar to the solution obtained when the tank circuit is replaced by a pure inductor. (See Ref. 3, page 50).

Note that in Fig. 7.4 the peak-to-peak amplitude appears to be nearly independent of $G_d\sqrt{L_1/C_1}$.

7.4 Distortion with Finite-Q Circuits

It has been shown (in Sec. 5.9) that under certain conditions, increasing Q_1 by increasing $\sqrt{L_1/C_1}$ can be expected to increase distortion and frequency departure. This property shall now be demonstrated by means of the two following examples. Again, in both cases, the biasing network has been neglected, or $R_B = 0$.

Example 7.1

For this example, $Q_1 = 10$, $G_d\sqrt{L_1/C_1} \simeq 1.0$, and $\omega_o = 2\pi\sqrt{1 - 1/100}$; or $f_o \simeq .995$ Hz. Again choosing the current scale 1 ma = 1 v, for the computer simulation, the circuit parameters are as follows:

$$R_1 = \frac{1}{70}$$

$$L_1 = \frac{1}{14\pi}$$

$$C_1 = \frac{7}{2\pi}$$

$$R_o = \frac{10}{7}$$

Using these values, the curves shown in Fig. 7.5 (corresponding to the values of V_B as indicated) have been obtained. These curves represent the steady-state solutions to V_D. It is seen that the nature of the solution depends on the value of V_B chosen. Note that for all curves considerable distortion and frequency departure are present. Fig. 7.5(c) can be compared to Fig. 7.4(b) and (c).

Example 7.2

In this case, $\sqrt{L_1/C_1}$ has been doubled (as compared to Example 7.1); and both R_1 and $1/\sqrt{L_1C_1}$ have been unchanged. Thus, $Q_1 = 20$, $G_d\sqrt{L_1/C_1} \simeq 2.0$, and $\omega_o = 2\pi\sqrt{1-1/400}$; or $f_o \simeq .999$ Hz. For a current scale of 1 ma = 1 v, the circuit parameters for the computer simulation will be

$$R_1 = \frac{1}{70} ,$$

$$L_1 = \frac{1}{7\pi} ,$$

$$C_1 = \frac{7}{4\pi} , \qquad \text{and}$$

$$R_o = \frac{40}{7} .$$

Note that R_o has been multiplied by a factor of four, as compared to Example 7.1.

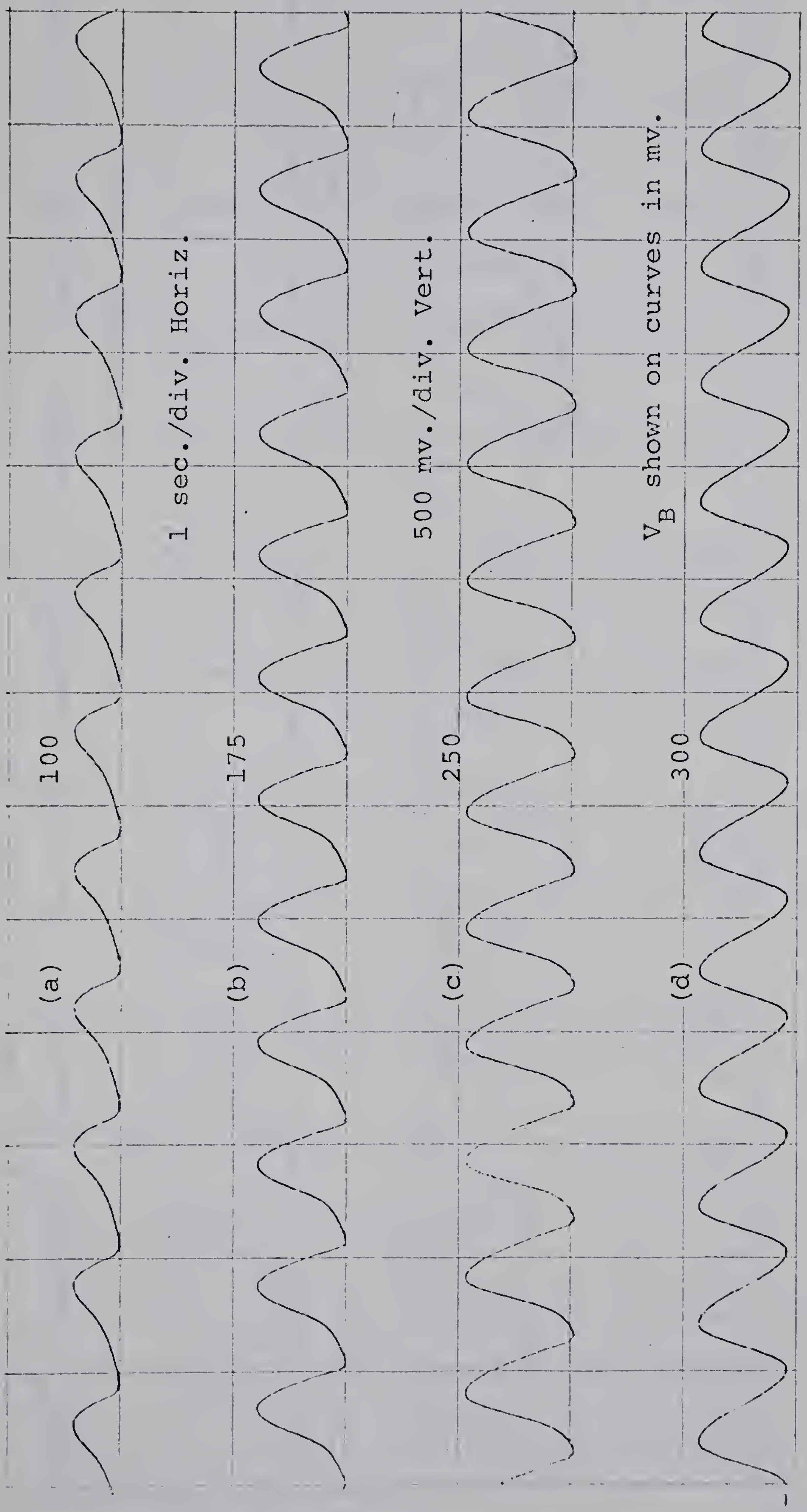

Figure 7.5

Waveforms Using a Tank Circuit with a Q of 10

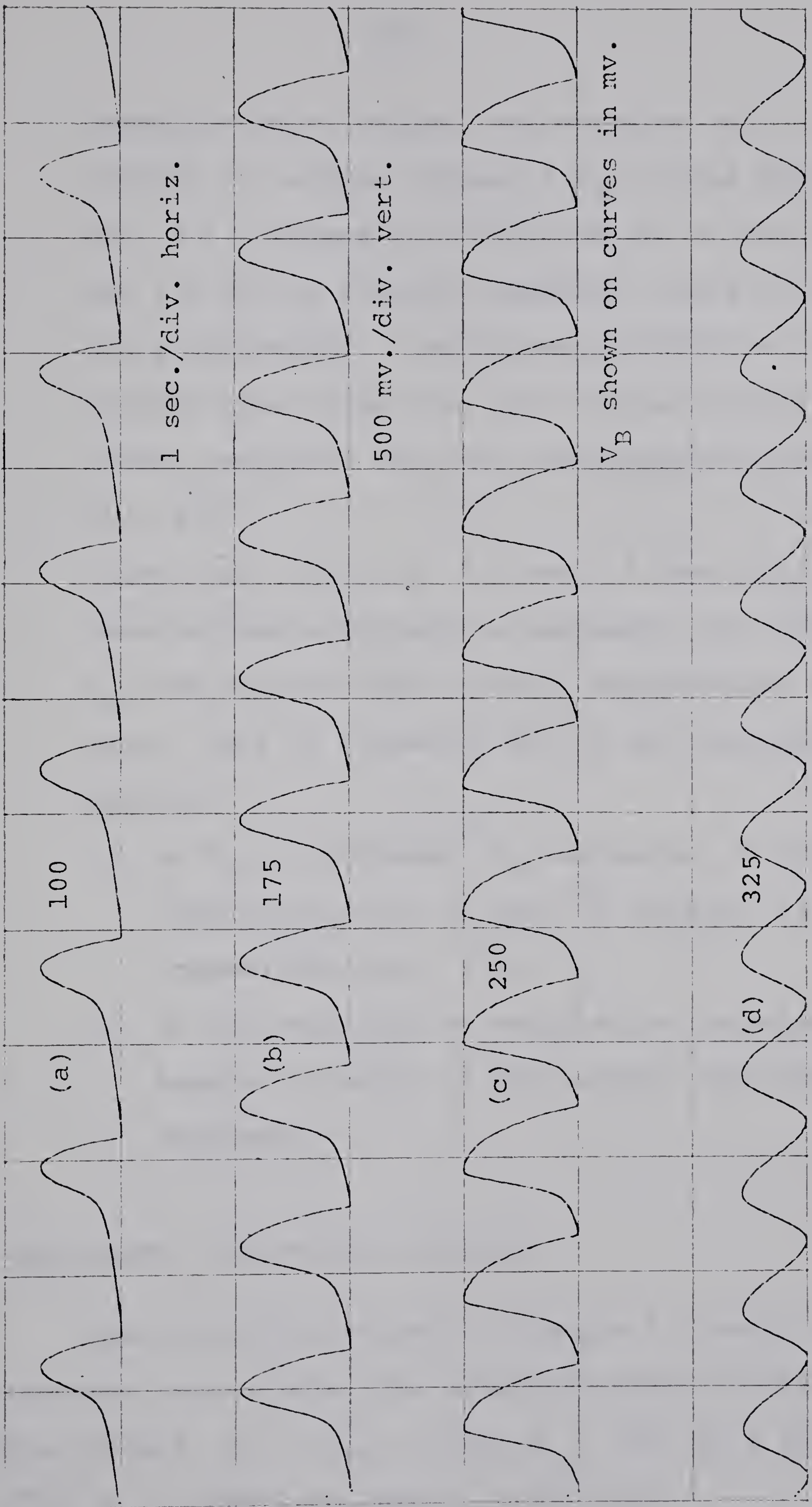

Figure 7.6
Waveforms Using a Tank Circuit with a Q of 20

Using the above values, the solution to V_D (corresponding to various values of V_B) are as shown in Fig. 7.6. Curves (a), (b), and (c) of Fig's. 7.5 and 7.6 can be directly compared, since the values of V_B correspond. The curves of Fig. 7.6 clearly exhibit more distortion and a higher degree of frequency departure than the corresponding curves of Fig. 7.5.

Curves (d), of Fig's. 7.5 and 7.6 show that as the peak-to-peak amplitude is decreased (by increasing V_B) the solution more closely approximates a sinusoid. This is primarily due to the following two factors:

1) as V_B is increased, r_d increases, so that the "open-loop gain" to the n^{th} harmonic is decreased (See Sec. 5.9);
2) as the amplitude of oscillation decreases, the harmonic content of the current wave-form also decreases.

7.5 Oscillator with Mutual Coupling

The circuit discussed in Example 6.1 shall now be simulated and tested using the schematic shown in Fig. A2.16. For this circuit, $(R_1 + R_B) = 125\Omega$, $Q_1 = \sqrt{70}$, $Q_2 = 50$, $F_f = \sqrt{1.4}$, $R_o = 1000/1.8\Omega$, and $V_B = 237.5$ mv.

Choosing

$$\frac{1}{L_1C_1} = 4\pi^2 \quad , \tag{7.6}$$

$$\omega_o = 2\pi\sqrt{1 - 1/70} \quad ; \quad \text{or} \quad f_o \simeq .993\text{Hz} \tag{7.7}$$

From (3.4) and (3.7)

$$\frac{R_o}{Q_1} = \sqrt{L_1/C_1} \quad ; \quad \text{or} \ \sqrt{L_1/C_1} = \frac{1000}{1.8\sqrt{70}} = 66.4\Omega \tag{7.8}$$

From (7.6) and (7.8),

$$L_1 = \frac{66.4}{2\pi} \quad , \qquad \text{and}$$

$$C_1 = \frac{1}{2\pi \times 66.4}$$

Since

$$Q_1 = \frac{1}{R_1}\sqrt{L_1/C_1} \quad , \quad R_1 = \frac{1}{Q_1}\sqrt{L_1/C_1} = \frac{66.4}{\sqrt{70}} \ ;$$

or $R_1 = 7.93\Omega$. Hence, $R_B = 125 - 7.93 = 117.07\Omega$.

Again choosing $1/\omega C_B = .01\ R_o$, $C_B = 100C_1/Q_1 = 11.96\ C_1$.

Note that in Eq's. A2.14, the only two quantities depending on the secondary tank circuit are $1/L_2C_2$ and R_2/L_2. From (6.21),

$$F_f^2 = \frac{L_2C_2}{L_1C_1} \quad , \quad \text{or} \quad \frac{1}{L_2C_2} = \frac{1}{F_f^2L_1C_1} \ .$$

Thus,

$$\frac{1}{L_2C_2} = \frac{4\pi^2}{1.4} \ .$$

Also,

$$\frac{1}{\sqrt{L_2C_2}} \cdot \frac{1}{Q_2} = \frac{1}{\sqrt{L_2C_2}} \cdot R_2 \sqrt{C_2/L_2} = \frac{R_2}{L_2} \quad ;$$

from which

$$\frac{R_2}{L_2} = \frac{2\pi}{\sqrt{1.4}} \cdot \frac{1}{50} = \frac{.04\pi}{\sqrt{1.4}}$$

For a current scale of 1 ma = 1 v, the circuit parameter for the computer simulation will be:

$R_1 = .00793$,

$L_1 = .01057$,

$C_1 = 2.395$,

$R_B = .11707$,

$C_B = 28.6$,

$R_o = .556$,

$\frac{1}{L_2C_2} = 28.2$, and

$\frac{R_2}{L_2} = .1062$.

Using the above values, the tracings shown in Fig's. 7.7 to 7.10 have been obtained. Fig. 7.7 shows the transient response of $H_1(S)$ (Fig. A2.16) to a unit step of voltage. This is equivalent to applying a 1 ma current step to the circuit shown in Fig. 6.1. The values of K^2 are indicated on the curves. K^2 has been adjusted as shown in Fig. A2.17 .

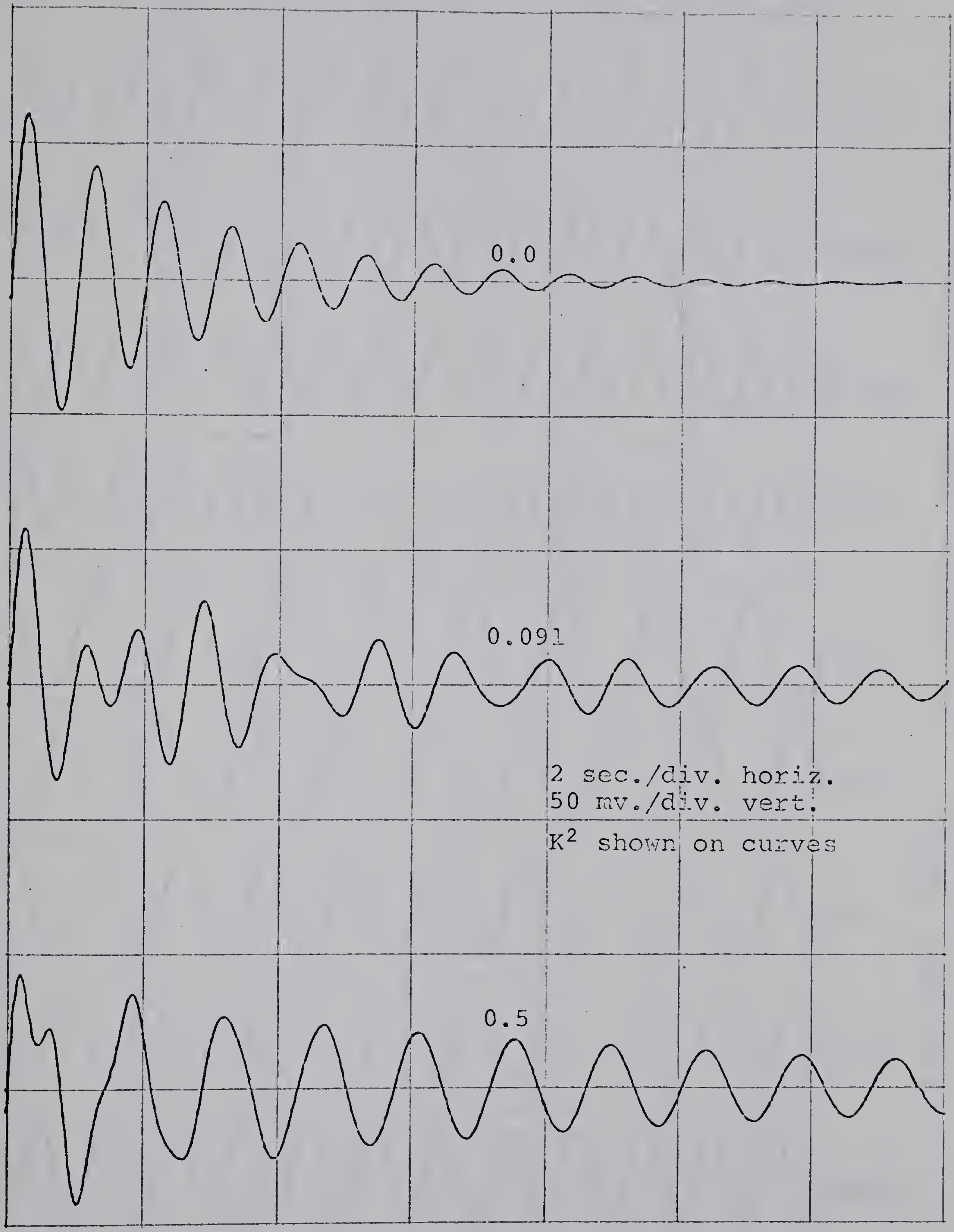

Figure 7.7

Transient Response of Mutually Coupled Circuits to a Current Step

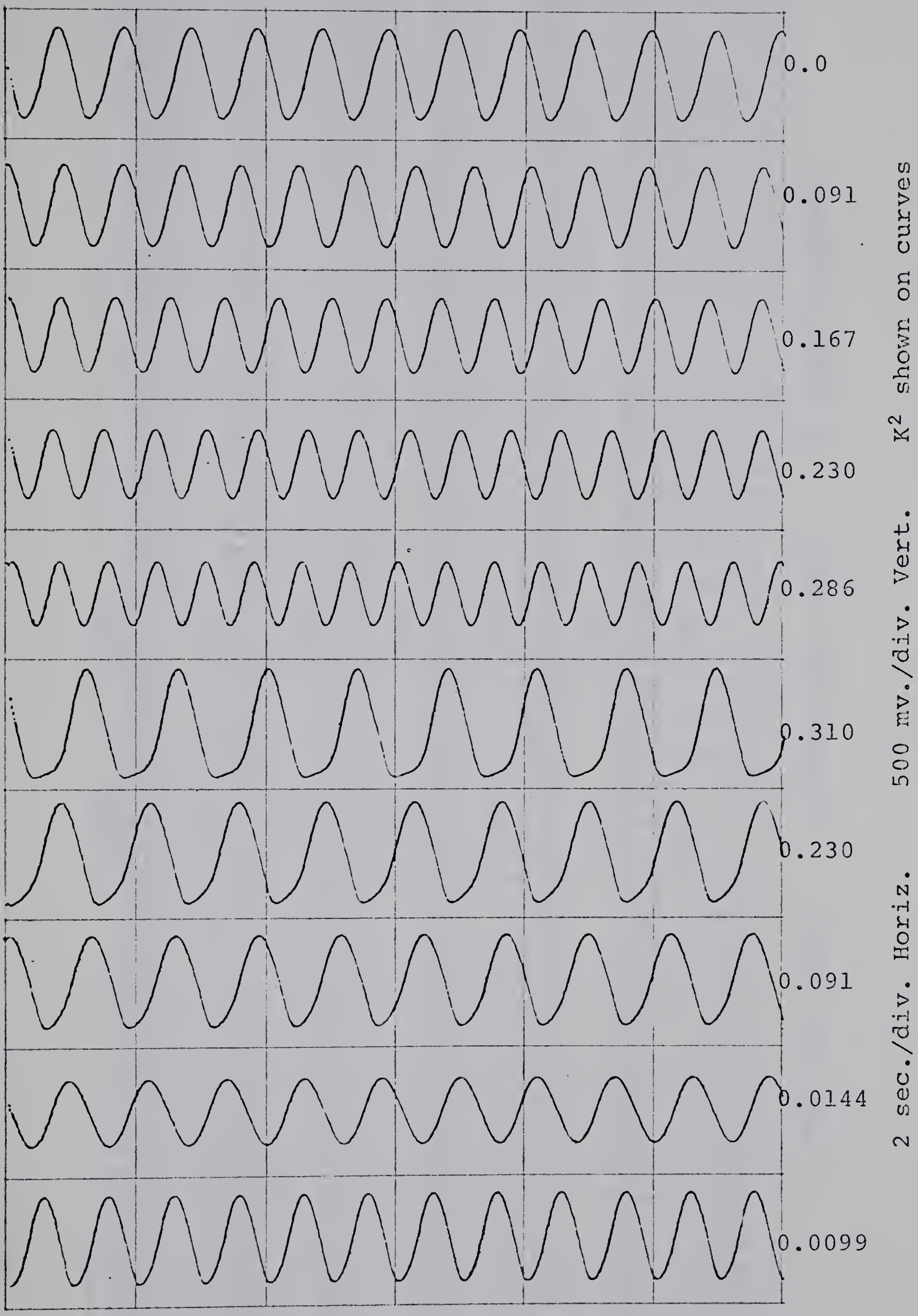

Figure 7.8

Voltage Waveforms with Mutually Coupled Tank Circuits

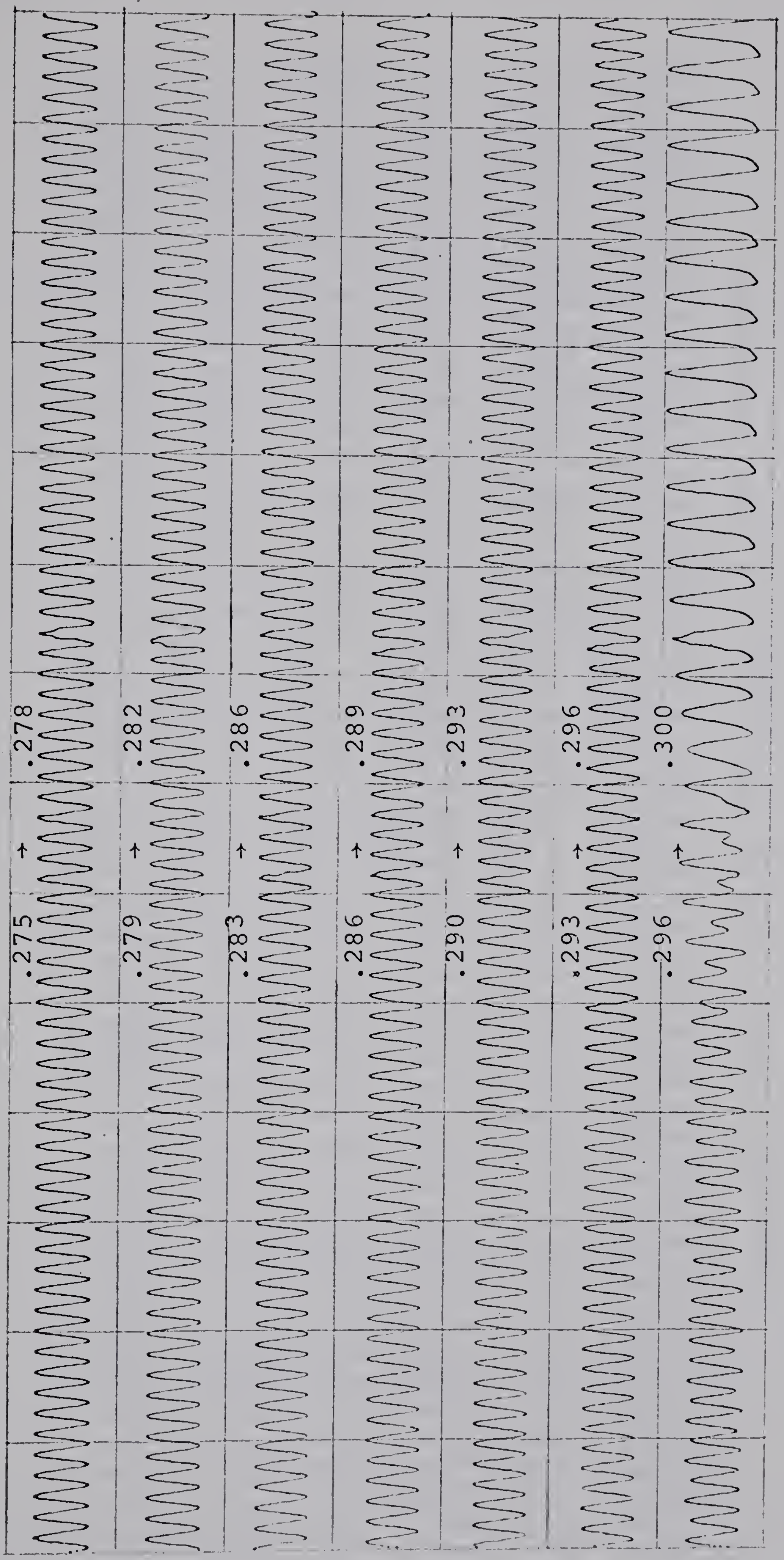

4 sec./div. Horiz. 500 mv./div. Vert. K^2 shown on curves

Figure 7.9
Continuous Solution with Increasing Coupling

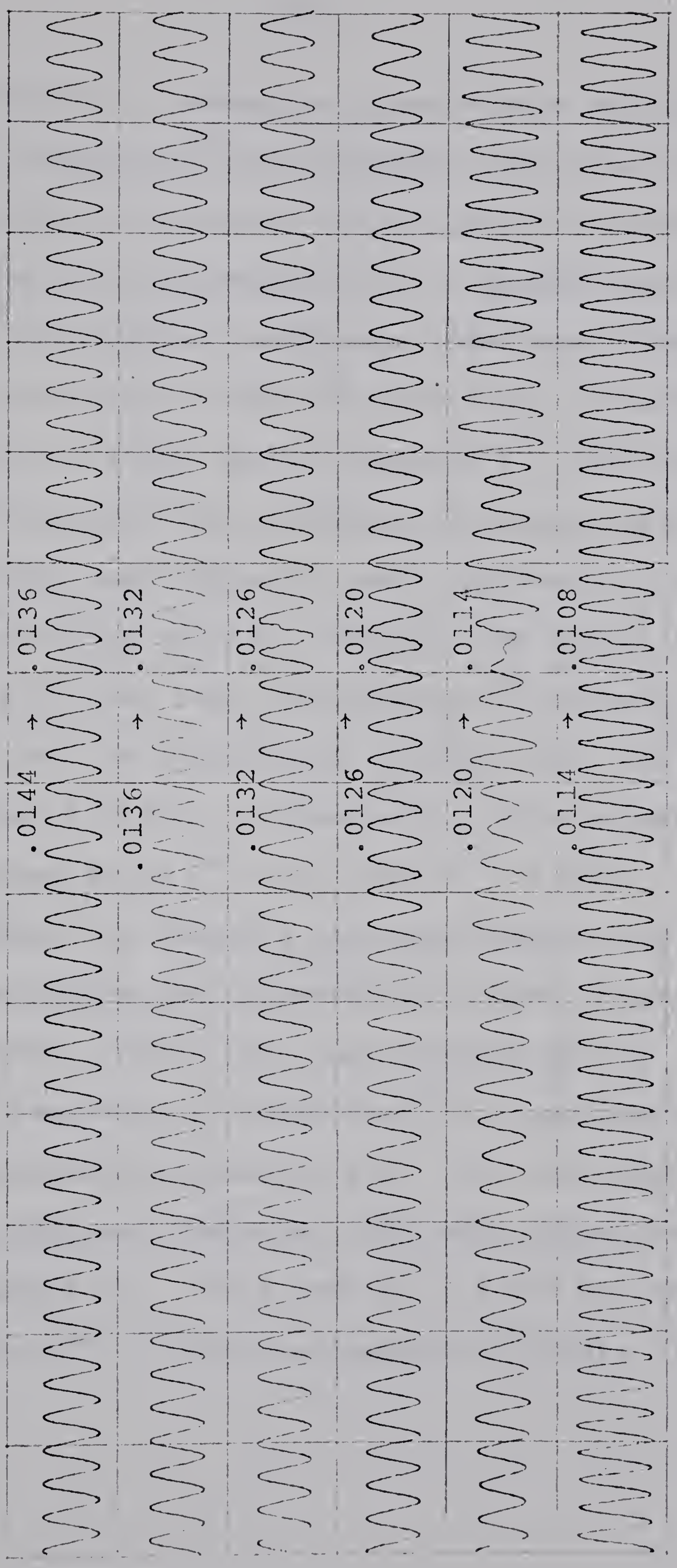

4 sec./div. horiz. 500 mv./div. vert. K^2 shown on curves

Figure 7.10

Continuous Solution with Decreasing Coupling

Figure 7.8 shows the steady-state solutions to V_D for the values of K^2 as indicated. Note that K^2 has first been increased in increments until a switch in modes occurred, and then similarily decreased until a second switch occurred. Each time K^2 was varied, sufficient time was allowed for the resulting transients to die out before the recording was made.

It was found that in varying K^2, the transients that were introduced had a tendency to precipitate the switch to either mode, thus making it very difficult to determine the exact switching points. However, the switch from State (1) to State (3) was seen to occur for K^2 somewhat larger than 0.286, and the switch back to State (1), for K^2 somewhat less than 0.0144. In Example 6.1, the switching points were calculated to be $K^2 = 0.37$ and $K^2 = 0.011$.

Table 7.2 compares the experimental and theoretical values of amplitude and frequency for three values of K^2. The experimental values have been taken from Fig. 7.8. For $K^2 = 0$, the frequency is given by (7.7); and the amplitude has been determined in Example 6.1. For the other two values of K^2, amplitude and frequency have been determined as outlined in Example 6.1. Note that $K^2 = 0.286$ corresponds to State (1), and $K^2 = 0.0144$ corresponds to State (3).

Table 7.2

Comparison of Results

K^2	Experimental A(mv)	Experimental f(H_Z)	Theoretical A(mv)	Theoretical f(Hz)
0.0	175	.989	177.5	.993
0.286	125	1.35	125	1.34
0.0144	125	.834	127.5	.833

In obtaining the curves shown in Fig's. 7.9 and 7.10, the pot $K^2/1-K^2$, of Fig. A2.17, was replaced by a servo-multiplier with a very slow ramp input as shown in Fig. 7.11.

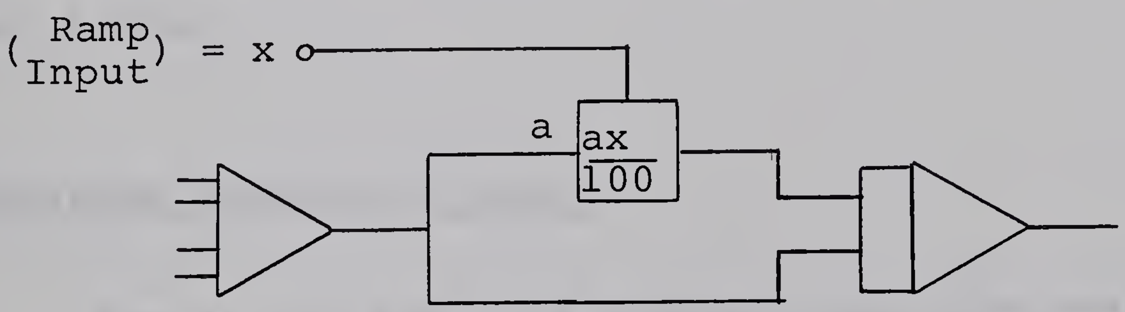

Figure 7.11
Servo-Multiplier Used to Vary Coupling

For Fig. 7.9, the ramp input, x, was chosen as $x(t) = 0.01t$, which corresponds to a linear variation of $K^2/1-K^2$ from 0.0 to 1.0, in 10^4 seconds. Thus, for any one cycle, K^2 can be considered as nearly constant.

Figure 7.9 shows the continuous solution to V_D, during the time in which K^2 was varied from 0.275 to 0.30. A few cycles were missed each time the recorder was repositioned.

Figure 7.10 is similar to Fig. 7.9, except that the system was initially oscillating in State (3), and K^2 was gradually decreased. In this case, x(t) was of the form $x(t) = x_o - 0.001t$. Figure 7.10 shows the solution to V_D during the time K^2 was decreased from 0.0144 to 0.0108.

From Fig. 7.9, the switch from State (1) to State (3) appears to start for $K^2 \simeq 0.293$; and from Fig. 7.10, the switch back to State (1) appears to start for $K^2 \simeq 0.0121$. In both cases, the minimum stable amplitude before the switch is about 125 mv.

7.6 Possible Sources of Error

Fig's. 7.9 and 7.10 indicate that the switch in modes (from either state) seems to occur slightly before the theoretical switching points are reached. This discrepancy could be the result of an error of 10 to 15 mv in V_B. Considering the number of amplifiers used in the system, an error of this magnitude could be accumulated from the individual d.c. offsets.

It is also possible that the switch from mode to mode could be precipitated by the presence of noise in the system. As well, noise at the input of the function generator could effectively alter the d.c. characteristic to some extent.

CONCLUSIONS

Both singly and doubly tuned tunnel diode oscillators have been analyzed in considerable detail, primarily by means of the describing - function method. This analysis has resulted in an explanation of the mode-switching phenomenon exhibited by the doubly tuned oscillator.

On the basis of the describing-function analysis, a system was designed, and then simulated by means of an analogue computer. The switching phenomenon was indeed exhibited.

The describing-function analysis of a tunnel diode oscillator (singly or doubly tuned) is complicated by the fact that the operating point of the tunnel diode depends on the amplitude of oscillation, and thus cannot be arbitrarily specified. For this reason, as well as for the sake of generality, the "Biasing Curves" and "Constant-G_{eq} Chart" have been introduced. These charts depend only on the tunnel diode characteristic, and can thus be used in the analysis of any circuit for which the describing-function method is applicable.

A similar approach could be taken in the describing-function analysis of most types of feedback oscillators using a single-valued non-linearity.

APPENDIX I

MATHEMATICAL JUSTIFICATIONS

Al.1 Proof of Theorem 5.1

The radius of curvature, ρ, for a function $y = f(x)$, is normally defined as

$$\rho = \frac{dS}{d\theta} = \frac{\left[1 + f'(x)^2\right]^{3/2}}{|f''(x)|} \; ; \quad f''(x) \neq 0 \qquad \text{(Al.1)}$$

(Ref. 4, page 430). This is shown in Fig. Al.1.

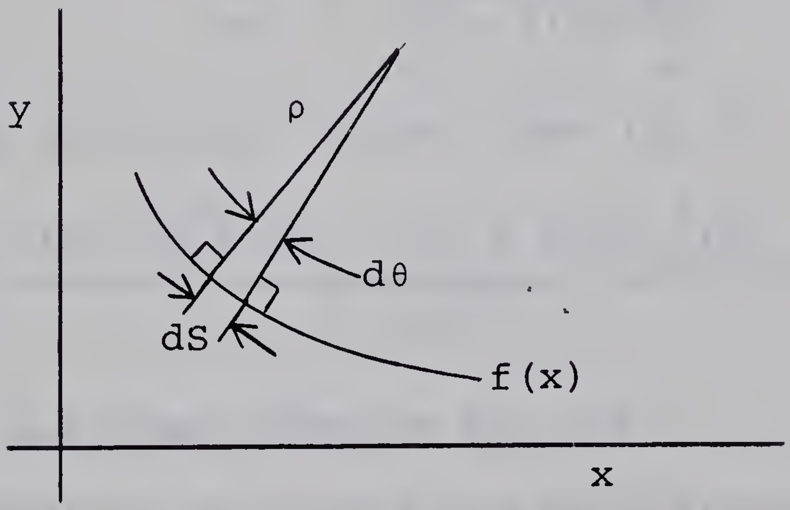

Figure Al.1
Radius of Curvature

It will, however, be more convenient to consider ρ as an algebraic quantity, whose sign depends on the sign of $f''(V)$. Thus, for the curve $I = f(V)$, ρ shall be defined as

$$\rho = \frac{\left[1 + f'(V)^2\right]^{3/2}}{f''(V)} \qquad \text{(Al.2)}$$

The quantity $d\rho/dS$ must now be found. Since

$$\frac{d\rho}{dS} = \frac{d\rho}{dV} \cdot \frac{dV}{dS} , \tag{A1.3}$$

the first step is to find $d\rho/dV$. Differentiating Eq. A1.2,

$$\frac{d\rho}{dV} = \frac{3f''(V)^2 f'(V)\left[1+f'(V)^2\right]^{\frac{1}{2}} - \left[1+f'(V)^2\right]^{3/2} f'''(V)}{f''(V)^2} \tag{A1.4}$$

Now since $dS^2 = dV^2 + dI^2$

$$= \left[1 + f'(V)^2\right] dV^2 , \quad dS = \left[1 + f'(V)^2\right]^{\frac{1}{2}} dV,$$

or

$$\frac{dV}{dS} = \frac{1}{\left[1 + f'(V)^2\right]^{\frac{1}{2}}} \tag{A1.5}$$

Substituting (A1.5) and (A1.4) into (A1.3),

$$\frac{d\rho}{dS} = \frac{3f''(V)^2 f'(V) - \left[1 + f'(V)^2\right] f'''(V)}{f''(V)^2} \tag{A1.6}$$

This result has been cited as Eq. 5.9.

Equation A1.6 must now be evaluated at the point $V = V_Q$. From Eq. 4.5, it is seen that $f^{(n)}(V_Q) = n!\, g_n(V_Q)$. Thus, it follows that:

$$\begin{aligned} &1) \quad f'(V_Q) = g_1 \; ; \\ &2) \quad f''(V_Q) = 2g_2 \; ; \quad \text{and} \\ &3) \quad f'''(V_Q) = 6g_3 \; . \end{aligned} \tag{A1.7}$$

Substituting (A1.7) into (A1.6),

$$\left.\frac{d\rho}{dS}\right|_{V=V_Q} = \frac{6g_1 g_2^2 - 3(1 + g_1^2)g_3}{2g_2^2} \tag{A1.8}$$

If V_Q is now restricted to the "negative resistance" region g_1 must be negative. Thus, the first term in the numerator of (A1.8) must be negative. Furthermore, the denominator of (A1.8) must always be positive or zero. Therefore, it is apparent that if:

$$1) \quad \left.\frac{d\rho}{dS}\right|_{V=V_Q} \geq 0 \ , \qquad g_3 < 0; \qquad (A1.9)$$

$$2) \quad \left.\frac{d\rho}{dS}\right|_{V=V_Q} = -3|g_1|, \ g_3 = 0; \qquad (A1.10)$$

$$3) \quad \left.\frac{d\rho}{dS}\right|_{V=V_Q} < -3|g_1|, \ g_3 > 0. \qquad (A1.11)$$

If the range {X} is now defined as the range $V_P < V_Q < V_v$, then for all values of V_Q belonging to {X}, $g_1(V_Q) < 0$. Assuming that $g_1(V_Q)$ is a continuous and single-valued function in {X}, $g_1(V_Q)$ can be represented as shown in Fig. A1.2.

The range {R} can similarily be defined as the range $V_2 \leq V_Q \leq V_3$, included by {X}, for which $\left.\frac{d\rho}{dS}\right|_{V=V_Q} \geq 0$ (if such a range exists). This is also illustrated in Fig. A1.2, assuming that $d\rho/dS$ is a continuous and single-valued function in the range of interest.

From (A1.9), it is now apparent that everywhere in {R}, $g_3(V_Q)$ must be negative (and non-zero).

If it is now assumed that $g_3(V_Q)$ is continuous and single-valued, it follows that there must be a larger range, {R'}, which includes {R}, for which $g_3(V_Q) \leq 0$. This range is designated as the range $V_1 \leq V_Q \leq V_4$, and is shown in Fig. A1.2.

It also follows from (A1.10) that at $V_Q = V_1$, $d\rho/dS = -3|g_1(V_1)|$; and at $V_Q = V_4$, $d\rho/dS = -3|g_1(V_4)|$. This proves Theorem 5.1.

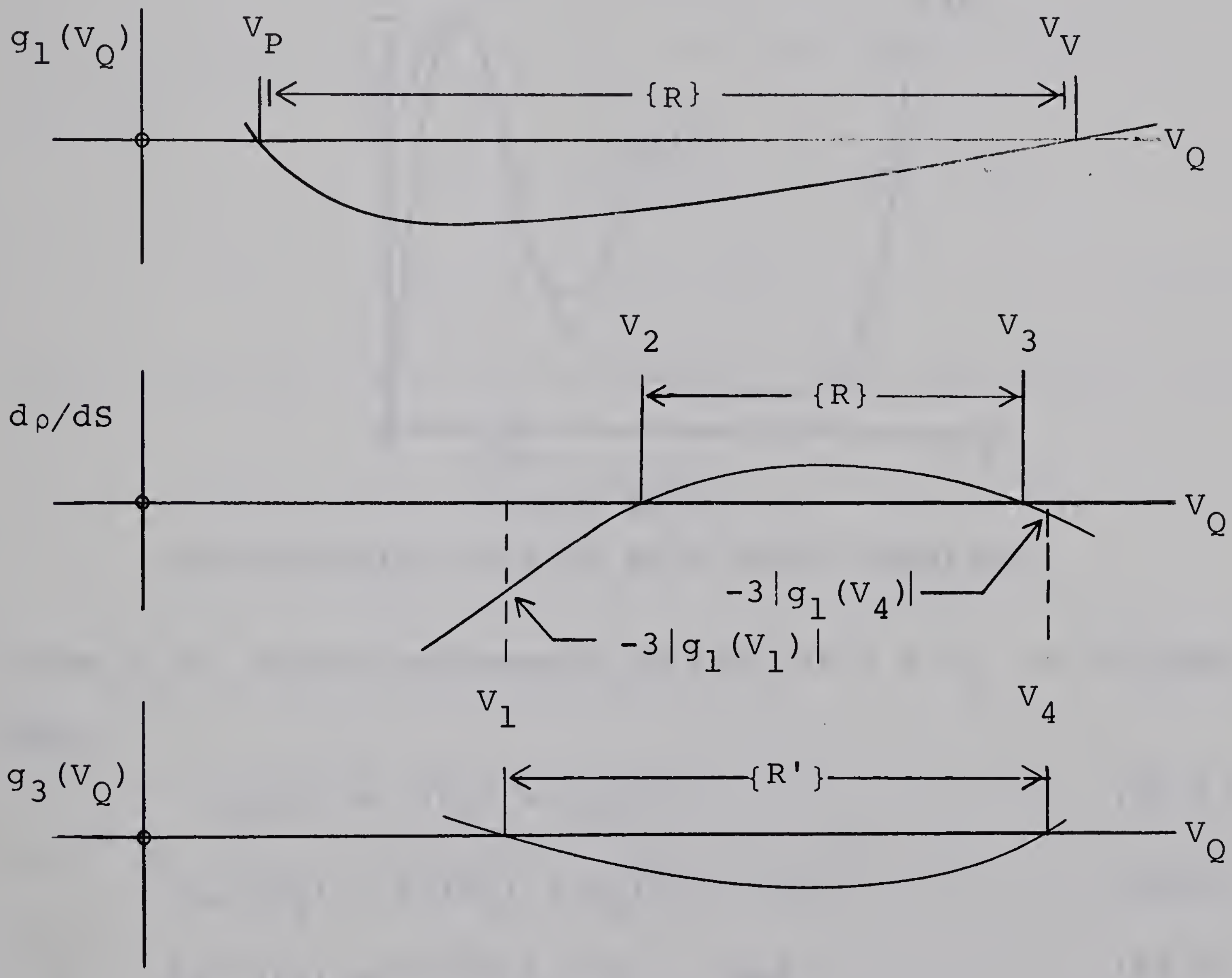

Figure A1.2
Graphical Representation of
$g_1(V_Q)$, $d\rho/dS$, and $g_3(V_Q)$

A1.2 Elliptic Contours

For a small region immediately surrounding the inflection point of the curve $I = f(V)$, a reasonable approximation to the function can be obtained by using a cubic equation of the form

$$f_T(V) = h_o' + h_1'V + h_2'V^2 + h_3'V^3 . \qquad (A1.12)$$

This is shown in Fig. A1.3.

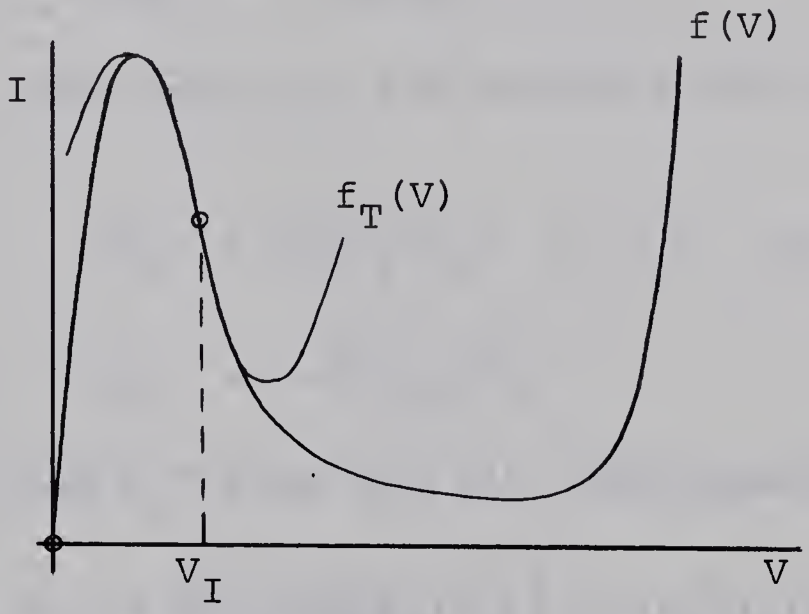

Figure A1.3

Approximation of f(V) by a Cubic Equation

Since $f_T(V)$ should correspond to $f(V)$ at $V = V_I$, it follows that:

$$f_T(V_I) = f(V_I) = g_o(V_I) ; \qquad (A1.13)$$

$$f_T'(V_I) = f'(V_I) = g_1(V_I) = -G_d ; \qquad (A1.14)$$

$$f_T''(V_I) = f''(V_I) = 0 ; \quad \text{and} \qquad (A1.15)$$

$$f_T'''(V_I) = f'''(V_I) = 6g_3(V_I) . \qquad (A1.16)$$

But from (A1.12):

$$f_T'(V_I) = h_1' + 2h_2'V_I + 3h_3'V_I^2 \; ; \qquad \text{(A1.17)}$$

$$f_T''(V_I) = 2h_2' + 6h_3'V_I \; ; \quad \text{and} \qquad \text{(A1.18)}$$

$$f_T'''(V_I) = 6h_3' \; . \qquad \text{(A1.19)}$$

Equating (A1.19) and (A1.16),

$$h_3' = g_3(V_I). \qquad \text{(A1.20)}$$

Substituting h_3' into (A1.18), and equating the result to (A1.15);

$$2h_2' + 6V_I g_3(V_I) = 0 \; ; \quad \text{or}$$

$$h_2' = -3V_I g_3(V_I) \qquad \text{(A1.21)}$$

Substituting h_2' and h_3' into (A1.17), and equating to (A1.14);

$$-G_d = h_1' + 2V_I\left[-3V_I g_3(V_I)\right] + 3V_I^2 g_3(V_I)$$

$$= h_1' - 3V_I^2 g_3(V_I) \; ; \qquad \text{from which}$$

$$h_1' = -G_d + 3V_I^2 g_3(V_I) \qquad \text{(A1.22)}$$

If $f_T(V)$ is now expanded about the general bias point V_Q, as was previously done with $f(V)$, the result will be

$$W_T(V) = f_T(V_Q + V)$$

$$= g_o' + g_1'V + g_2'V^2 + g_3'V^3; \qquad \text{(A1.23)}$$

where

$$g_n' = \frac{f_T^{(n)}(V_Q)}{n!} = g_n'(V_Q) \ . \qquad \text{(A1.24)}$$

Note that (A1.23) and (A1.24) are identical to (4.4) and (4.5), if K = 3.

From (4.36), the describing-function in terms of the three coefficients g_n', will now be

$$G_{eq}'(A,V_Q) = g_1' + \frac{3}{4} g_3'A^2 \qquad \text{(A1.25)}$$

But from (A1.24), $g_1' = f_T'(V_Q)$

$$= h_1' + 2h_2'V_Q + 3h_3'V_Q^2 \qquad \text{(A1.26)}$$

Substituting (A1.22), (A1.21), and (A1.20) into (A1.26);

$$\begin{aligned} g_1' &= \left[-G_d + 3V_I^2 g_3(V_I)\right] + 2\left[-3V_I g_3(V_I)\right]V_Q \\ &\quad + 3g_3(V_I)V_Q^2 \\ &= -G_d + 3g_3(V_I)(V_I^2 - 2V_IV_Q + V_Q^2) \\ &= -G_d + 3g_3(V_I)(V_Q - V_I)^2 \qquad \text{(A1.27)} \end{aligned}$$

Also, from (A1.24),

$$g_3' = \frac{f_T'''(V_Q)}{6} = \frac{6h_3'}{6} = h_3' = g_3(V_I); \text{ so that}$$

$$\frac{3}{4} g_3'A^2 = \frac{3}{4} g_3(V_I)A^2 \qquad \text{(A1.28)}$$

Substituting (A1.28) and (A1.27) into (A1.25),

$$G_{eq}'(A,V_Q) = -G_d + 3g_3(V_I)(V_Q - V_I)^2 + \frac{3}{4} g_3(V_I)A^2 . \qquad \text{(A1.29)}$$

The contour $G_{eq}'(A,V_Q) = \Gamma$ is now defined by the equation

$$-G_d + 3g_3(V_I)(V_Q - V_I)^2 + \frac{3}{4} g_3(V_I)A^2 = \Gamma, \quad \text{or}$$

$$\Gamma + G_d = \frac{3}{4} g_3(V_I)A^2 + 3g_3(V_I)(V_Q-V_I)^2 . \qquad \text{(A1.30)}$$

Equation A1.30 can be rewritten as

$$\frac{A^2}{(\Gamma + G_d)\dfrac{4}{3g_3(V_I)}} + \frac{(V_Q - V_I)^2}{(\Gamma + G_d)\dfrac{1}{3g_3(V_I)}} = 1 . \qquad \text{(A1.31)}$$

Equation A1.31 defines an ellipse in the AV_Q-plane, with centre at $(0,V_I)$, major axis of $4\sqrt{\dfrac{\Gamma + G_d}{3g_3(V_I)}}$; and minor axis of $2\sqrt{\dfrac{\Gamma + G_d}{3g_3(V_I)}}$. The major axis is parallel to the A-axis. The above results have been stated in Sec. 5.4.

As a point of interest, is should be noted that if the d.c. characteristic were in fact a cubic (for all values of V), all contours would be elliptic.

Al.3 Gradient of $G_{eq}(A,V_Q)$

By introducing the notion of the gradient of G_{eq} or $\vec{\nabla} G_{eq}$, Eq. 5.20 can be derived.

The differential vector operator, $\vec{\nabla}$, is defined in the AV_Q-plane as

$$\vec{\nabla} = \vec{i}\,\frac{\partial}{\partial A} + \vec{j}\,\frac{\partial}{\partial V_Q} \quad ; \tag{Al.32}$$

where $\vec{i}$ and $\vec{j}$ are unit vectors parallel to the A- and V_Q-axes respectively. Then $\vec{\nabla} G_{eq}$, or Grad G_{eq}, is defined as

$$\vec{\nabla} G_{eq} = \vec{i}\,\frac{\partial G_{eq}}{\partial A} + \vec{j}\,\frac{\partial G_{eq}}{\partial V_Q} \; . \tag{Al.33}$$

At some point P_1, $\vec{\nabla} G_{eq}$ can be graphically interpreted as a vector, in the direction of increasing G_{eq}, and perpendicular to the contour $G_{eq} = \Gamma_1$, which passes through the point P_1. This is illustrated in Fig. Al.4.

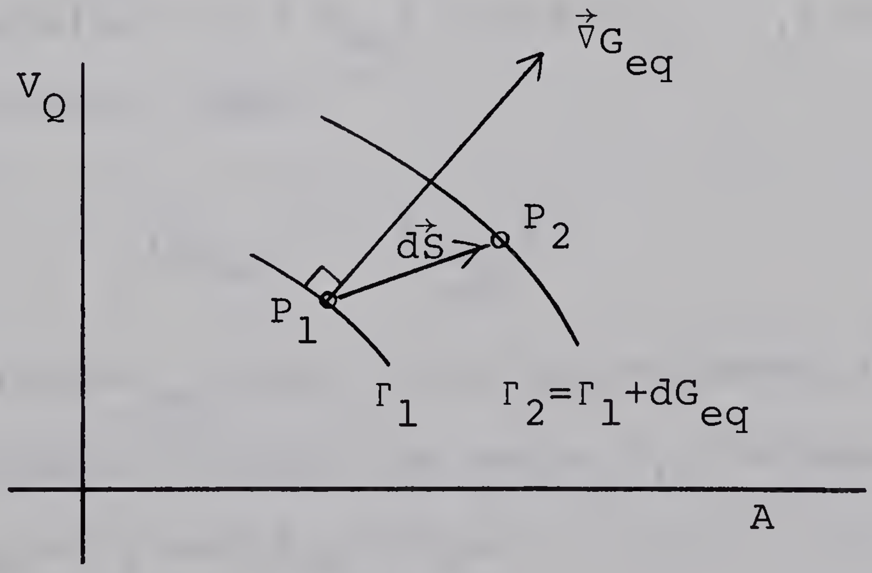

Figure Al.4
Graphical Interpretation of the Gradient Vector

In moving the incremental distance, $\vec{dS}$ from P_1 to P_2, G_{eq} changes from Γ_1 to Γ_2. This incremental change will be given by

$$d\,G_{eq} = \vec{\nabla}\,G_{eq} \cdot \vec{dS} \quad ; \qquad (A1.34)$$

where

$$\vec{dS} = \vec{i}\,dA + \vec{j}\,dV_Q \ .$$

Normally, however, the two partial derivatives of G_{eq} are not known, so that a graphical means of determining $\vec{\nabla}\,G_{eq}$ is desired.

If $\vec{dS}$ is first taken to be parallel to $\vec{\nabla}\,G_{eq}$, then

$$\vec{\nabla}G_{eq} \cdot \vec{dS} = |\vec{\nabla}G_{eq}| \cdot |\vec{dS}| = \Gamma_2 - \Gamma_1 \ ; \quad \text{or}$$

$$|\vec{\nabla}G_{eq}| = \frac{\Gamma_2 - \Gamma_1}{|dS|} \ .$$

If $\vec{dS}$ is now replaced by $\vec{\Delta S}$, which is a small but finite distance (parallel to $\vec{\nabla}\,G_{eq}$), then $(\Gamma_2 - \Gamma_1)$ will also be small but finite. Then

$$|\vec{\nabla}G_{eq}| \simeq \frac{\Gamma_2 - \Gamma_1}{|\Delta S|} \qquad (A1.35)$$

On the Constant-G_{eq} Chart, $|\Delta S|$ can be taken as the perpendicular distance, through the point P_1, between two adjacent contours $G_{eq} = \Gamma_1$ and $G_{eq} = \Gamma_2$.

If $\vec{\nabla}G_{eq}$ makes angle α with the horizontal axis, it is now apparent that

$$\vec{\nabla}G_{eq} \simeq \frac{\Gamma_2 - \Gamma_1}{|\Delta S|}(\vec{i}\cos\alpha + \vec{j}\sin\alpha). \qquad \text{(A1.36)}$$

Since $\vec{\Delta}G_{eq}$ is now known, the incremental change, dG_{eq}, corresponding to any arbitrary displacement $d\vec{S}$ can be found from (A1.34).

If $d\vec{S}$ makes angle β with the horizontal axis, then $d\vec{S} = \vec{i}\,dA + \vec{j}\,dV_Q = \vec{i}\,dA + \vec{j}\tan\beta\,dA = (\vec{i} + \vec{j}\tan\beta)dA$.

Hence, $dG_{eq} = \vec{\nabla}G_{eq}\cdot d\vec{S}$

$$\simeq \frac{\Gamma_2 - \Gamma_1}{|\Delta S|}(\vec{i}\cos\alpha + \vec{j}\sin\alpha)(\vec{i} + \vec{j}\tan\beta)dA, \text{ or}$$

$$dG_{eq} \simeq \frac{\Gamma_2 - \Gamma_1}{|\Delta S|}(\cos\alpha + \sin\alpha\tan\beta)dA\ . \qquad \text{(A1.37)}$$

Equation A1.37 can be rewritten as

$$\frac{dG_{eq}}{dA} \simeq \frac{\Gamma_2 - \Gamma_1}{|\Delta S|}\left(\frac{\cos(\alpha-\beta)}{\cos\beta}\right) \qquad \text{(A1.38)}$$

In Sec. 5.7, $d\vec{S}$ has been chosen to be along the curve $V_Q(A)$.

The results derived in this section can also be used to prove Theorems 5.2 and 5.3.

A1.4 Proof of Theorem 5.2

Proof of this theorem is based on the gradient of G_{eq}, as discussed in Sec. A1.3.

Consider any point, P_1, in the AV_Q-plane. If $d\vec{S}$ is chosen to be parallel to the A-axis, then $d\vec{S} = \vec{i}\,dA$, so that $dV_Q = 0$, and $\beta = 0$ (in Eq. A1.38). Now, from (A1.34), $dG_{eq} = \vec{\nabla} G_{eq} \cdot d\vec{S}$; and from (A1.33),

$$\vec{\nabla} G_{eq} = \vec{i}\,\frac{\partial G_{eq}}{\partial A} + \vec{j}\,\frac{\partial G_{eq}}{\partial V_Q} .$$

Thus, for $dV_Q = 0$, $dG_{eq} = \partial G_{eq}/\partial A \cdot dA$ or

$$\frac{dG_{eq}}{dA} = \frac{\partial G_{eq}}{\partial A} . \qquad \text{(A1.39)}$$

If the point P_1 is now chosen to lie on the V_Q-axis, then at P_1, $A = 0$. However, Eq. 5.4 shows that $\left.\frac{\partial G_{eq}}{\partial A}\right|_{A=0} = 0$. Thus, from (A1.39), at P_1, $dG_{eq}/dA = 0$. But since $\beta = 0$, from (A1.38),

$$\frac{dG_{eq}}{dA} \simeq \frac{\Gamma_2 - \Gamma_1}{|\Delta S|} \cos\alpha . \qquad \text{(A1.40)}$$

Equation A1.40 implies that $\cos\alpha = 0$, or $\alpha = \pm 90^\circ$. Thus, all contours must meet the V_Q axis at right angles, as $\vec{\nabla} G_{eq}$ is always perpendicular to the contour through the point P_1.

Also, since moving in any direction from the point $(0, V_I)$ corresponds to increasing G_{eq}, it follows that if $V_Q > V_I$, $\alpha = +90^\circ$, and if $V_Q < V_I$, $\alpha = -90^\circ$. This is shown in Fig. A1.5 .

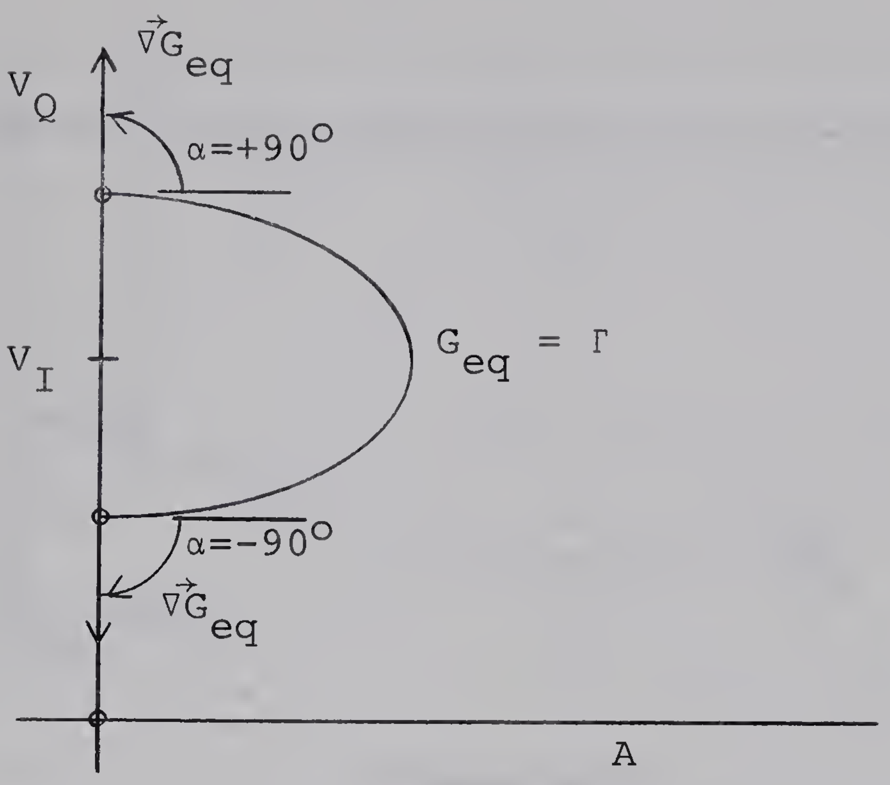

Figure A1.5
Illustration of Theorem 5.2

A1.5 Proof of Theorem 5.3

Proof of this theorem is based on the results obtained in both Sec's. A1.3 and A1.4.

Consider a curve $G_{eq}(A,V_{Q_2})$, such that $\left.\frac{\partial^2 G_{eq}}{\partial A^2}\right|_{A=0} < 0$. This curve will clearly concave downward at A = 0. One such curve is shown in Fig. 5.4(a), and again in Fig. A1.6. Now since $\left.\frac{\partial G_{eq}}{\partial A}\right|_{A=0} = 0$ (Eq. 5.4), it follows that there must exist a small positive number ε, for which

$$\left.\frac{\partial G_{eq}}{\partial A}\right|_{A=\varepsilon} < 0 .$$

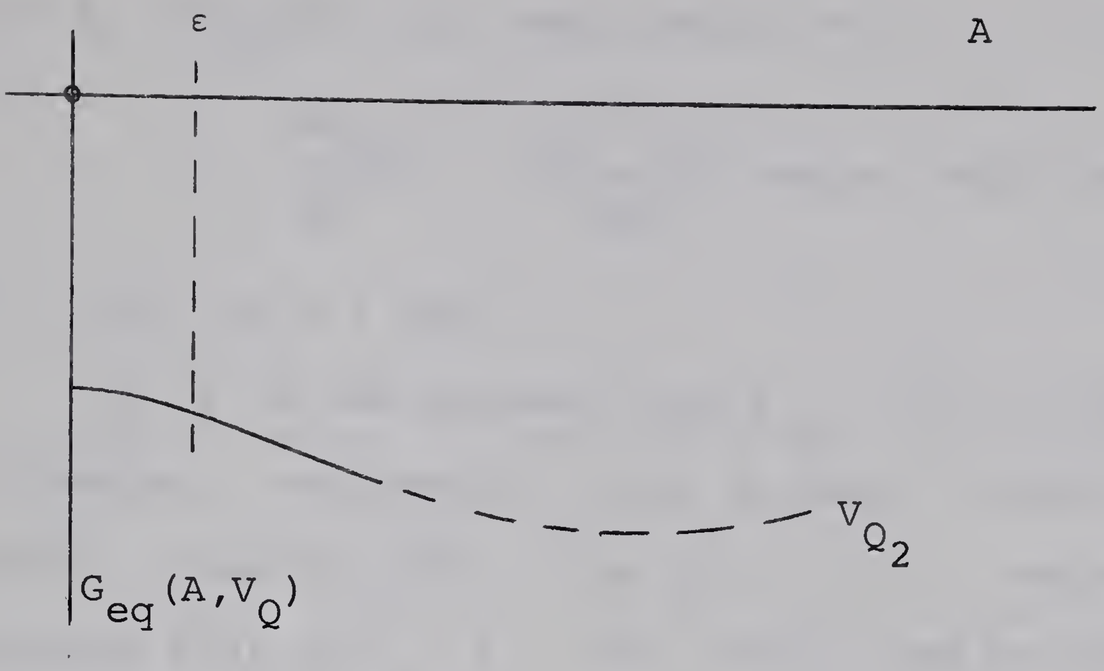

Figure A1.6
Describing Function Curve Near the Vertical Axis

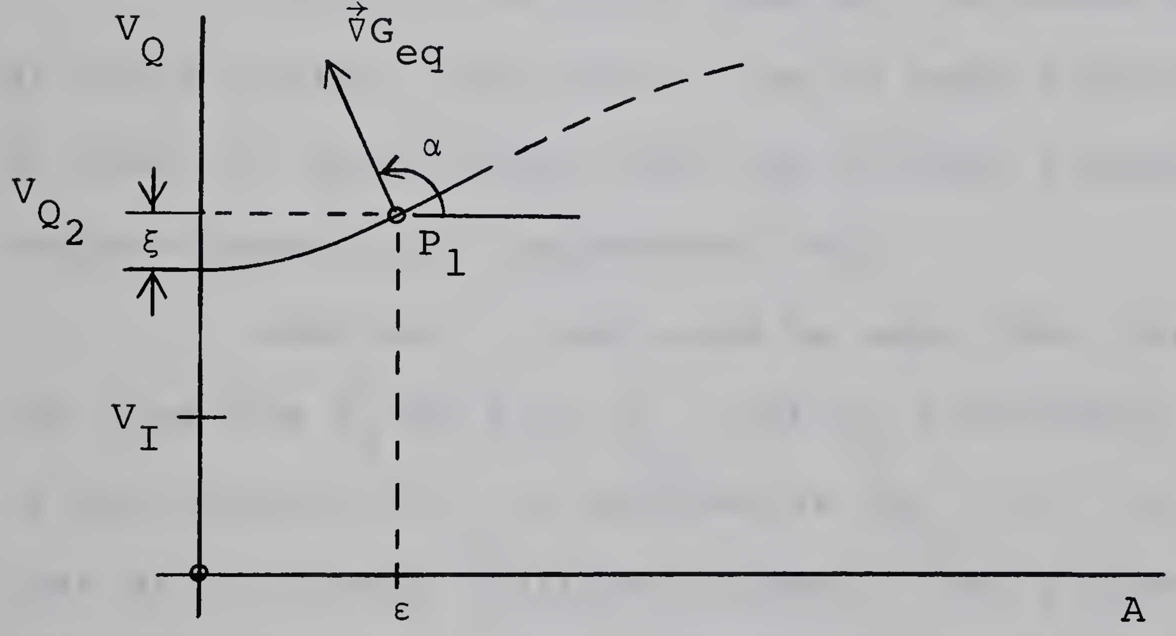

Figure A1.7
Contour Near the Vertical Axis

If the point (ε, V_{Q_2}) is now chosen as P_1, in the AV_Q-plane, and $d\vec{S}$ is chosen parallel to the A-axis, then, in Eq. A1.38, $\beta = 0$, and by (A1.39) $\frac{dG_{eq}}{dA} = \left.\frac{\partial G_{eq}}{\partial A}\right|_{A=\varepsilon}$

Thus, at P_1, $dG_{eq}/dA < 0$. But since $\beta = 0$,

$$\frac{dG_{eq}}{dA} \simeq \frac{\Gamma_2 - \Gamma_1}{|\Delta S|} \cos \alpha, \text{ which implies}$$

that $\alpha > +90^\circ$, or $\alpha > -90^\circ$.

If it is now assumed that $V_{Q_2} > V_I$, it is apparent that by making ε arbitrarily close to zero, α can be made arbitrarily close to $+90^\circ$. (See Fig. A1.5). Hence, it can be concluded that at P_1, $\alpha > +90^\circ$, which implies that the contour through P_1 must have a positive slope at P_1. This is shown in Fig. A1.7.

Since it is known that all contours meet the V_Q-axis at right angles, and since ε can be made arbitrarily close to zero, it now follows that the contour through P_1 must be concave upward as A approaches zero.

However, it can also be seen that this contour will not meet the V_Q-axis at V_{Q_2}, but at a slightly smaller value. If this value of V_Q is defined as $(V_{Q_2} - \xi)$, it is apparent that as ε is made arbitrarily small (but finite) the same will be true of ξ. For a specific ε, ξ will of course depend on the degree of curvature of the contour in the vicinity of P_1.

If the range $\{V_{Q_2}\}$ is now defined as the range $V_1 \leq V_Q \leq V_2$, such that $V_1 > V_I$, and such that all curves $G_{eq}(A,V_Q)$ corresponding to $\{V_{Q_2}\}$ are concave downward at $A = 0$, then it can be concluded that all contours meeting

the V_Q-axis in the range $V_1 - \xi_1 \leq V_Q \leq V_2 - \xi_2$ must be concave upward at A = 0. Now by making ε arbitrarily small, ξ_1 and ξ_2 will also be made aribtrarily small, so that the range $V_1 - \xi_1 \leq V_Q \leq V_2 - \xi_2$ can be made to correspond, as closely as desired, to the range $\{V_{Q_2}\}$. The end points of the two ranges, however, cannot be made to coincide, since ε, and thus ξ_1 and ξ_2 must remain finite.

A similar argument can be used to prove the remainder of Theorem 5.3.

APPENDIX II

ANALOGUE COMPUTER SIMULATION

It has been shown in Sec. 7.1, that the tunnel diode oscillator (with or without mutual coupling) can be accurately simulated on an analogue computer, by means of three basic system components. Computer schematics for these basic components will now be derived.

A2.1 Function Generator

A function generator which will produce the d.c. characteristic, I = f(V), will first be designed. This is done by using an actual tunnel diode, so that the resulting function will be as close as possible to the actual curve for the diode. This function generator has been used to obtain the characteristic shown in Fig. 4.1(a).

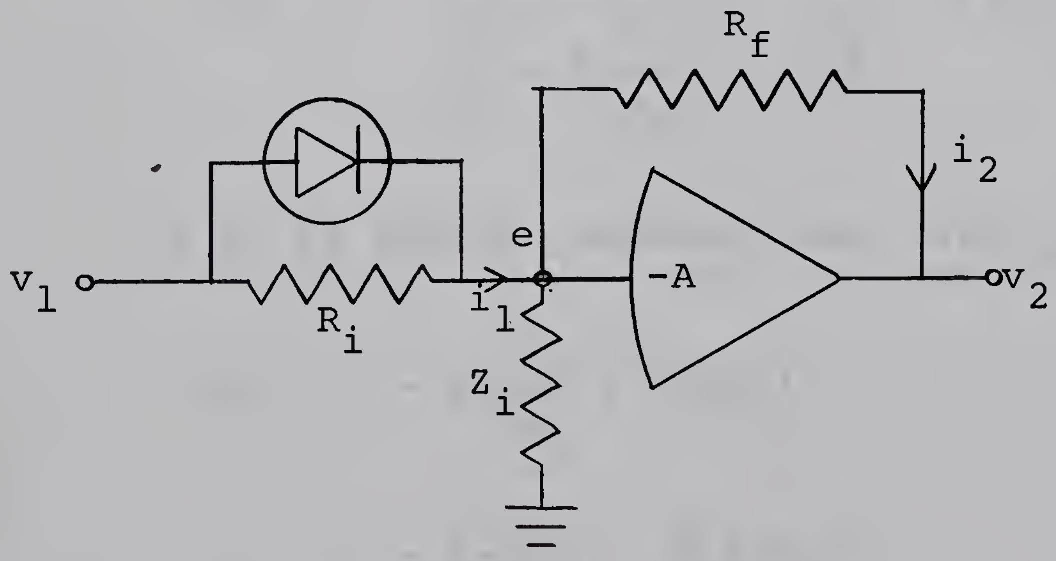

Figure A2.1
Derivation of the Function Generator

Figure A2.1 shows an ordinary operational amplifier, with open-loop gain of A, input impedance of Z_i, and a feedback resistor, R_f. A tunnel diode is placed in parallel with the input resistor, R_i.

If it is assumed that the grid voltage, e, is much less than V_1 or $-V_2$, then $i_1 \simeq V_1/R_i + f(V_1)$, and $i_2 \simeq Ae/R_f$. Since $e = (i_1 - i_2)Z_i$, it follows that

$$e \simeq \left[\frac{V_1}{R_i} + f(V_1) - \frac{Ae}{R_f}\right] Z_i \quad ; \quad \text{or}$$

$$e\left[1 + A\left(\frac{Z_i}{R_f}\right)\right] \simeq \left[\frac{V_1}{R_i} + f(V_1)\right] Z_i \; . \quad \text{But } e = -V_2/A,$$

so that

$$-\frac{V_2}{A}\left[1 + A\left(\frac{Z_i}{R_f}\right)\right] \simeq \left[\frac{V_1}{R_i} + f(V_1)\right] Z_i, \quad \text{from which}$$

$$V_2 \simeq -\frac{AZ_i}{\left[1 + A\left(\frac{Z_i}{R_f}\right)\right]} \cdot \left[\frac{V_1}{R_i} + f(V_1)\right].$$

If it is further assumed that $A(Z_i/R_f) >> 1$, then

$$V_2 \simeq -R_f\left[\frac{V_1}{R_i} + F(V_1)\right]$$

$$= -\left(\frac{R_f}{R_i}\right)V_1 - R_f f(V_1).$$

If the quantity $(R_f/R_i)V_1$ is now added to V_2, the

result will be $-R_f f(V_1)$. This can be done as shown in Fig. A2.2.

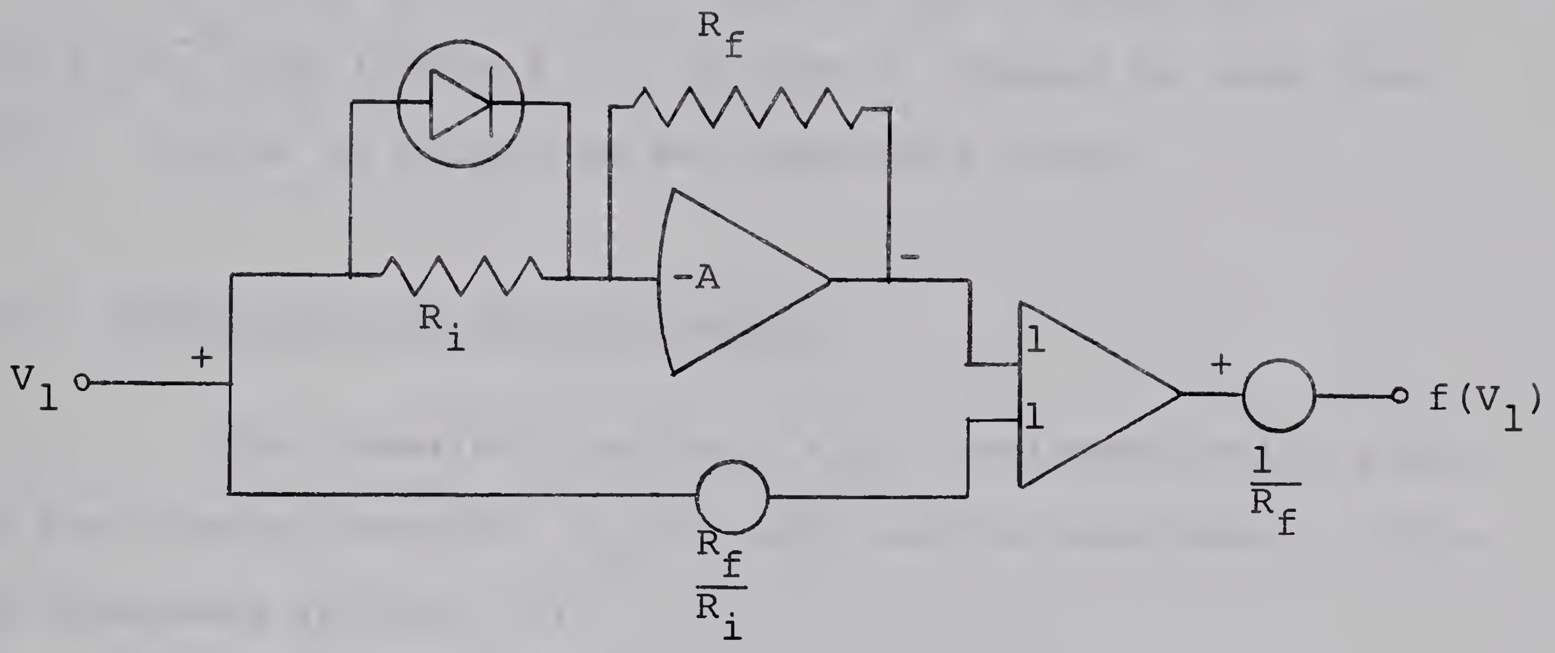

Figure A2.2
The Function Generator

The reason for including R_i, in parallel with the tunnel diode, is to prevent self-oscillation of the diode (in conjunction with the circuitry of the analogue computer), as discussed in Sec. 5.10. To assure that this does not occur, R_i can be connected directly to the leads of the tunnel diode (so that parasitic elements will be minimized); and can be chosen in magnitude so that the resulting combination does not exhibit a "negative resistance" region. Thus, from Fig. A2.1,

$$\frac{d_{i_1}}{dV_i} > 0, \qquad \text{or} \qquad \frac{1}{R_i} > -f'(V_1).$$

Since the maximum value of $-f'(V_1)$ is G_d (Eq. 1.2), this implies that $1/R_i > G_d$, or $R_i < 1/G_d$.

For a 1N2940 tunnel diode, G_d is typically 6.6×10^{-3} mho (Table 4.1), so that R_i should be less than 150 Ω. R_f can be chosen as any desirable value.

A2.2 Simulation of Biasing Network

The transfer function, $H_2(S)$, mathematically equal to the biasing network, $Z_B(S)$, will now be simulated. (This is discussed in Sec. 7.1)

From Fig. 2.1(b),

$$Z_B(S) = \frac{R_B \cdot 1/SC_B}{R_B + 1/SC_B}$$

$$= \frac{R_B}{SC_BR_B + 1} = H_2(S)$$

The computer schematic for this transfer function can very easily be derived, and is shown in Fig. A2.3.

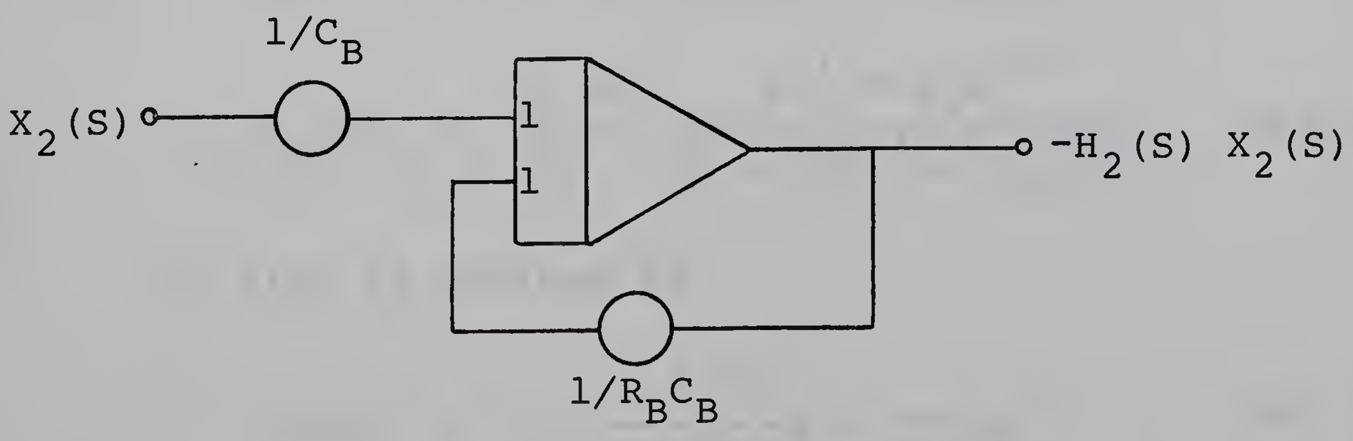

Figure A2.3

Simulation of the Biasing Network

A2.3 Simulation of Single Tank Circuit

The computer schematic for the transfer function $H_1(S)$, equal to the impedance function, $Z_T(S)$ for a single tank circuit will now be derived.

From Eq. 3.1,

$$Z_T(S) = \frac{R_1 + SL_1}{S^2L_1C_1 + SC_1R_1 + 1} = H_1(S) \qquad \text{(A2.1)}$$

Equation A2.1 can be rewritten as

$$H_1(S) = \frac{1}{C_1}\left[\frac{S + \frac{R_1}{L_1}}{S^2 + \frac{R_1}{L_1}S + \frac{1}{L_1C_1}}\right]$$

$$= \frac{1}{C_1}\left[\frac{S + a_o}{S^2 + b_1S + b_o}\right] \qquad \text{(A2.2)}$$

where a_o, b_1, and b_o are implicitly defined. Letting $H_1(S) = C_1(S)/R_1(S)$, (A2.2) can be rewritten as

$$\frac{C_1(S)}{R_1(S)} = \frac{1}{C_1}\left[\frac{S^{-1} + a_oS^{-2}}{1 + b_1S^{-1} + b_1S^{-2}}\right] \quad , \text{ or}$$

$$C_1(S) = \frac{R_1(S)}{C_1}\left[\frac{S^{-1} + a_oS^{-2}}{1 + b_1S^{-1} + b_oS^{-2}}\right] \qquad \text{(A2.3)}$$

If E(S) is defined as

$$E(S) = \frac{R_1(S)}{C_1(1 + b_1S^{-1} + b_oS^{-2})} \quad ; \qquad \text{(A2.4)}$$

(A2.3) can be expressed as

$$C_1(S) = E(S)(S^{-1} + a_o S^{-2}) \qquad (A2.5)$$

Now, (A2.4) can be rewritten as

$$E(S)(1 + b_1 S^{-1} + b_o S^{-2}) = \frac{R_1(S)}{C_1}; \quad \text{or}$$

$$E(S) = \frac{R_1(S)}{C_1} - b_1 S^{-1} E(S) - b_o S^{-2} E(S) \; . \qquad (A2.6)$$

Using the method of Signal Flow, (A2.6) can be represented as shown in Fig. A2.4.

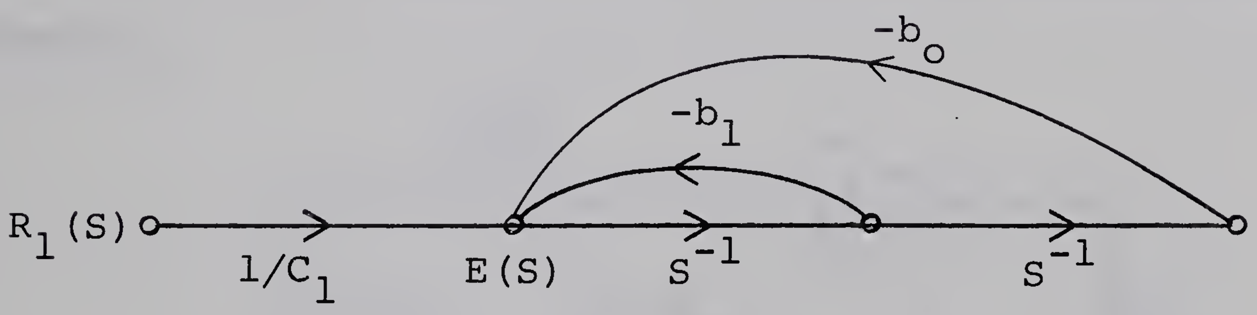

Figure A2.4
Signal Flow Graph for Equation A2.6

Similarily, (A2.5) can be represented as shown in Fig. A2.5.

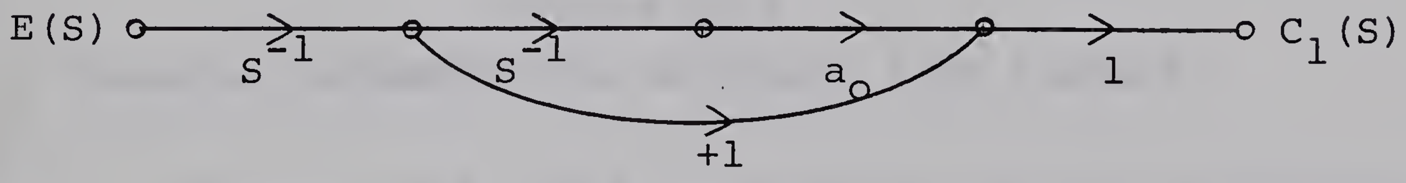

Figure A2.5
Signal Flow Graph for Equation A2.5

Combining Fig's. A2.4 and A2.5 results in the complete Signal Flow Graph for $H_1(S)$, which is shown in Fig. A2.6.

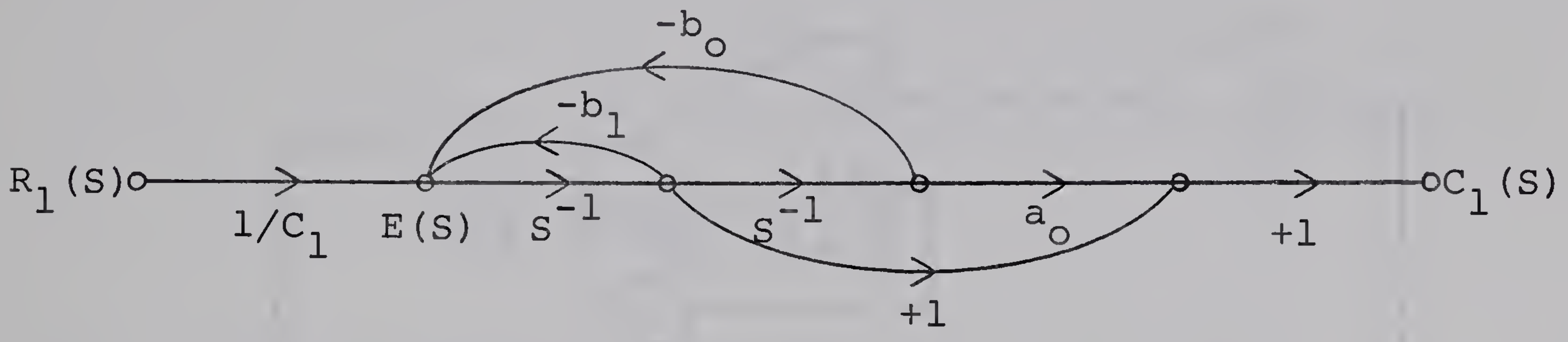

Figure A2.6
Signal Flow Graph for a Single Tank Circuit

The computer schematic can now be drawn directly from Fig. A2.6, and is shown in Fig. A2.7. The values of a_o, b_o, and b_1 (as defined by (A2.2)) are shown on the schematic.

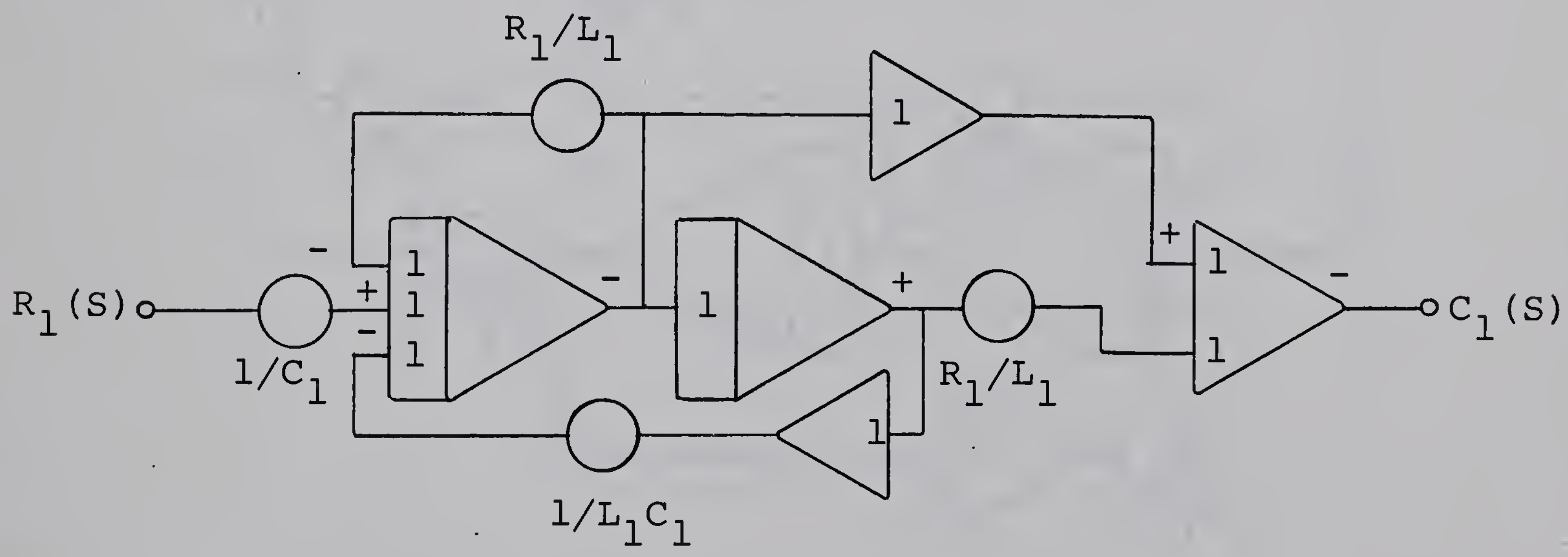

Figure A2.7
Computer Schematic for a Single Tank Circuit

Figures A2.2, A2.3, and A2.7 can now be combined to form the complete simulation of the circuit shown in Fig. 2.2. The resulting schematic is shown in Fig. A2.8 (See Fig. 7.1).

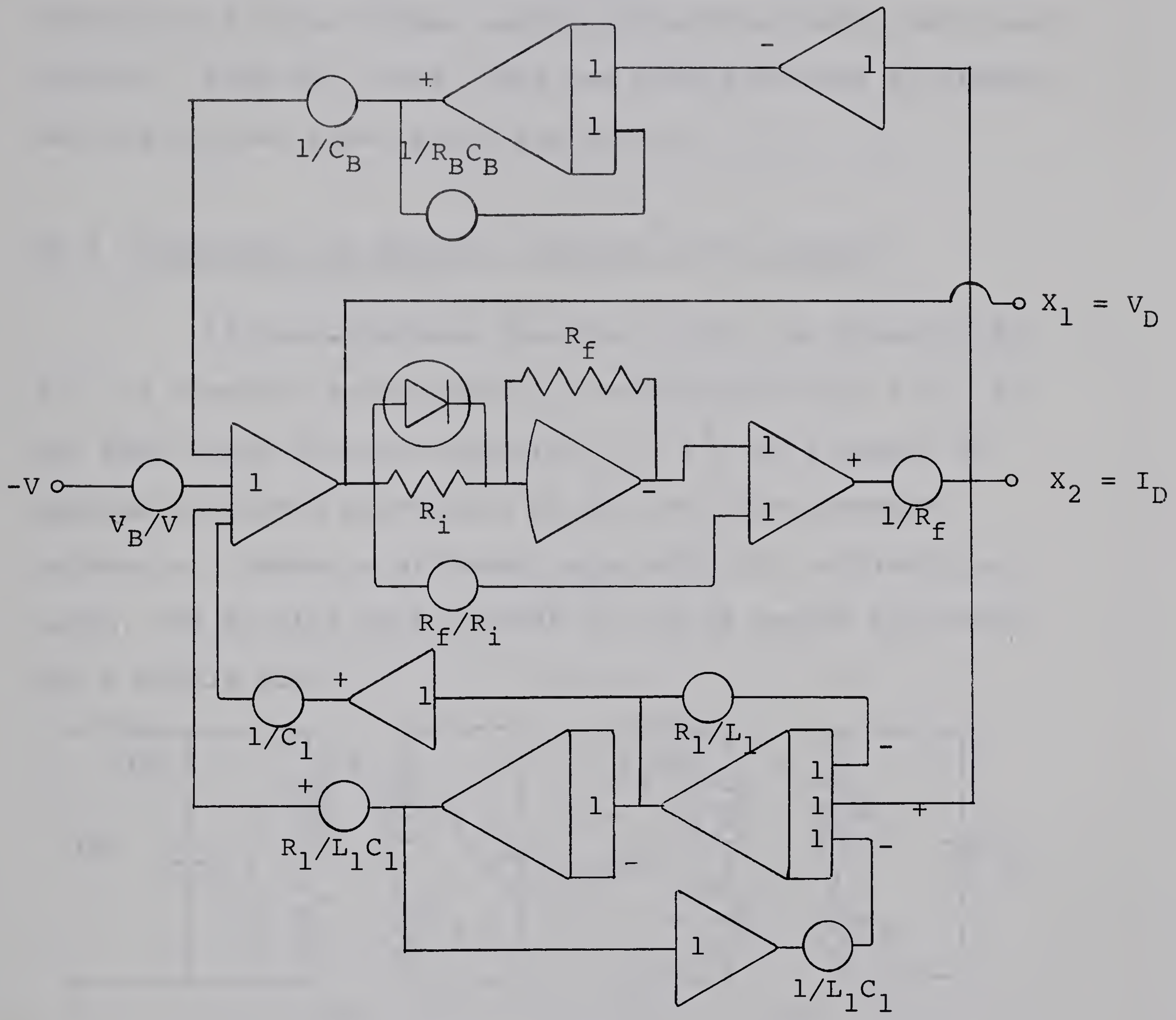

Figure A2.8
Computer Schematic for an Oscillator
Using a Single Tank Circuit

[illegible]

It was suggested in Sec. 5.9, that the dependence of distortion on the factor $G_d\sqrt{L_1/C_1}$ could be investigated by simulating a tunnel diode oscillator with an infinite-Q tank circuit. From Fig. A2.8, this can easily be done by disconnecting the two pots, R_1/L_1 and R_1/L_1C_1.

A2.4 Simulation of Mutually Coupled Tank Circuits

If the impedance function, $Z_T(S)$, as given by Eq. 6.2, is directly synthesized, as was done for Eq. A2.1, it has been found that the quantity $(1 - K^2)$ will appear in several different parameters on the resulting computer schematic. Hence, a different approach will initially be taken, and it will be seen that K^2 can be varied by adjusting a single pot.

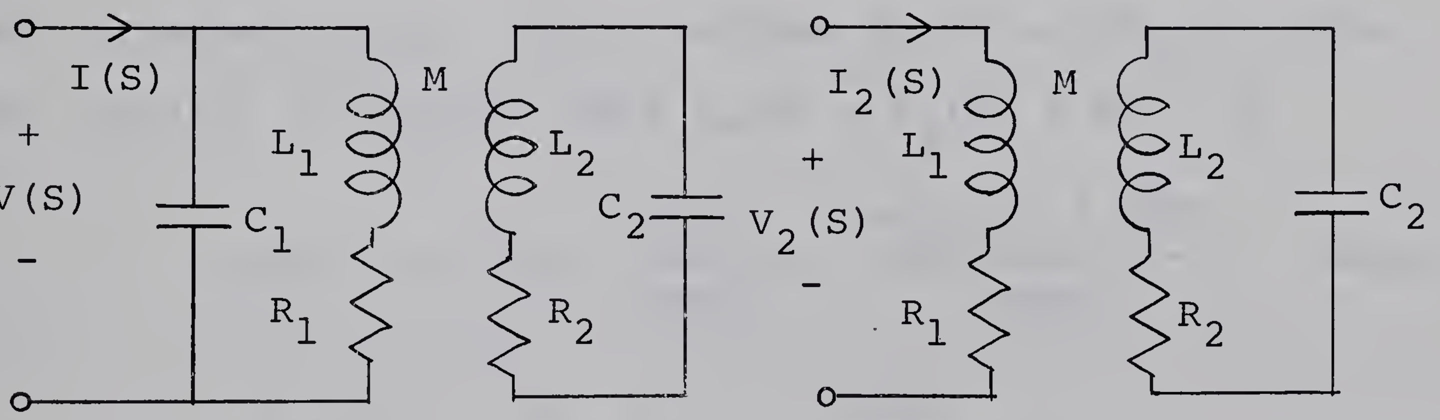

(a) (b)

Figure A2.9
Circuits with Mutual Coupling

It is desired to simulate a transfer function $H_1(S)$, equal to $Z_T(S) = V(S)/I(S)$, as shown in Fig. A2.9(a).

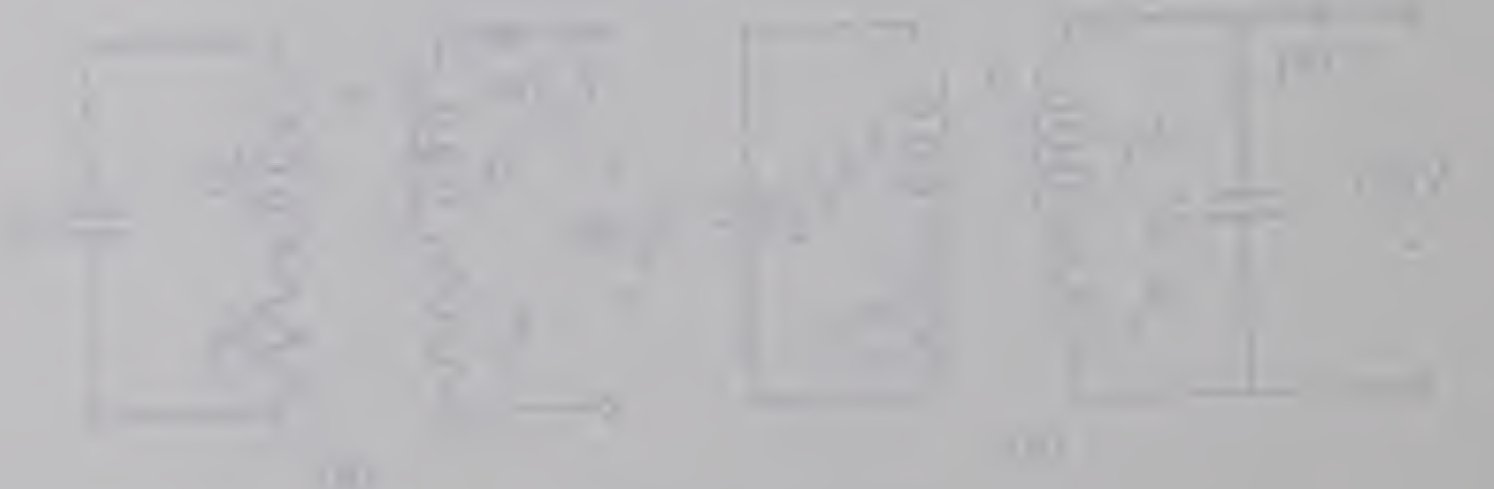

Consider first the circuit shown in Fig. A2.9(b), where $Z_2(S) = V_2(S)/I_2(S)$. This circuit is identical to that shown in Fig. 6.2, except that R_1 has been added. Thus, $Z_2(S) = R_1 + Z_1(S)$, where $Z_1(S)$ is defined by Eq. 6.8; or

$$Z_2(S) = R_1 + \frac{SL_1\left[S^2L_2C_2(1-K^2) + SR_2C_2 + 1\right]}{(S^2L_2C_2 + SR_2C_2 + 1)} .$$

This can be rewritten as

$$Z_2(S) = \frac{S^3L_1L_2C_2(1-K^2) + S^2(L_1R_2C_2+R_1L_2C_2) + S(L_1+R_1R_2C_2) + R_1}{(S^2L_2C_2 + SR_2C_2 + 1)} \tag{A2.7}$$

Now let

$$Y_2(S) = \frac{1}{Z_2(S)} = \frac{N(S)}{D(S)} ; \tag{A2.8}$$

where N(S) and D(S) are the denominator and numerator of (A2.7) respectively. Also, letting $Y_T(S) = 1/Z_T(S)$, from Fig. A2.9(a) it follows that $Y_T(S) = Y_2(S) + SC_1$, or

$$Y_T(S) = SC_1 + \frac{N(S)}{D(S)} = \frac{SC_1D(S) + N(S)}{D(S)} .$$ Hence,

$$Z_T(S) = \frac{1}{Y_T(S)} = \frac{D(S)}{SC_1D(S) + N(S)} ,$$ which can

be rearranged as

$$Z_T(S) = \frac{\dfrac{1}{SC_1}}{1 + \dfrac{N(S)}{SC_1D(S)}} .$$

Thus, the problem is now to simulate the transfer function

$$H_1(S) = \frac{\dfrac{1}{SC_1}}{1 + \dfrac{N(S)}{SC_1 D(S)}} = \frac{C_1(S)}{R_1(S)}$$

The closed loop system shown in Fig. A2.10 will have this transfer function.

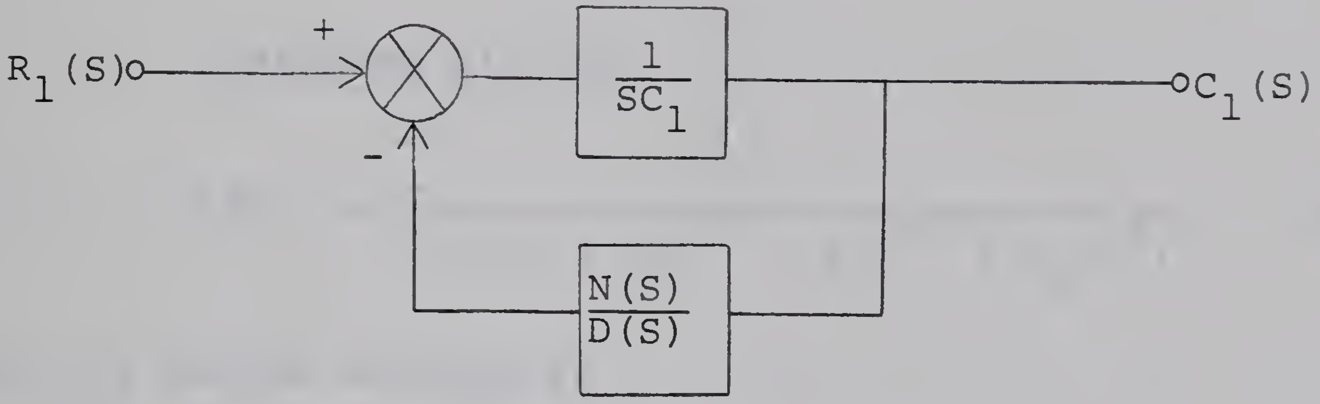

Figure A2.10
Block Schematic for Simulation of
Mutually Coupled Tank Circuits

The feedback portion of Fig. A2.10 can now be simulated by the same means as was Eq. A2.1. From Eq. A2.7,

$$\frac{N(S)}{D(S)} = \frac{S^2L_2C_2 + SR_2C_2 + 1}{S^3L_1L_2C_2(1-K^2)+S^2(L_1R_2C_2+R_1L_2C_2)+S(L_1+R_1R_2C_2)+R_1} \qquad \text{(A2.9)}$$

which can be written as

$$\frac{N(S)}{D(S)} = \frac{1}{L_1}\left[\frac{S^2 + S\,\dfrac{R_2}{L_2} + \dfrac{1}{L_2C_2}}{S^3(1-K^2)+S^2(\dfrac{R_2}{L_2}+\dfrac{R_1}{L_1})+S(\dfrac{1}{L_2C_2}+\dfrac{R_1R_2}{L_1L_2}) + \dfrac{R_1}{L_1L_2C_2}}\right]$$

$$= \frac{1}{L_1}\left(\frac{S^2 + a_1S + a_o}{b_3S^3 + b_2S^2 + b_1S + b_o}\right). \qquad \text{(A2.10)}$$

Letting N(S)/D(S) = C(S)/R(S), (A2.2) can be expressed as

$$\frac{C(S)}{R(S)} = \frac{1}{L_1}\left(\frac{S^{-1} + a_1S^{-2} + a_oS^{-3}}{b_3 + b_2S^{-1} + b_1S^{-2} + b_oS^{-3}}\right) \quad ; \quad \text{or}$$

$$C(S) = \frac{R(S)}{L_1}\left(\frac{S^{-1} + a_1S^{-2} + a_oS^{-3}}{b_3 + b_2S^{-1} + b_1S^{-2} + b_oS^{-3}}\right). \quad (A2.11)$$

Defining E(S) as

$$E(S) = \frac{R(S)}{L_1(b_3 + b_2S^{-1} + b_1S^{-2} + b_oS^{-3})}, \quad (A2.12)$$

(A2.11) can be written as

$$C(S) = E(S)(S^{-1} + a_1S^{-2} + a_oS^{-3}) \quad (A2.13)$$

Also, (A2.12) can be rewritten as

$$E(S)(b_3 + b_2S^{-1} + b_1S^{-2} + b_oS^{-3}) = \frac{R(S)}{L_1} \quad ; \quad \text{or}$$

$$b_3E(S) = \frac{R(S)}{L_1} - b_2S^{-1}E(S) - b_1S^{-2}E(S) - b_oS^{-3}E(S) \quad (A2.14)$$

Equation A2.14 can be represented by the Signal Flow Graph shown in Fig. A2.11

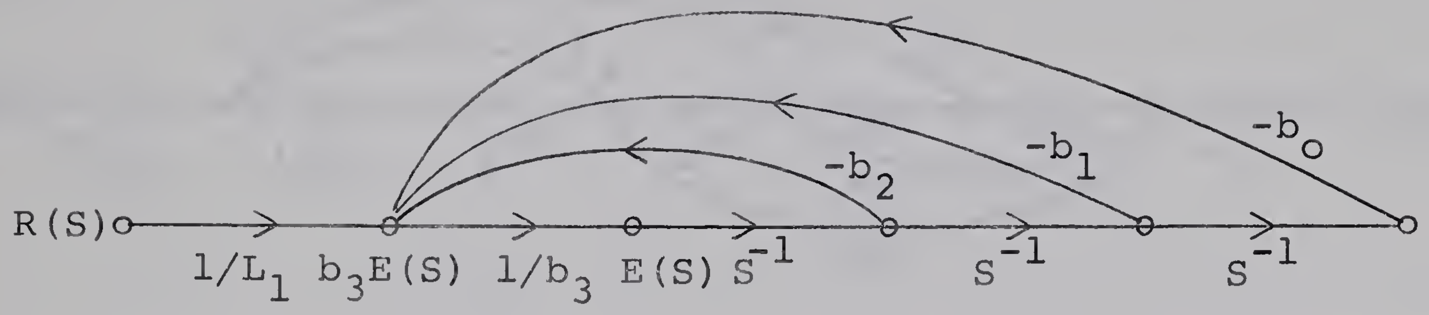

Figure A2.11
Signal Flow Graph for Equation A2.14

Also, Eq. 2.13 can be represented by Fig. A2.12.

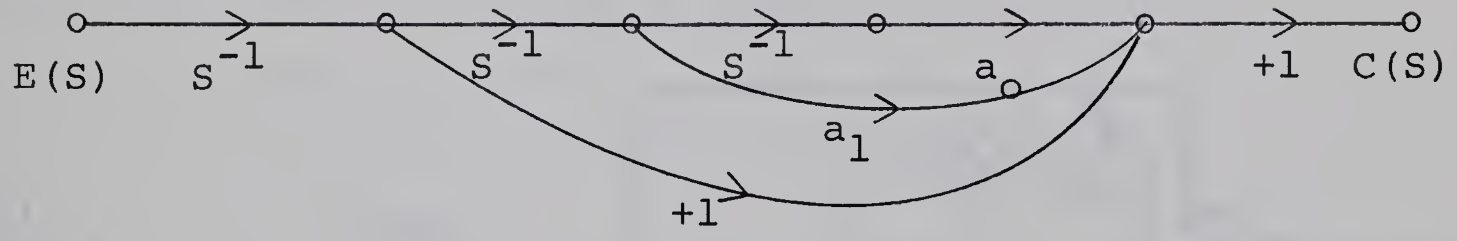

Figure A2.12
Signal Flow Graph for Equation A2.13

Combining Fig's. A2.11 and A2.12, the Signal Flow Graph for the feedback function N(S)/D(S) results. This is shown in Fig. A2.13. Note that b_3, which is $(1-K^2)$, appears only once in this figure.

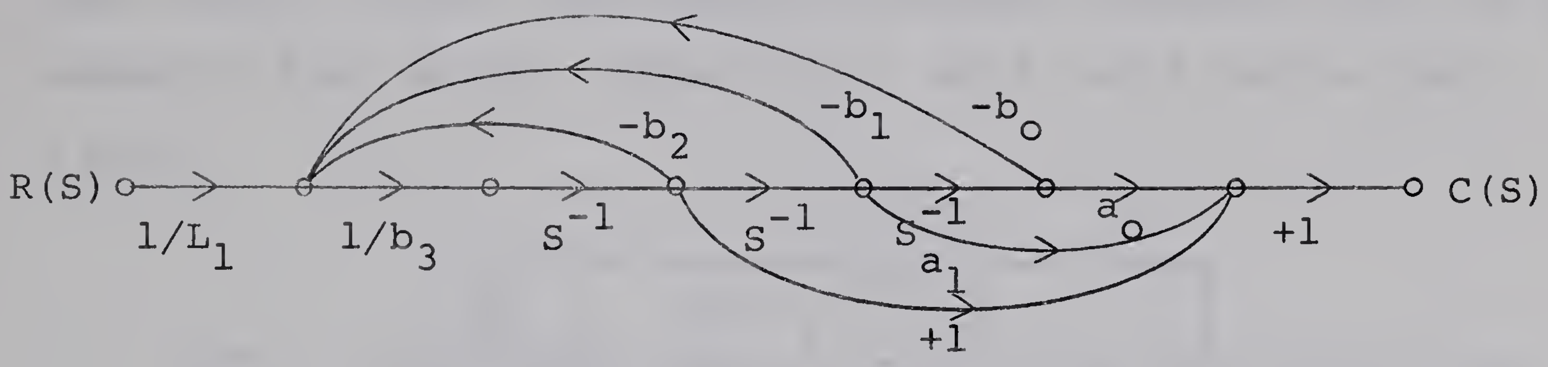

Figure A2.13

Signal Flow Graph for Feedback Portion of Fig. A2.10

The computer scheme for N(S)/D(S) can now be drawn from Fig. A2.13, and is shown in Fig. A2.14.

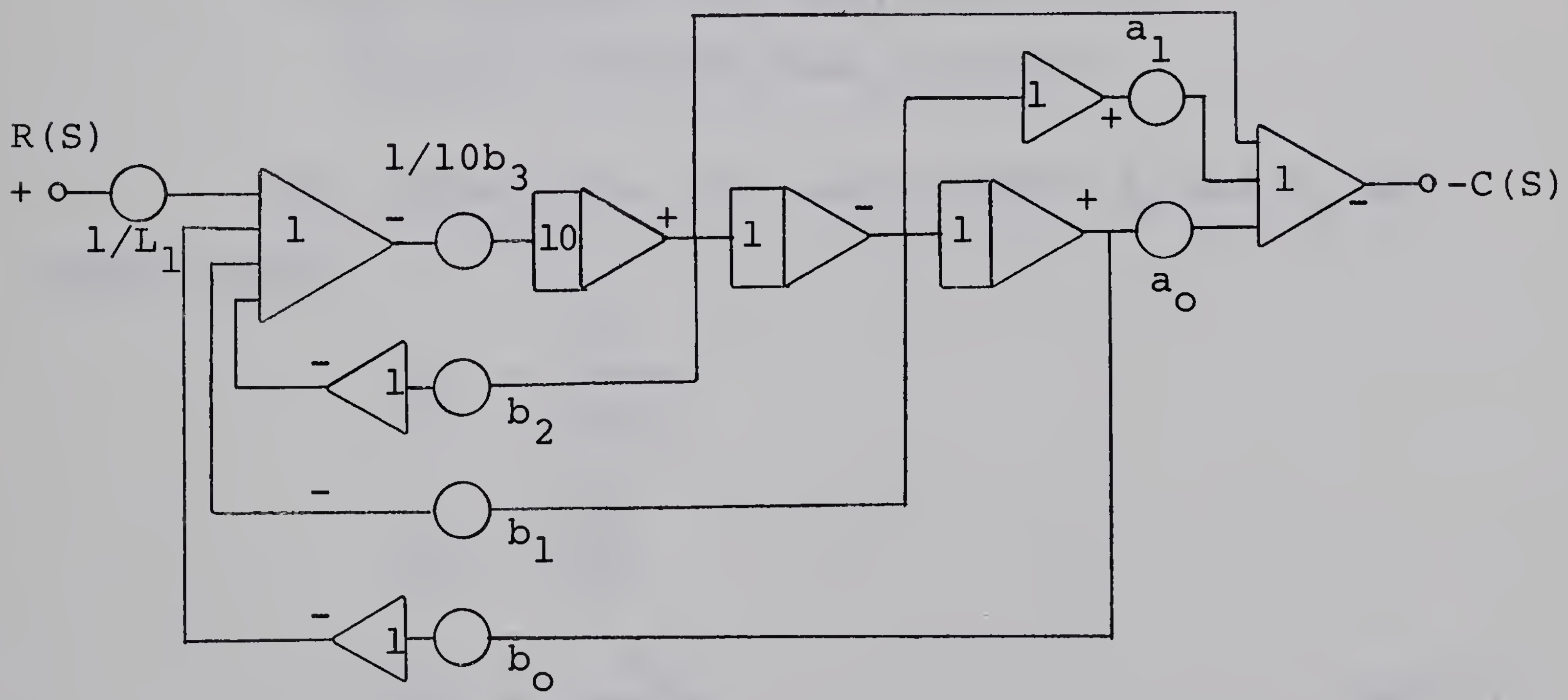

Figure A2.14

Computer Schematic for Feedback Portion of Fig. A2.10

From Fig. 7.1, the block diagram for the complete simulation, with mutual coupling, will now be as shown in

Fig. A2.15. Thus, the complete computer schematic will be as shown in Fig. A2.16. (From Fig's. A2.2, A2.3, A2.14, and A2.15).

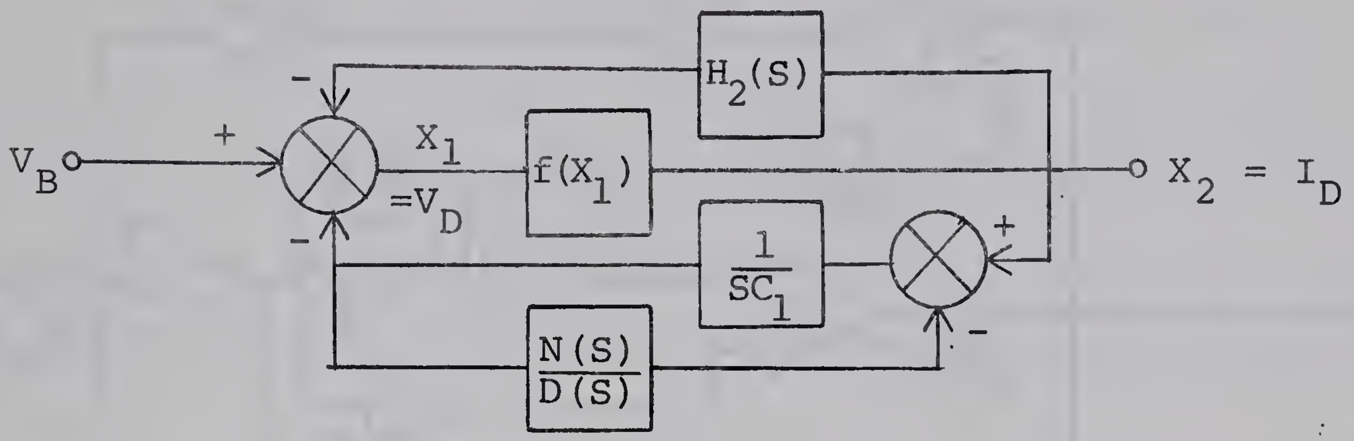

Figure A2.15
Block Schematic for Oscillator with
Mutually Coupled Tank Circuits

For convenience, the coefficients a_n and b_n are listed below.

$$\begin{aligned}
a_o &= \frac{1}{L_2C_2} \\
a_1 &= \frac{R_2}{L_2} \\
b_o &= \frac{R_1}{L_1L_2C_2} \qquad \text{(A2.14)} \\
b_1 &= \frac{1}{L_2C_2} + \frac{R_1R_2}{L_1L_2} \\
b_2 &= \frac{R_2}{L_2} + \frac{R_1}{L_1} \\
b_3 &= (1 - K^2)
\end{aligned}$$

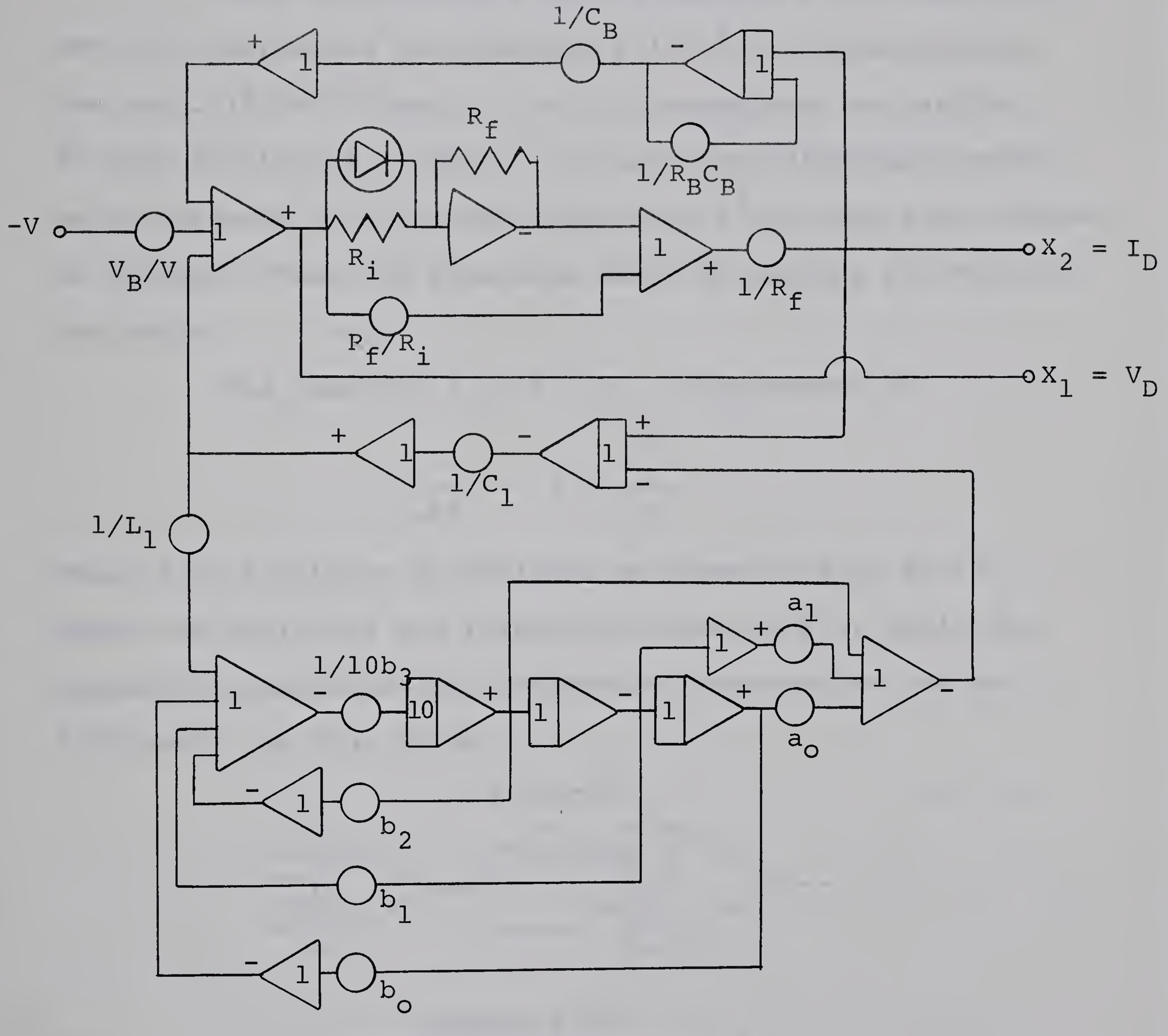

Figure A2.16
Computer Schematic for Oscillator with
Mutually Coupled Tank Circuits

A2.5 Accurate Adjustment of K^2

Note that in Fig's. A2.14 and A2.16, the coefficient $1/b_3$ represents the quantity $1/(1-K^2)$, so that varying the pot $1/10(1-K^2)$ from 0.1 to 1.0 corresponds to varying K^2 from 0.0 to 0.9. However, in practice, difficulty would be encountered in accurately adjusting K^2 to very small values, or to zero. Thus, an alternate means of varying K^2 would be desirable.

The quantity $1/(1-K^2)$ can be expressed as

$$\frac{1}{1-K^2} = 1 + \frac{K^2}{1-K^2} .$$

Thus, Fig. A2.16 can be modified as shown in Fig. A2.17, where the amplifier and integrator shown in Fig. A2.17 represent the amplifier and integrator connected to the pot $1/10(1-K^2)$, in Fig. A2.16

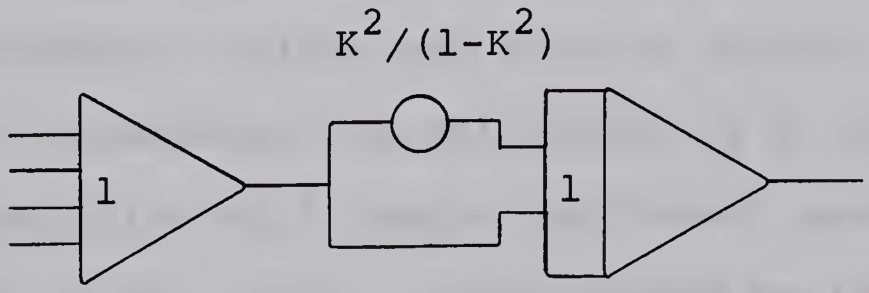

Figure A2.17
Accurate Adjustment of K^2

Hence, varying the pot $K^2/(1-K^2)$ from 0.0 to 1.0 corresponds to varying K^2 from 0.0 to 0.5. For very small values of K^2, $K^2/(1-K^2) \simeq K^2$, and for $K^2 = 0$, the pot can be disconnected.

A2.6 Scaling

For the computer simulation of any practical oscillator circuit (with or without mutual coupling) frequency scaling will be required. This can be done by simply scaling the impedance functions, $Z_T(S)$ and $Z_B(S)$, to any desired frequency, and using the resulting circuit elements to determine the pot-settings and gains for the computer schematics.

It is shown by Skilling (Ref. 2, page 501) that

$$Z(R, \frac{L}{n}, \frac{C}{n}, nS) = Z(R,L,C,S) \qquad (A2.15)$$

Thus, if it were desired to simulate a circuit that was known to oscillate at 1.0 MHz,and the simulation was desired to oscillate at 1.0 Hz, in Eq. A2.15, $n = 10^{-6}$. Hence, for the simulation, all resistors would be unchanged, and all inductors and capacitors would be multiplied by 10^6.

Impedance scaling can also be applied if desired. If all linear impedances are multiplied by a factor, m, the form of the solution will remain unaltered, provided that the diode characteristic, f(V), is multiplied by 1/m.

It should be kept in mind that, on the computer simulation, X_1 is the actual voltage appearing across the tunnel diode, and thus must not be allowed to exceed the operating range of the diode. Any desirable scale can be chosen for X_2, which represents the diode current.

REFERENCES

1. Gibson, J.E.: Non-Linear Automatic Control, McGraw-Hill Co., 1963.

2. Skilling, H.H.: Electrical Engineering Circuits, John Wiley & Sons, Inc., 1957.

3. Giorgis, J., Gottlieb, E., Lawry, H.R., and Weischedel, R.C., Contributors: General Electric Tunnel Diode Manual, First Edition.

4. Taylor, A.E.: Calculus with Analytic Geometry, Prentice-Hall, Inc., 1959.

B29876